

STORAX CONTAINING HYDROXYETHYL CHITOSAN-CARRAGEENAN
HYDROGEL / ASYMMETRIC POLYCAPROLACTONE MEMBRANE
BILAYER WOUND DRESSING

A THESIS SUBMITTED TO
THE GRADUATE SCHOOL OF NATURAL AND APPLIED SCIENCES
OF
MIDDLE EAST TECHNICAL UNIVERSITY

BY

MUSTAFA NAKİPOĞLU

IN PARTIAL FULFILLMENT OF THE REQUIREMENTS
FOR
THE DEGREE OF DOCTOR OF PHILOSOPHY
IN
BIOTECHNOLOGY

JANUARY 2023

Approval of the thesis:

**STORAX CONTAINING HYDROXYETHYL CHITOSAN-
CARRAGEENAN HYDROGEL / ASYMMETRIC POLYCAPROLACTONE
MEMBRANE BILAYER WOUND DRESSING**

submitted by **MUSTAFA NAKİPOĞLU** in partial fulfillment of the requirements
for the degree of **Doctor of Philosophy in Biotechnology, Middle East Technical
University** by,

Prof. Dr. Halil Kalıpçılar
Dean, Graduate School of **Natural and Applied Sciences**

Assoc. Prof. Dr. Yeşim Soyer
Head of the Department, **Biotechnology**

Prof. Dr. Ayşen Tezcaner
Supervisor, **Biotechnology, METU**

Assoc. Prof. Dr. Can Özen
Co-Supervisor, **Biotechnology, METU**

Examining Committee Members:

Prof. Dr. Ayşe Karakeçili
Chemical Engineering, Ankara University

Prof. Dr. Ayşen Tezcaner
Biotechnology, METU

Prof. Dr. Dilek Keskin
Engineering Sciences, METU

Prof. Dr. İrem Erel Göktepe
Chemistry, METU

Assist. Prof. Dr. Özge Erdemli
Molecular Biology and Genetics, Başkent University

Date: 18.01.2023

I hereby declare that all information in this document has been obtained and presented in accordance with academic rules and ethical conduct. I also declare that, as required by these rules and conduct, I have fully cited and referenced all material and results that are not original to this work.

Name Last name : Mustafa Nakipođlu

Signature :

ABSTRACT

STORAX CONTAINING HYDROXYETHYL CHITOSAN-CARRAGEENAN HYDROGEL / ASYMMETRIC POLYCAPROLACTONE MEMBRANE BILAYER WOUND DRESSING

Nakipođlu, Mustafa
Doctor of Philosophy, Biotechnology
Supervisor : Prof. Dr. Ayşen Tezcaner
Co-Supervisor: Assoc. Prof. Dr. Can Özen

January 2023, 133 pages

Despite the advancement of modern technology, wound care is still based on traditional methods such as suture, staple and gauze around the world. Although, these methods provide affordable treatment for various types of wounds, they fall short in easy and effective treatment to facilitate healing process. Enabling a quicker and more convenient wound healing necessitates a comprehensive approach to wound dressing development to include simple yet multifunctional and versatile designs. In this work, we focused on the development of a multifunctional wound dressing composed of two layers; polydopamine coated asymmetric polycaprolactone membrane (PCL-DOP) and *Liquidambar orientalis* Mill. storax loaded hydroxyethyl chitosan (HECS)-carrageenan (kC) based hydrogel (HECS-kC). PCL-DOP membrane was prepared by non-solvent induced phase separation (NIPS) followed by polydopamine coating and demonstrated an excellent barrier against bacteria while allowing optimal oxygen and water vapor exchange in addition to good adhesive-cohesive properties. Storax loaded HECS-kC hydrogel, on the other hand, was tested on different pH environment *in vitro* and optimized to provide necessary conditions to facilitate wound healing. The hydrogels showed

ultra-stretchability, capability to absorb wound exudates, allow oxygen and water vapor transmission while the storax incorporation enabled enhanced antimicrobial and antioxidant activity. Furthermore, rat full-thickness skin defect model showed that the developed bilayer wound dressing could significantly facilitate wound healing compared to Tegaderm and control groups. This study displays that the bilayered wound dressing have a potential to be used a simple and effective wound care system.

Keywords: Polycaprolactone, Chitosan, Carrageenan, *Liquidambar orientalis* Mill., Wound dressing

ÖZ

SIĞLA YAĞI İÇEREN HİDROKSİETİL KİTOSAN-KARAGENAN HİDROJEL / ASİMETRİK POLİKAPROLAKTON MEMBRAN ÇİFT TABAKALI YARA ÖRTÜSÜ

Nakipoğlu, Mustafa
Doktora, Biyoteknoloji
Tez Yöneticisi: Prof. Dr. Ayşen Tezcaner
Ortak Tez Yöneticisi: Doç. Dr. Can Özen

Ocak 2023, 133 sayfa

Günümüzde modern teknolojideki ilerlemelere rağmen yara bakımı, dünyada yaygın bir şekilde sargı bezi, dikiş, cerrahi zımba kullanımı gibi geleneksel yöntemlere dayanmaktadır. Çeşitli yaraların bakımında bu yöntemler ekonomik tedaviler sunsa da yara iyileşme sürecini kolaylaştıracak kolay ve etkili bir çözüm sağlamakta yetersiz kalmaktadır. Yaraların daha hızlı ve güvenilir bir şekilde bakımını sağlamak, basit ancak çok fonksiyonlu ve farklı yara tiplerine uygun kapsamlı bir tasarımsal yaklaşım gerektirmektedir. Bu çalışmada çok fonksiyonlu, iki tabakalı bir yara örtüsünün geliştirilmesi üzerinde çalışılmıştır; polidopamin kaplı asimetrik polikaprolakton membran (PCL-DOP) ve *Liquidambar orientalis* Mill. bitkisinden elde edilen sıgla yağı içeren hidroksietil kitosan (HECS)-karagenan (kC) temelli hidrojel (HECS-kC). PCL-DOP membran çözgen olmayan çözücü ile indüklenmiş faz ayrımı yöntemi ile hazırlandıktan sonra polidopamin kaplanmış ve bakteri geçişine karşı çok etkili bir bariyer özelliği gösterirken iyi mekanik ve yapışkanlık özellikleri yanında aynı zamanda uygun seviyede oksijen ve su buharı geçirgenliği göstermiştir. Diğer taraftan, sıgla yağı yüklü HECS-kC hidrojel farklı pH

ortamlarında in vitro test edilerek optimize edilerek yaranın iyileşmesi ile uyumlu bir şekilde bozunabilen bir kompozisyon elde edilmiştir. Elde edilen hidrojel sıradışı bir gerdirilebilme özelliğine ek olarak uygun *ex vivo* yapışkanlık, yara akıntılarını emebilme, oksijen ve su buharı geçirgenliği yanında yüklenen sığla yağı sayesinde daha etkin antimikrobiyal ve antioksidan etkiler göstermiştir. Ayrıca sıçanlarda gerçekleştirilen tam-tabaka ekzisyonel yara modeli geliştirilen çift tabakalı yara örtüsünün yara iyileşmesini Tegaderm ve control grubuna göre anlamlı olarak kolaylaştırdığı gözlenmiştir. Bu çalışma, geliştirilen çift tabakalı yara örtüsünün basit ve etkili bir yara bakım sistemi olarak kullanılabilme potansiyeline sahip olduğunu göstermektedir.

Anahtar Kelimeler: Polikaprolakton, Kitosan, Karagenan, *Liquidambar orientalis* Mill., Yara örtüsü

It is He who brought me forth from the womb of my mother when I knew nothing and gave me hearing, sight, intelligence and affections; that I may give thanks.

ACKNOWLEDGMENTS

I would like to express my sincere gratitude to my thesis supervisor Dr. Ayşen Tezcaner, supporting, always positive and considerate. With her dedicated supervision and guidance, I was able to put my study onto a well-planned academic structure. Her academic expertise and positive stance have always helped me to see the study through difficult times during this lengthy endeavor.

I deeply thank to my thesis committee members Dr. Ayşe Karakeçili, Dr. Dilek Keskin, Dr. İrem Erel Göktepe and Dr. Özge Erdemli for their advice and support in biannual thesis committee meetings and during my thesis defence. I greatly appreciate the Turkish Fulbright Commission for the grant (TR-VSR-2019-14) that has not only helped me to expand my academic expertise during my program in University of California, Los Angeles (UCLA) but also enabled me to have a global perspective to many cultures and contemporary issues. In addition, I thank BIOMATEN and all its staff who allowed me to utilize the facility and provided technical assistance. I would like to acknowledge Dr. Siyami Karahan and Dr. Yasin Özkabadayı for their significant contribution during animal experiments. Furthermore, I would like to express my gratitude to Dr. Can Özen for his support during my program. I also thank all my lab colleagues whom I keep in my thoughts for valuable experiences we shared together.

It was also impossible without the boundless support, consideration and immense devotion of my wife, Funda Nakipoğlu.

This work is partially funded by Scientific and Technological Research Council of Turkey under grant number TUBİTAK 222S018.

TABLE OF CONTENTS

| | |
|--------------------------------|------|
| ABSTRACT..... | v |
| ÖZ..... | vii |
| ACKNOWLEDGMENTS | x |
| TABLE OF CONTENTS..... | xi |
| LIST OF TABLES | xii |
| LIST OF FIGURES | xiii |
| LIST OF ABBREVIATIONS..... | xx |
| | |
| 1 INTRODUCTION | 1 |
| 2 MATERIALS AND METHODS..... | 17 |
| 3 RESULTS AND DISCUSSION | 37 |
| 4 CONCLUSION..... | 93 |
| | |
| REFERENCES | 95 |
| APPENDICES | 125 |
| CURRICULUM VITAE..... | 133 |

LIST OF TABLES

| | |
|---|----|
| Table 1.1 Biomaterial based commercial wound dressing products | 2 |
| Table 1.2 Bioadhesives with antimicrobial properties through the addition of antimicrobial agents..... | 7 |
| Table 3.1 Korsmeyer-Peppas values of hydrogels with HECS:kC ratios of 1:1 and 1:2 for different pH environments..... | 76 |

LIST OF FIGURES

| | |
|---|----|
| Figure 2.1. Scheme of hydroxyethylation of chitosan | 18 |
| Figure 3.1. FTIR spectra of CS and HECS. | 38 |
| Figure 3.2. XRD analysis for CS and HECS. | 39 |
| Figure 3.3. Porosity of hydrogel of different HECS:kC ratios (2:1, 1:1, 1:2). * denotes significant difference between groups ($p < 0.05$, $n=3$). | 40 |
| Figure 3.4. Scanning electron micrographs of hydrogels with HECS:kC ratios of 2:1, 1:1, 1:2 (w/w)..... | 41 |
| Figure 3.5. Swelling equilibria of HECS:kC hydrogels with 2:1 (a) 1:1 (b) 1:2 (c) ratio in 37°C at different pH ($n=3$). (d) Swelling ratios of the hydrogels after 24 hours of incubation at 37°C. * denotes significant difference between the groups ($p < 0.05$, $n=3$). | 43 |
| Figure 3.6. Remaining dry weights after 14 days with respect to the initial dry weights of incubation in PBS with varying pH. Significant differences between the groups are shown by * ($p < 0.05$, $n=3$). | 45 |
| Figure 3.7. Oxygen permeability of HECS-kC hydrogels. * denotes significant difference between the groups ($p < 0.05$, $n=3$)..... | 46 |
| Figure 3.8. Water vapor transmission rate of the HECS-kC hydrogels. No significant difference was observed between the hydrogel groups. * denotes significant difference between the control and hydrogel groups ($p < 0.05$, $n=3$)..... | 47 |
| Figure 3.9. Typical compressive stress-strain curves of HECS-kC hydrogels with ratios of 1:1 and 1:2. Inset figure show trendlines for calculation of Young's modulus..... | 49 |
| Figure 3.10. Compressive moduli of HECS-kC hydrogels with ratios 1:1 and 1:2. * denotes significant differences between the groups ($p < 0.05$, $n=3$). | 49 |
| Figure 3.11. Typical tensile stress-strain curves of HECS-kC hydrogels with ratios of 1:1 and 1:2. Inset figure show trendlines for calculation of Young's modulus.. | 50 |

| | |
|---|----|
| Figure 3.12. Elastic moduli (right) and tensile strength at 140% strain (left) for HECS-kC hydrogels with ratios 1:1 and 1:2. * denotes significant differences between the groups ($p < 0.05$, $n=3$)..... | 51 |
| Figure 3.13. Rheological properties of hydrogels with HECS:kC ratios of 2:1, 1:1 and 1:2 in terms of storage and loss moduli versus angular frequency (left), temperature effect on G' & G'' of the hydrogels between 20-60 °C (right). | 52 |
| Figure 3.14. Temperature effect on the viscosity of the hydrogels with HECS:kC ratios of 2:1, 1:1 and 1:2 between 20-60 °C..... | 53 |
| Figure 3.15. <i>Ex vivo</i> adhesion strength of hydrogels with HECS:kC ratios of 1:1 and 1:2. * denotes significant difference between the groups ($p < 0.05$, $n \geq 3$). | 55 |
| Figure 3.16. Representative images of <i>S. aureus</i> agar-plates treated with blank and storax loaded hydrogels with different HECS:kC ratios. 2:1, 1:1 and 1:2 represents the HECS:kC ratio in the hydrogels and S+ represents the hydrogels loaded with storax (1 mg/mL) while S- represents the blank hydrogels..... | 56 |
| Figure 3.17. Antimicrobial activity of blank and storax loaded hydrogels with different HECS:kC ratios against <i>S. aureus</i> . 2:1, 1:1 and 1:2 represents the HECS:kC ratio in the hydrogels and S+ represents the hydrogels loaded with storax (1 mg/mL) while S- represents the blank hydrogels (* $p < 0.05$, $n=3$). | 57 |
| Figure 3.18. FTIR spectra of PCL and PCL-DOP..... | 58 |
| Figure 3.19. Water vapor transmission rate of asymmetric PCL membranes (* $p < 0.05$, $n=6$). | 59 |
| Figure 3.20. Oxygen permeability of asymmetric PCL-DOP membrane (* $p < 0.05$, $n=3$)..... | 61 |
| Figure 3.21. Representative tensile stress-strain curve of PCL-DOP membrane. The inset figure shows the representative stress-strain curve used to compute the elastic modulus. | 62 |
| Figure 3.22. <i>In vitro</i> adhesion strength of asymmetric PCL and PCL-DOP membranes on hydrogels with HECS:kC ratios of 1:1 and 1:2. * denotes significant differences ($p < 0.05$, $n \geq 3$). | 63 |

| | |
|---|----|
| Figure 3.23. Microbial penetration from PCL-DOP membrane.* denotes significant difference between the groups ($p < 0.05$, $n=3$). | 64 |
| Figure 3.24. Water contact angle analysis for PCL and PCL-DOP membranes. Inset figure shows representative contact angles (* $p < 0.05$, $n=3$). | 66 |
| Figure 3.25. Porosity of PCL and PCL-DOP membranes. * denotes significant difference between the groups ($p < 0.05$, $n=3$). | 67 |
| Figure 3.26. Scanning electron microscopy images of PCL and PCL-DOP membranes. | 68 |
| Figure 3.27. Cytocompatibility of storax on L929 mouse fibroblast cells. * denotes significant difference between the groups ($p < 0.05$, $n=3$). | 69 |
| Figure 3.28. Cytocompatibility of blank and storax loaded HECS:kC hydrogels. * denotes significant difference between the groups ($p < 0.05$, $n=3$). | 70 |
| Figure 3.29. Relative cell viability of L929 fibroblasts treated with H_2O_2 in the presence of HECS:kC and HECS:kC+Storax. * denotes significant difference between the groups ($p < 0.05$, $n=5$). | 72 |
| Figure 3.30. Morphological analysis of L929 fibroblasts L929 fibroblasts treated with H_2O_2 in the presence of HECS:kC and HECS:kC+Storax. (a-d) Inverted phase contrast microscopy images obtained on day 7; (e-h) confocal laser scanning microscopy images obtained on day 14. Cells treated with; only 250 μM H_2O_2 (a, e), 250 μM H_2O_2 and HECS:kC (b, f), 250 μM H_2O_2 and HECS:kC+Storax (c, g) and 0 μM H_2O_2 (d, h). Red arrow heads show globular cells under excessive oxidative stress. | 74 |
| Figure 3.31. Cell spreading areas of L929 fibroblasts treated with H_2O_2 in the presence of HECS:kC and HECS:kC+Storax. * denotes significant difference between the groups ($p < 0.05$, $n>50$). | 74 |
| Figure 3.29. Storax release profiles from the hydrogels with HECS:kC ratios; 1:1 (left) and 1:2 (right) in different pH environment ($n \geq 3$). | 77 |
| Figure 3.30. Scanning electron microscopy images of storax loaded hydrogels (HECS:kC ratio of 1:1) after 10 days of storax release in PBS at 37°C. | 77 |

Figure 3.31. Application of HECS:kC/PCL-DOP bilayer wound dressing on rat full-thickness skin defect model. Photographs were taken on day 0 (a, b) and day 10 (c, d)..... 79

Figure 3.32. Representative images of the gross appearance of full-thickness skin defects over 10 days. 79

Figure 3.33. Wound closure rate at different periods of post wounding. * denotes significant difference between the groups ($p < 0.05$, $n=7$). 80

Figure 3.34. Histological evaluation of Masson’s trichrome stained full-thickness skin defect representative tissue samples on day 5. (a) Control, (b) Tegaderm, (c) HECS:kC hydrogel, (d) Storax loaded HECS:kC hydrogel. Scale bar: 250 μm . (a) Granulation tissue in defect area (double headed black arrow), normal skin tissue-defect border (double headed green arrow), epidermal thickening on defect edge (black arrow), scab formation (white asterix). (b) Granulation tissue in defect area (double headed black arrow), normal skin tissue-defect border (double headed green arrow), epidermal thickening on defect edge (black arrow), insufficient epithelialization (arrow head). (c) Granulation tissue in defect area (double headed black arrow), normal skin tissue-defect border (double headed red arrow), partial epithelialization and epidermal thickening (black arrow), insufficient epithelialization at the center of the defect (arrow head). (d) Granulation tissue in defect area (double headed black arrow), normal skin tissue-defect border (double headed green arrow), sufficient epithelialization on defect area and subsequent epidermal thickening (black arrow)..... 81

Figure 3.35. Histological evaluation of Masson’s trichrome stained full-thickness skin defect representative tissue samples on day 10. (a) Control, (b) Tegaderm, (c) HECS:kC hydrogel, (d) Storax loaded HECS:kC hydrogel. Scale bar: 250 μm . (a) Thick granulation tissue (double headed green arrow), normal skin-defect border (double headed black arrow), partial epithelialization and epidermal thickening (black arrow), insufficient epithelialization at the center of the defect (arrow head), neovascularization (red arrows), normal skin (red asterix). (b) Granulation tissue in defect area (double headed black arrow), normal skin (red asterix), insufficient

epithelialization and epidermal thickening (red arrow), insufficient epithelialization at the center of the defect (arrow head), neovascularization (black arrow). (c) Granulation tissue in defect area (double headed black arrow), normal skin (red asterix), type-1 collagen remodeling areas (black arrow), epidermis and epithelialization similar to normal skin (blue arrow). (d) Granulation tissue in defect area (double headed black arrow), type-1 collagen remodeling in granulation tissue (red asterix), normal skin (white asterix), epidermis and epithelialization similar to normal skin (black arrow)..... 83

Figure 3.36. Control group, day 5. Hematoxylin-eosin stained full-thickness skin defect representative tissue samples. Scale bar: (a) 250 μm , (b) 50 μm . (a) Normal skin-defect border (double headed black arrow), normal skin (double headed green arrow), scab formation (asterix), insufficient epithelialization (black arrow), neovascularization (arrow head). (b) 40X view the marked section; neutrophil granulocytes (black arrow), macrophages (arrow head), dermal fibroblasts (red arrow)..... 84

Figure 3.37. Tegaderm group, day 5. Hematoxylin-eosin stained full-thickness skin defect representative tissue samples. Scale bar: (a) 250 μm , (b) 50 μm . (a) Normal skin-defect border (double headed black arrow), scab formation (double headed green arrow), normal skin (asterix), partial epithelialization (green arrow), granulation tissue (double headed blue arrow), neovascularization (black arrow). (b) 40X view the marked section; neutrophil granulocytes (yellow arrow), macrophages (red arrow head)..... 84

Figure 3.38. HECS:kC hydrogel group, day 5. Hematoxylin-eosin stained full-thickness skin defect representative tissue samples. Scale bar: (a) 250 μm , (b) 50 μm . (a) Normal skin-defect border (red arrow), granulation tissue (double headed white arrow), muscle tissue (yellow asterix). (b) 40X view the marked section; neutrophil granulocytes (red arrow), macrophages (yellow arrow), neovascularization (green arrow head). 85

Figure 3.39. Storax loaded HECS:kC hydrogel group, day 5. Hematoxylin-eosin stained full-thickness skin defect representative tissue samples. Scale bar: (a) 250

µm, (b) 50 µm. (a) Normal skin-defect border (white arrow), granulation tissue (double headed black arrow), scab formation (arrow head), partial epithelialization and epidermal thickening (black arrow), muscle tissue (asterix). (b) 40X view the marked section; neutrophil granulocytes (black arrow), macrophages (arrow head), dermal fibroblasts (green arrow).86

Figure 3.40. Control group, day 10. Hematoxylin-eosin stained full-thickness skin defect representative tissue samples. Scale bar: (a) 250 µm, (b) 50 µm. (a) Normal skin (asterix), partial epithelialization and epidermal thickening (black arrow), insufficient epithelialization at the center of the defect (yellow arrow), neovascularization (red arrow). (b) 40X view the marked section; neutrophil granulocytes (yellow arrow), macrophages (green arrow head), neovascularization (red arrow).87

Figure 3.41. Tegaderm group, day 10. Hematoxylin-eosin stained full-thickness skin defect representative tissue samples. Scale bar: (a) 250 µm, (b) 50 µm. (a) Normal skin-defect border (red arrow), partial epithelialization (blue arrow), granulation tissue (double headed black arrow), neovascularization (black arrow). (b) 40X view the marked section; neutrophil granulocytes (green arrow), macrophages (red arrow head), dermal fibroblasts (yellow arrow).87

Figure 3.42. HECS:kC hydrogel group, day 10. Hematoxylin-eosin stained full-thickness skin defect representative tissue samples. Scale bar: (a) 250 µm, (b) 50 µm. (a) Normal skin (asterix), granulation tissue (double headed black arrow), sufficient epithelialization (black arrow). (b) 40X view the marked section; macrophages (yellow arrow), neovascularization (red arrow), dermal fibroblasts (green arrow head).89

Figure 3.43. Storax loaded HECS:kC hydrogel group, day 10. Hematoxylin-eosin stained full-thickness skin defect representative tissue samples. Scale bar: (a) 250 µm, (b) 50 µm. (a) Normal skin (asterix), granulation tissue (double headed black arrow), sufficient epithelialization (black arrow). (b) 40X view the marked section; macrophages (yellow arrow), neovascularization (red arrow), dermal fibroblasts

(green arrow head), hair follicles (asterix), normal skin appearance of epidermis as a result re-epithelialization (double headed white arrow). 89

Figure 3.44. Histological scoring of tissue samples based on (a) epithelialization, (b) inflammation, (c) fibroplasia, (d) neovascularization, (e) collagen density, (f) collagen thickness, (g) collagen arrangement. Lower scores indicate better outcomes. Solid colored bars indicate parameters obtained on day 5. Horizontally striped bars indicate parameters obtained on day 10. White dots on bars are individual data points, same letters show significant differences ($p < 0.05$). 91

LIST OF ABBREVIATIONS

| | |
|-------------------|--|
| ASTM | American Society for Testing and Materials |
| CS | Chitosan |
| CF | Chloroform |
| DCM | Dichloromethane |
| dH ₂ O | Distilled water |
| DAPI | 4',6-diamidino-2-phenylindole |
| DMEM | Dulbecco`s Modified Eagle Media |
| DMF | Dimethylformamide |
| DOP | Dopamine |
| FDA | Food and Drug Administration, USA |
| FTIR | Fourier-transform infrared spectroscopy |
| HECS | Hydroxyethyl chitosan |
| kC | Kâppa-carrageenan |
| M _n | Number-Average Molecular Weight |
| NMR | Nuclear Magnetic Resonance |
| SEM | Scanning Electron Microscopy |
| THF | Tetrahydrofuran |
| PBS | Phosphate buffered saline |
| PCL | Poly(ϵ -caprolactone) |
| PDA | Polydopamine |
| PEC | Polyelectrolyte complexation |
| PVA | Polyvinyl alcohol |
| XRD | X-ray Diffraction |

CHAPTER 1

INTRODUCTION

Intact skin is a barrier that covers the human body to help the maintenance of homeostasis by regulating heat and fluid loss. Upon injury, this barrier slits open and, depending on the size of the wound, it loses the ability to modulate heat and moisture loss. Even worse, the body becomes exposed to microbial infections, which may lead to various health issues. Wounds are categorized as pressure ulcers, venous leg ulcers, diabetic foot ulcers, traumatic wounds and surgical wounds. The basic treatment of these wounds focuses on two main points; preventing bacterial infection and absorption of the exudates off from the wound site (Vowden & Vowden, 2017). Additionally, keeping the wound site moist is vital to facilitate a rapid recovery of the damaged tissue.

Wound dressing materials used traditionally, such as gauze and tulle, cover the wound site and allow gas exchange. However, they may adhere to the wound site causing further damage when removed and fall short in the ability to facilitate the healing of complicated wounds. Hydrogels, on the other hand, possess promising features that can be utilized to develop a wound dressing that can address the above-mentioned issues. Hydrogels are composed of 90 wt% water and 10 wt% natural or synthetic polymers which can be functionalized in accordance with the type of wound. High water content of hydrogels keeps the wound site moist enabling a faster recovery while absorbing the necrotic tissues and foreign materials (Sahiner et al., 2016). The obvious superiority of hydrogel based wound dressings encouraged many companies to develop clinical products (**Table 1.1**) as the global market (including non-hydrogel wound dressings) is expected to generate \$13.4 billion revenue by 2030 (Prescient & Strategic Intelligence, 2022).

Table 1.1 Biomaterial based commercial wound dressing products

| Base Polymer | Brand Name | Company |
|-----------------------|---|--------------------------------|
| Alginate | Nu-Gel® | Systagenix |
| | Tegagel® | 3M GmbH |
| | Algosteril® | 4M Medical GmbH |
| | Curasorb® | Medtronic |
| | Sorbsan® | B. Braun Melsungen AG |
| | Comfeel Plus Flexible® | Coloplast AG |
| | Kendall™ Hydrocolloid Dressing | Medtronic |
| Chitosan | KytoCel® | MasterCare Medical GmbH |
| | Chitoderm® plus | Trusetal Verbandstoffwerk GmbH |
| Collagen | CellerateRX® | Wound Care Innovations LLC |
| | Regenecare® Wound Gel | MPM Medical Inc. |
| | Wun'Dres® | Coloplast AG |
| | Biobrane® | Smith & Nephew |
| | CollaSorb® | Paul Hartmann AG |
| | Fibracol® | Acelity |
| | Medifil® | Human Bio Science, Inc. |
| Synthetic | Stimulen™ | Southwest Technologies, Inc. |
| | FlexiGel ® | Smith & Nephew |
| | Oakin® | Amerigel |
| Hyaluronic Acid | AquaClear® | Paul Hartmann AG |
| | Hyalofill® | Anika Therapeutics |
| | Hyalosafe® | Anika Therapeutics |
| PVA/ Chitosan | Hyalo Regen | Fidia Pharma GmbH |
| | Biatain Ibu™ (0.5 mg·cm ⁻¹ ibuprofen) | Coloplast AG |
| Alginate/ Collagen | Regenecare® Wound Gel (2% lidocaine) | MPM Medical, Inc. |

There are many commercially available hydrogel-based bioadhesives, both of biological and synthetic origin (Bal-Ozturk et al., 2021). Biological bioadhesives such as fibrin glue (Ge & Chen, 2020) are biocompatible; however, they suffer from low mechanical properties and limited adhesion to wet surfaces. On the other hand, synthetic bioadhesives such as cyanoacrylate and polyethylene glycol (PEG) based

bioadhesives (Pinnaratip et al., 2019) have great mechanical properties but they may cause serious inflammatory response due to their toxic degradation products. PEG is biocompatible and it is approved by the Food and Drug Administration (FDA). However, it is very hydrophilic and it may swell up to four times of its original size and cause problems of compression, e.g. of sensitive tissues such as nerves (Ge & Chen, 2020). Designing new bioadhesives with multiple functionalities including high adhesion, biocompatibility, biodegradability, antimicrobial properties, capability to regenerate damaged tissue is essential.

Sealing wound areas as quickly as possible through the use of bioadhesive can provide better medical outcomes (Tavakoli et al., 2020a). Immunocompromised patients, however, might require certain drugs (Zehtabchi et al., 2012), which can be delivered locally by bioadhesives (Coccolini et al., 2021). Microbial infections in wound sites can cause serious problems and negatively affect the healing processes (Daeschlein et al., 2013). Therefore, wound dressing materials should be able to protect wounds from infections (Zhu et al., 2021).

Bioadhesive wound dressing with antimicrobial properties can be made by three ways in general; through the loading of antimicrobial drugs (1), through the incorporation of nanomaterials (2), or through the use of polymers that are inherently antimicrobial (3).

Antimicrobial drugs can be directly loaded into bioadhesives to physically trap drug molecules in polymeric matrices to be released by diffusion. Secondly, antimicrobial drugs can be chemically bound to polymeric matrices and they can be released upon an external stimulus (Liang et al., 2019)(Kumar et al., 2014) or through the degradation of polymeric matrices dependent (Xu et al., 2017)(Sumitha et al., 2021). Among examples, antimicrobial peptides were covalently incorporated into a gelatin based hydrogel (Annabi et al., 2017) and ciprofloxacin were physically embedded into a chitosan based film (García et al., 2017).

Use of nanomaterials in bioadhesive hydrogels can provide simultaneous effects, both advantageous and disadvantageous. Until now, metal nanoparticles (Jia et al., 2021), micelles (Khalil et al., 2020), liposomes (Hurler et al., 2012), carbon nanotubes (Ren et al., 2021) were used to provide antimicrobial properties to hydrogels. Application of nanomaterials in hydrogels can also enable the local delivery of compounds which have impaired mobility in aqueous environments due to their hydrophobic nature. Curcumin, for example, were loaded into Pluronic based micelles and loaded into chitosan based bioadhesive (Qu et al., 2018). Another example includes the use of metal nanoparticles (zinc) for both antimicrobial activity and secondary crosslinking of carrageenan based polymeric matrix (Tavakoli et al., 2020a).

When polymers with inherent antimicrobial properties were used to prepare hydrogel, the necessity for antimicrobial drugs or nanomaterials might disappear (Watson et al., 2016)(Berg et al., 2021). The most well-known antimicrobial polymer is derived from insect chitin, which is acetylated to obtain easier dissolved chitosan. Other examples include cellulose (H. Tan et al., 2021), dextran (Q. Yang et al., 2021), hyaluronic acid (S. Liu et al., 2020) and polylysine (R. Wei et al., 2021). The first such example of hydrogel was developed by utilizing two polymers polydextran aldehyde and polyethylenimine. While these two polymers readily formed Schiff base to form a hydrogel, remaining uncoupled functional groups, especially those of polyethylenimine, enabled contact dependent antimicrobial activity due to the densely packed positively charged atoms on the surface of the hydrogel (Giano et al., 2014). Such cationic groups have seen a tremendous interest over the years to develop antimicrobial wound dressing materials (Q. Yang et al., 2021).

Recent attempts to develop innovative wound dressing bioadhesives with antimicrobial properties led to the exploitation of multiple mechanisms. For example

a recent study took the advantage of both nanomaterials and inherently antimicrobial polymers to have synergistic antimicrobial activity (Yu et al., 2022).

Wound dressing bioadhesives have been developed using natural and synthetic polymers, antimicrobial drugs or peptides and nanomaterials. While some of the developed bioadhesives were shown to perform even better than some commercial products, others were hampered by mechanical weaknesses or cytotoxicity (**Table 1.2**) (Y. Yang et al., 2022). Antimicrobial agents incorporated to bioadhesives can have negative effect on materials properties and biocompatibility. One approach to minimize such disadvantages were the employment of metal ions in polymeric matrices instead of metal nanoparticles. Zinc ions, for example, were used as an antimicrobial agent in a polyethylene glycol based hydrogel while enhancing the mechanical stiffness of the hydrogel through coordination with catechol groups in the polymeric matrix (Y. Yang et al., 2022).

Antimicrobial drugs loaded into polymeric matrices depend on diffusion mechanism for release and their release profiles are usually affected by surface modification of bioadhesives. Chitosan films were dendronized to increase adhesive strength, however ciprofloxacin release was drastically slowed in the first six hours (García et al., 2017). Excessively slow antibiotic release should be avoided as the antimicrobial activity of such wound dressings would mainly be based on the concentration of antibiotics released in the vicinity of wounds (Gimeno et al., 2015). Achieving minimum inhibitory concentration as quickly as possible can inhibit any biofilm formation in the wound area and greatly facilitate the healing process. Other modifications may cause the opposite effect, increasing antimicrobial agent release while decreasing adhesion. For instance, usnic acid release was improved by the addition of polyvinylpyrrolidone into carboxymethylcellulose polymeric matrix. However, this was achieved at the cost of decreased adhesion strength due to the depletion of functional groups on carboxymethylcellulose that would interact with tissues otherwise (Pagano et al., 2019).

Antimicrobial drugs' physicochemical properties may have critical importance in terms of mechanical properties of hydrogels even at low concentrations. Negatively charged cefuroxime axetil, for example, was shown to decrease the adhesive strength of chitosan, which has positively charged groups whereas increasing adhesion when used together with hydroxypropyl methylcellulose (Timur et al., 2019). Similarly, porogen agents can increase the burst release of antimicrobials to have a strong initial antimicrobial effect while having a negative impact on other material properties (Timur et al., 2019).

Alternative methods used to minimize the disadvantages of incorporating antimicrobial agents into bioadhesive wound dressings include the use of antimicrobial peptides. These peptides are designed to possess a rich sequence of cationic aminoacids to interact with and disrupt bacterial membrane without having any significant cytotoxicity or negative effect on the mechanical properties of wound dressing materials (Lei et al., 2019)(Annabi et al., 2017)(Ageitos et al., 2017; Mercer & O'Neil, 2020). One such antimicrobial peptide example included rich tryptophan and arginine sequences and it was incorporated into polyethylene glycol and chitosan based hydrogel to demonstrate good antibacterial activity (L. Huang et al., 2019).

In summary, antimicrobial agent incorporation is easy and quick method to develop antimicrobial wound dressing materials, however, this approach necessitates a careful assessment of all the components chemically or physically interacting with each other. Another important aspect of antimicrobial loaded wound dressings is that the antimicrobial activity must remain throughout the treatments, which means that the antimicrobial agent release should continue from the wound dressing and remain at minimum inhibitory concentration (S. Liu et al., 2020). Failing to achieve this can provide a favorable environment for drug-resistant bacterial strains, which can seriously complicate the treatment (B. Li & Webster, 2018). Antimicrobial agents normally used topically without any toxicity may cause adverse effects when they

come into contact with exposed tissues and should be meticulously assayed on effectiveness-dose-toxicity axis (Pagano et al., 2019)(Mou et al., 2019).

Table 1.2 Bioadhesives with antimicrobial properties through the addition of antimicrobial agents.

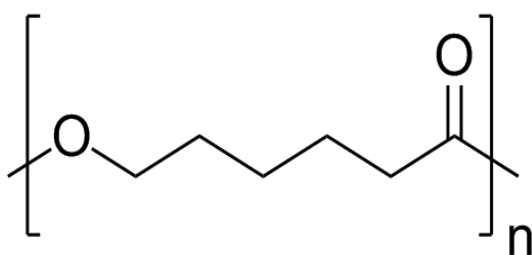
| No | Composition | Outcomes | Ref. |
|----|--|--|---------------------------|
| 1 | PEG200, β -cyclodextrin, silk sericin; 2.5% Gentamicin | Three-point-bend test on bovine rib demonstrated better results with less inflammation. Strong antibacterial activity against <i>E. coli</i> , <i>S. aureus</i> , <i>P. aeruginosa</i> . Rat sternal closure model for 7 days demonstrated promising results. | (Balcioglu et al., 2022) |
| 2 | Modified hyaluronic acid, azide conjugated carboxymethylcellulose (CMC); 0.2% Amoxicillin | Peeling test on porcine skin demonstrated an adhesive strength of ~500 kPa. Effective antibacterial activity against <i>E. coli</i> , <i>S. aureus</i> for 2 days <i>in vitro</i> . Performed better than a commercial product in mice full-thickness skin defect model. | (Mao et al., 2022) |
| 3 | Polyethylene glycol (PEG) monomethyl ether modified glycidyl methacrylate functionalized chitosan, methacrylamide dopamine; 0.18% Zinc ions | Lap shear test on porcine skin showed good adhesion. Antimicrobial activity against <i>E. coli</i> , Methicillin resistant <i>S. aureus</i> (MRSA). Achieved quicker healing <i>in vivo</i> compared to a commercial product. | (Y. Yang et al., 2022) |
| 4 | Ferric iron/Tannic acid-cellulose; 0.2% Tetracycline | Probe pull test conducted on porcine skin demonstrated mild adhesion performance. Strong antibacterial activity versus <i>E. coli</i> , <i>S. aureus in vitro</i> . Poor cytocompatibility <i>in vitro</i> . | (Y. Chen et al., 2022) |
| 5 | Quaternized carboxymethyl chitosan, oxidized hyaluronate; 2,2,6,6-tetramethylpiperidine-1-oxyl (15% of molar concentration of aldehyde groups) | Weak adhesive performance on porcine skin. Superb antimicrobial activity against <i>E. coli</i> , <i>S. aureus</i> . Highly biocompatible based on <i>in vitro</i> NIH 3T3 cells and <i>in vivo</i> rat wound model test results. | (Q. Wei et al., 2022) |
| 6 | Hydroxypropyl methylcellulose, Pluronic F127, Pluronic F68, benzalkonium chloride; 1% Itraconazole | Residence time and probe pull tests on cow vaginal tissue exhibited good adhesion. Rat candidiasis model <i>in vivo</i> showed effective decrease in fungal viability. | (Permana et al., 2021) |
| 7 | Silk fibroin, indocyanine green; 0.005% Vancomycin | Tensile test on mice skin demonstrated mild adhesion. Strong antimicrobial activity against MRSA both <i>in vitro</i> and <i>in vivo</i> . | (Urie et al., 2021) |
| 8 | Gelatin, snail slime; 4.76 w/w Fluconazole | Adhesion strength was analysed by rheometry on pig ear tissue. Enabled effective use of fluconazole against many fungal pathogens <i>in vitro</i> . Promising results in rat candidiasis model. | (di Filippo et al., 2021) |
| 9 | Polyvinylpyrrolidone (PVP) K-90 and propylene glycol with CMC; 1% Zingiber cassumunar Roxb extract | Probe pull test on rat skin demonstrated mild adhesiveness. <i>S. aureus</i> infected rat skin wound model yielded positive outcomes. | (Rahman et al., 2021) |
| 10 | Oxidized pectin coated chitosan nanofibers; Cationic amphiphilic antimicrobial peptides (loaded as 1 mg/mL on nanofiber membrane) | Probe pull on porcine esophagus tissue demonstrated mild adhesion. pH-responsive antimicrobial release enabled strong activity against <i>S. gordonii</i> and <i>S. mutans</i> . <i>In vitro</i> cytocompatibility tests on human oral keratinocytes and MC3T3-E1 cells showed good results. | (Boda et al., 2020) |
| 11 | CMC, Polyvinylpyrrolidone (PVP) K90, bentonite nanoclay; 3% Red onion extract | Probe pull test was conducted on pig skin and showed mild adhesion. Demonstrated antioxidant activity along with antimicrobial activity against <i>E. faecalis</i> , <i>S. aureus</i> , <i>S. epidermidis</i> , <i>L. innocua</i> . Considerable cytotoxicity on HaCaT cell line. | (Pagano et al., 2020) |
| 12 | <i>Avena sativa</i> based biopolymer and polyvinyl alcohol (PVA) with hydroxyethylcellulose; 0.3% Bacitracin zinc | Probe pull test on rabbit intestinal tissue demonstrated good adhesion. Antimicrobial activity was shown on a variety of bacterial species such as <i>E. coli</i> , <i>M. luteus</i> , <i>S. aureus</i> , <i>P. aeruginosa</i> . <i>In vivo</i> experiments of rat wound model also demonstrated good results. | (e) Hosary et al., 2020) |

In the past few years multi-layered hydrogel based wound dressings have drawn attention due to the possibility of incorporation of layers with different features and purposes. There are many recent studies focusing on the development of hydrogel based multi-layer wound dressings. In one recent study, a fifteen bilayered chitosan-alginate polyelectrolyte film carrying pirfenidone was developed for surgical wound healing (Mandapalli et al., 2016). Their *in vivo* results showed that the anti-fibrotic agent pirfenidone gradually decreased TGF- β expression and accelerated the wound contraction. In another study, chitosan was crosslinked with genipin and it was brought together with partially oxidized polysaccharide of *Blettita stritata* to obtain a wound dressing with quicker gelation times, higher water retention capacity in addition to higher L929 proliferation compared to chitosan crosslinked only with genipin (Ding et al., 2017). Their *in vivo* results demonstrated mature epidermization in mice during 7 days. Zhou et al. developed a methacrylated gelatin based wound dressing in order to decrease the reoccurrence of bacterial infection. They have encapsulated antimicrobial and fluorescent vesicles that respond to the microbiota of the wound site and release the loaded antimicrobials only when specific toxins are secreted from the pathogenic bacteria (Zhou et al., 2018). Another bilayered wound dressing composed of polycaprolactone and polylactic acid was developed to facilitate both wound healing and skin regeneration. The two electrospun layers were loaded with vitamin E to enhance angiogenesis. Their results showed good *in vitro* cell attachment and proliferation as well as quicker wound healing in scratch assay (Zahid et al., 2019). Another gelatin and polycaprolactone based bilayered membrane developed for wound healing purposes was obtained by a novel two-step spin coating combined with in situ crosslinking to generate a biocompatible polycaprolactone/gelatin bottom layer and an antibacterial polycaprolactone/2-(methacryloyloxy) ethyl] trimethylammonium top layer (Y. Huang et al., 2019). Their *in vitro* tests showed promising antibacterial potency and biocompatibility. Contardi et. al. developed a transparent wound dressing composed of polyvinylpyrrolidone/hyaluronic acid top layer and polyvinylpyrrolidone bottom layer releasing an antiseptic and an antibiotic. They tested the bilayer wound

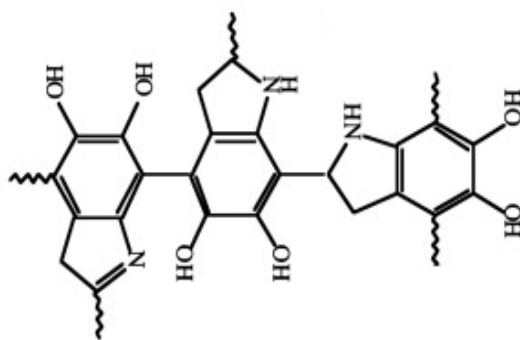
dressing's *in vitro* antibacterial performance and reported 3 log reduction in colony count. In the *in vivo* tests the bilayer wound dressing has been 50% reabsorbed in the wound site in 24 hours. (Contardi et al., 2019).

Similar to the hydrogels, asymmetrical polymeric membranes have been demonstrated to be promising wound dressings for the treatment of skin wounds. With their asymmetrical structure, they present the characteristics required from an ideal wound dressing. This type of membrane contains a dense surface skin layer and interconnected micropores designed to protect the wound from physical damage and microorganism penetration while the sponge-like sublayer allows the adsorption of fluids, the drainage of the wound by capillary and the facilitation of tissue regeneration (Morgado et al., 2014a).

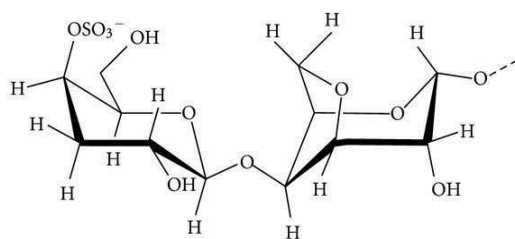
Whether it may be a hydrogel or membrane, choice of the polymer is very important in the development of a wound dressing. Many studies have focused on the utilization of natural or synthetic polymers either alone or as blends. Among these are alginate, collagen, chitosan, hyaluronic acid, pullulan, cellulose, gelatin, pectin, keratin, silk fibroin, polyurethane-dextran, cellulose acetate (Mogoşanu & Grumezescu, 2014). Although these wound dressing materials achieved promising successes, there are still many parameters to improve for achieving a complete healing; enhanced mechanical stability, expansion of absorbing capacity and more suitable adherence to wound site (Gupta et al., 2019). While some polymers such as hyaluronic acid perform well their advantages are vitiated by their cost. Other animal derived materials (especially collagen and gelatin) carry a risk of pathogen transmission (Koehler et al., 2018). Although some commercialized wound dressings carrying bioactive signals perform well, their costs are too high to be economically feasible for many regions around the world (Spanò et al., 2018).



Poly(ϵ -caprolactone) (PCL) is one of the widely used synthetic polymers for tissue engineering applications. It is well known by its mechanical strength, flexibility, proper degradation profile (Ehterami et al., 2018).



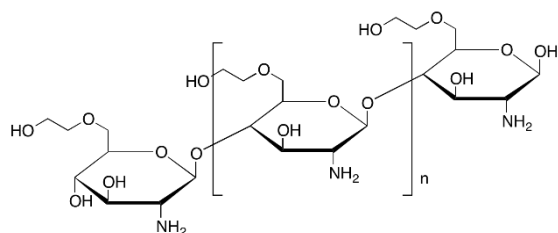
Polydopamine (PDA) has been used for mussel-inspired coating of biomaterials recently. PDA coating has advantages in terms of simplicity, inexpensiveness and low cytotoxicity (Zuppolini et al., 2020). PDA coating enables adhesion to wet surfaces (such as hydrogels) and enhances hydrophilicity.



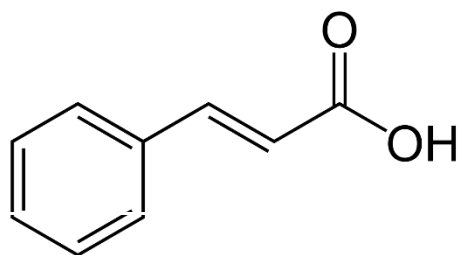
Carrageenans are a family of sulphated polysaccharides that are present in many species of red algae. They find applications in structuring and stabilizing of products' aqueous phases in numerous food products and in fat replacement. Kappa-carrageenans (kCs)

are valued due to their ability to form highly thermoreversible gels in the presence of specific cations (Hoffmann et al., 1996). kCs are also one of the most studied polysaccharides for the development of wound dressing, since, besides their inherent

biocompatibility, they show blood coagulation and immune activities that are helpful in the wound healing process (Zepon et al., 2019a).



Chitosan (CS) is a product derived from N-deacetylation of chitin in the presence of hot alkali. In chitosan, degree of deacetylation ranges from 40% to 98% and the molecular weight ranges between 5×10^4 Da and 2×10^6 Da (Hejazi & Amiji, 2003). Hydroxyethyl-chitosan (HECS) is a multifunctional derivative of chitosan with a good water-solubility. Introduction of hydroxyethyl group improves the spatial structure, weakens the intermolecular forces and increases the water-solubility thus improving the moisturizing property of HECS (Shao et al., 2015a). Excellent physical and chemical properties of HECS make this polymer to be used as antioxidant, and material for medical dressings, tissue engineering and drug carrier applications (Shao et al., 2015a).



Storax, obtained from oriental sweet gum (*Liquidambar orientalis* Mill.) tree, has been used for centuries to treat common ailments such as skin problems, coughs, and ulcers. Recently, storax has proven to be a strong antimicrobial agent even against multidrug resistant bacteria such as methicillin-resistant *Staphylococcus aureus*. It is also used for treating some skin diseases in Turkish folk medicine. Cinnamic acid is the key component in storax. (Lingbeck et al., 2015)(Sağdıç, Özkan, Özcan, & Özçelik, 2005)(Ocsel et al., 2012).

In developing a wound dressing, the way that the polymers are brought together is equally important to the choice of polymers. Polyelectrolyte complexation (PEC) employs oppositely charged polymers to electrostatically attract each other in an aqueous solution to form hydrogel (Shchipunov, 2020). In PEC, the ratio of molecular weights and concentrations of oppositely charged polyelectrolytes, their chemical structure, and the stoichiometry of their composition are the important parameters for their structural stability and integrity (Zezin & Kabanov, 1982). The phenomenon has been known since the beginning of 20th century as the spontaneous phase separation in solutions of oppositely charged polyelectrolytes and it has been widely utilized in food, pharmaceutical, agrochemical, and textile industries (Shchipunov, 2020). The concept of PEC has drawn interest in the field of biomaterials recently as well. Between the years of 2015 and 2020, there are more than 10 research articles employing PEC method to obtain hydrogels of various natural and synthetic polyelectrolytes such as chitosan (Miller et al., 2018), polyvinyl alcohol (Cutiongco et al., 2015), eudragite L100 (Varshosaz et al., 2015), xanthan (Varshosaz et al. 2015), and carbopol 934 (Varshosaz et al., 2015), carboxymethyl cellulose (Mejía et al., 2019), carboxymethyl starch (Mejía et al., 2019), alginate (Costa-Almeida et al. 2017), hyaluronic acid (Lalevée et al., 2017), methacrylated hyaluronic acid (Costa-Almeida et al., 2017), chondroitin sulfate (Costa-Almeida et al. 2017), poly(sodium 4-styrenesulfonate) (Murakawa et al. 2019), poly(diallyldimethylammonium chloride) (Murakawa et al., 2019). Particularly, chitosan and kappa-carrageenan polyelectrolyte complex hydrogel has been developed for controlled drug release platform (Kamel & Abbas, 2013) and bone tissue engineering (Patel, Zaky, et al., 2020).

1.1 Aim of the study

An effective and biocompatible wound dressing should have the ability to prevent bacterial infections (I), to minimize water loss (II), to permit O₂ and CO₂ transfer

(III), to drape well to the surface irregularities of wound (IV), to adhere to wound site mildly (V) and absorb the wound exudates. With this consideration, we aim to develop a novel storax incorporated bilayer wound dressing that will be composed of microporous, hydrophobic PCL membrane as top layer and kC -HECS hydrogel as bottom layer. With its storax-incorporated hierarchical structure, we anticipate to obtain a wound dressing that performs better than many current commercial products in terms of cost-effectiveness for the healing of acute (such as abrasions & lacerations), surgical and chronic wounds such as pressure, arterial, venous and neuropathic (diabetic) ulcers.

1.2 Hypothesis of the study

Our hypothesis was that a top layer asymmetric PCL membrane will minimize water loss and bacterial exposure of wound site while allowing gas transfer. Bottom layer hydrogel composed of HECS and kC with storax will prevent the proliferation of bacteria in wound site, absorb wound exudates, adapt to the irregular geometry of wound site and adhere only mildly to wound site. Bilayered wound dressing combined by a PDA-mediated adhesion, will facilitate the healing of acute and chronic wounds

1.3 Novelty of the study

To the best of our knowledge, this work will be the first to develop a wound dressing composed of two-layers:

- Incorporating storax to prevent bacterial infections
- PCL-DOP membrane produced via non-solvent induced phase separation

- Hydroxyethyl chitosan and kappa-carrageenan hydrogel by polyelectrolyte complexation
- PCL-DOP and HECS/kC as the whole composition for the purpose of developing a bilayer wound dressing.

CHAPTER 2

MATERIALS AND METHODS

2.1 Materials

Water (dH₂O), ~2-5 MΩ × cm at 25°C. Chitosan (CS) (medium molecular weight), Chloroethanol, Polycaprolactone (80 kDa), Potassium hydroxide (KOH), Isopropyl alcohol, Sodium chloride (NaCl), Acetic acid, Dichloromethane (DCM), Tris, Dopamine hydrochloride, Magnesium chloride (MgCl₂), Sodium hydroxide (NaOH), Sodium thiosulfate were purchased from Sigma-Aldrich (USA). Absolute ethanol, Mangan (II) sulphate monohydrate and Iodide were obtained from Merck (USA). Dulbecco's modified eagle's medium was obtained from Sartorius (Germany). Dimethylsulfoxide (DMSO) was purchased from Serva (Germany). κ-Carrageenan obtained from a local provider (food grade), confirmed with ¹H NMR analysis (**Appendix A Figure 1**) and dialyzed (12-14 kDa molecular weight cut-off) at 30 °C for 24 h to remove any impurities and very low length polymer chains. Starch and Storax of *Liquidambar orientalis* Mill. was obtained from a local provider.

2.2 Methods

2.2.1 Preparation of Hydroxyethyl chitosan

1 g CS was added to 20.0 mL KOH (45%) and stirred for 12 h at 40°C. Then, the mixture of CS was left in the refrigerator at -5°C for 48 h; after alkalization, the redundant KOH was filtered out. Afterwards, 20.0 mL chloroethanol and 10 mL isopropyl alcohol were added under continuous stirring at 85°C and incubated at this

temperature for 24 h (**Figure 2.1**). The white solid product was washed with alcohol for many times, and then, it was dried in vacuum at 40°C (Z. Li et al., 2017). Prepared hydroxyethyl chitosan (HECS) was characterized by FITR analysis in BIOMATEN-Turkey; XRD (Rigaku MiniFlex) and ¹H NMR (Bruker Biospin 300Mhz) analyses in METU Central Laboratory-Turkey (Shao et al., 2015a).

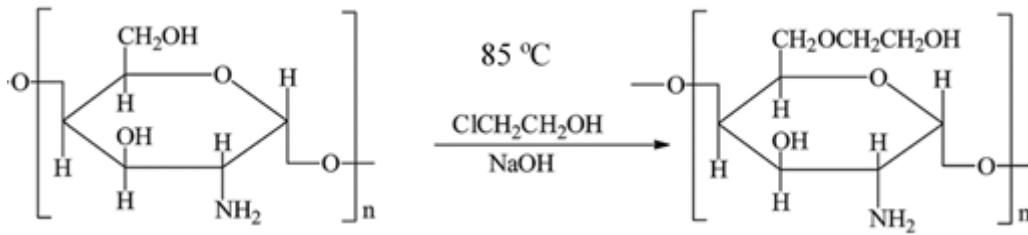


Figure 2.1. Scheme of hydroxyethylation of chitosan

2.2.2 Viscosity-Average Molecular Weight of k-Carrageenan

kC (1 gr) was dissolved in distilled water (200 mL) at 60 °C for 2 hours and dialyzed at 30 °C for 1 day with the water changed several times prior to complete freezing at -80 °C and then freeze-dried. This dialysed kC was used in all the experiments.

The molecular weight estimation of kC was conducted in Institute of Materials Science and Nanotechnology Bilkent University (UNAM) according to a previous method (Toumi et al., 2021). Briefly, dynamic viscosities of 0.1 M NaCl solution and five kC solutions with concentrations ranging from 2×10^{-3} to 1×10^{-2} mg/mL prepared in 0.1 M NaCl at 25 °C were measured with Antor Paar rheometer (USA) attached to a cone and a CP 60 plate device after confirming the Newtonian behavior. Measured dynamic viscosities were used to calculate the specific viscosities of each kC solution according to the following equation;

$$\eta_{sp} = \frac{\eta_{dyn} - \eta_0}{\eta_0}$$

where η_{sp} is specific viscosity, η_{dyn} is dynamic viscosity of the kC solutions and η_0 is the dynamic viscosity of the solution with only NaCl. After determining the specific viscosity of each kC solution, the intrinsic viscosity of kC was determined by the following equation;

$$[\eta] = \lim_{C \rightarrow 0} \frac{\eta_{sp}}{C}$$

where C is the concentration of the solutions. The average molecular weight (Mw) of kC was determined by equation of Mark-Houwink Sakurada as represented below:

$$[\eta] = K \cdot Mw^a$$

where, K and a refer to the parameters of Mark-Houwink, with K equal to $8.84 \cdot 10^{-5}$ mL/mg and a equal to 0.86, according to the literature (Vreeman et al., 1980).

Based on these, the viscosity average molecular weight of kC was estimated to be 397.46 kDa. Other studies with kC reported average molecular weights of 223 kDa (Toumi et al., 2021), 385 kDa (Fan et al., 2011)(Lefnaoui & Moulai-Mostefa, 2015), 472 kDa (Darmayanti et al., 2016).

2.2.3 Preparation of Bottom Layer of the Wound Dressing; HECS-kC Hydrogel

The hydrogel was prepared with the complexation of polyanion kC and polycation HECS. 1% kC and 1% HECS stock solutions were prepared in distilled water at 80°C. kC solution was adjusted to pH 6.5 with 5% acetic acid. After complete dissolution, both solutions were mixed to yield hydrogels with 2:1, 1:1 and 1:2 HECS:kC (wt%) ratios to yield 2% total polymer concentration. The mixed solutions

in 80°C were vortexed for 1 min and dispensed to their molds for complete complexation and gelation in room temperature for 2 hours. For storax loaded hydrogels, storax were added before gelation occurred to obtain 1 mg/mL of storax in hydrogels. Concentrations higher than 1 mg/mL disrupted the gelation process due to the hydrophobicity of storax.

2.2.4 Preparation of Top Layer of the Wound Dressing; Asymmetric PCL-DOP Membrane

PCL solutions with various concentrations (w/v) were prepared in 1 mL dichloromethane and the viscous casting solution at 4°C was immediately spread onto a glass support. Afterwards, it was immediately immersed in absolute ethanol coagulation bath for phase inversion. The membrane was stored in this closed container for 24 hours at room temperature for complete phase inversion process (Yen et al., 2009). The thickness of the membrane was adjusted to be ~200 µm. Following the fabrication, the membranes were immersed in 1 mg/mL dopamine solution (prepared in 10 mM Tris, pH 8.5) and incubated on orbital shaker at 250 rpm for 24 hours (Zuppolini et al., 2020). Afterwards, the membranes were thoroughly washed with distilled water and freeze-dried.

2.2.5 Swelling Equilibrium of HECS:kC Hydrogels

Cylindrical hydrogels were prepared at dimensions; 6 mm radius and 3 mm height for water uptake analysis. Samples were placed in PBS (pH 6.4, 7.4 and 8.4) and incubated for various time intervals (0.5, 1, 2, 3, 4, 24 h) at 37°C. At each time point, wet specimens were weighed until no weight change was observed. Following equation was used to determine the swelling equilibrium of the specimens:

Swelling (%): $[(W_w - W_i)/W_i] \times 100$

where W_w refers to the weight of the samples after awaiting in PBS for defined periods of time, and W_i is the initial weight of the samples.

2.2.6 *In vitro* Degradation Analysis of HECS:kC Hydrogels

The specimens were first immersed in bottles containing PBS with pH 6.4, 7.4 and 8.4, then placed in a water bath set at 37 °C for 2 weeks. After the predetermined incubation periods, the specimens were drained first and their wet weights were measured. Finally, dry weights were measured after freeze-drying. The structural integrity of specimens was assessed visually after incubations (Aktürk & Keskin, 2016). Change in the wet and dry weights was determined using the following formula:

Mass Loss (%) = $[(W_i - W_f)/ W_i] \times 100$

where W_i refers to the initial dry or wet weight of the samples and W_f refers to the final dry or wet weight of the samples.

2.2.7 Water Vapor Transmission Rate Analysis of HECS:kC Hydrogels and Asymmetric PCL-DOP Membrane

Water vapor transmission rates (WVTR) was determined according to the ASTM method E96-90, Procedure D. An evaporimeter was constructed in a closed chamber to prevent variations owing to ambient conditions. Briefly, the system consisted of a plastic box with an air tight cover and isothermal ambience at 35 °C, a digital hygrometer with a continuous percent relative humidity and temperature display, and a reservoir of a saturated magnesium chloride solution to maintain the relative humidity at 50±2 % after equilibration. A cylindrical, plastic permeability cup filled with 20 g of deionized water and sealed with the test sample at the top was placed inside the system. Evaporation of water through the test sample was monitored by measuring weight change in the plastic cup as an indication of daily loss of water. Then, the water vapor transmission rate (WVTR) was calculated by dividing the daily loss of water with the evaporation area of the permeability cup (L. Wang et al., 2018).

2.2.8 Oxygen Permeability Analysis of HECS:kC Hydrogels and Asymmetric PCL-DOP Membrane

Oxygen penetration through specimens was determined according to a previously reported method (Wittaya-areekul & Prahsarn, 2006). Briefly, the samples were placed in the screw lid of a flask containing 150 ml of deionized water and being held in place (test area: 3.14 cm²). The negative control was a closed flask with a plastic bottle cap while the positive control was an open flask allowing oxygen to enter the flask and dissolve in the water as recipient. The test flasks were placed in an open environment under constant agitation for 24 h. The collected water samples were then analyzed for dissolved oxygen according to Winkler's method (Glazer et al., 2004; Winkler, 1888). The sample was titrated with 0.0375M sodium thiosulfate

solution with the addition of starch solution as an indicator until blue color vanished. Results was expressed as the amount of dissolved oxygen (ppm).

2.2.9 Microbial Penetration Analysis of Asymmetric PCL-DOP Membrane

The ability of membranes to prevent microbial penetration was tested by attaching the membranes to the top of glass test tubes containing 20 ml of standard nutrient broth used as growth media in microbiological studies (Wittaya-arekul & Prahsarn, 2006). Before the tests, nutrient broth and glass test tubes were sterilized by autoclaving at 121°C for 20 mins. The negative control was a sterile nutrient broth in glass test tube closed with cotton ball and aluminum foil while the positive control was a sterile nutrient broth in test tube open to air. The test tubes were placed in an open environment for 1 week. The cloudiness of the nutrient broth in any tube was considered as microbial contamination. Also, spectrophotometric evaluation at 600 nm wavelength was carried out with a microplate spectrophotometer (Hitachi U-2800A Spectrophotometer UV/Vis Reader, Japan).

2.2.10 Mechanical Properties of HECS:kC Hydrogels and Asymmetric PCL-DOP Membrane

Tensile of the hydrogels and asymmetric membranes were performed with mechanical testing device (Univert, CellScale, Canada). Dumbbell sample pattern was used to prevent the slippage of membranes at the grip side during tensile tests. The stretch tests were carried out at test conditions of 25°C and 50±3 % relative humidity. The crosshead speed of the system adjusted was to 10 mm/min to get a constant strain rate of 100 %/min. The test results were obtained as load versus

deflection curves, which are converted into stress-strain data by the computer program. Young's modulus was calculated from the stress-strain curves (Ying et al., 2019).

For the unconfined compression test, hydrogel discs of 1 cm diameter and 5 mm height were obtained using 10 mm diameter biopsy punch and discs were placed in PBS at 25°C. Compression tests were done using 10 N load cell at a force rate of 1 mm/min up to 60% of the total height of hydrogels using mechanical testing device (Univert, CellScale, Canada). Compressive moduli and strength of the hydrogels were calculated from stress–strain curves (Fathi- Achachelouei et al., 2020).

2.2.11 Rheological Analysis of HECS:kC Hydrogels

Oscillatory shear rheology was conducted to characterize the rheological properties of the hydrogels prepared in various ratios using an MCR 302 Rheometer (Anton Paar, Graz, Austria) in Bilkent University National Nanotechnology Research Center (UNAM). A parallel plate geometry (8 mm with a sandblasted measuring plate, PP08/S) was used to load the samples, following equilibration at room temperature. To register the viscoelastic moduli, for all samples at 25°C in the linear viscoelastic region. The gels were maintained hydrated during the oscillatory frequency sweep was performed at 0.1-100 rad s⁻¹ under a small oscillatory strain and ~0.1% frequency was registered. Experiments (total time ~ 12.5 min) were conducted in an enclosed chamber. The viscoelastic moduli versus angular frequency were recorded (Sheikhi et al., 2019).

2.2.12 *Ex vivo* Adhesion Strength of HECS:kC Hydrogels

Assessing the adhesion strength between the hydrogel and dermal tissues is important because insufficient adhesion between these two can prevent sealing and expose the wound. On the other hand, an excessively strong adhesion may prevent on-demand removal of the wound dressing by causing secondary injuries on removal (Nam & Mooney, 2021). In order to assess the adhesive behavior of the hydrogels, lap shear strength was determined according to a modified ASTM test (F2255-05) (Shirzaei Sani et al., 2019). Fresh sheep and chicken skin were obtained, shaved clean and scraped from the excessive fat and washed with PBS before the tests. Sheep skin samples were cut in 2x1 cm pieces and the terminal sections with approximately 1x1 cm dimensions were used to overlap two layers of skin (either sheep or chicken). On the other hand, chicken skin pieces of approximately 1x1 cm were first glued to a leather support with a cyanoacrylate-based glue. After injecting ~50 uL of warm pre-gel polymer solution on dermal tissues, the layers were carefully overlapped and left for gelation at room temperature for 1 hour. The lap shear strength of the adhesives was then measured under the tensile stress at a rate of 1 mm/min using a mechanical testing device (Univert, CellScale, Canada). The ultimate stress was reported as the shear strength of the bioadhesives ($n \geq 3$).

2.2.13 Adhesion Strength Between Asymmetric Membrane and Hydrogel

Lap shear tests of the asymmetric membrane and the hydrogels were conducted similarly to the *ex vivo* adhesion tests of the hydrogels. After washing with distilled water, asymmetric PCL and PCL-DOP membranes were cut in ~1x1 cm dimensions and they were glued on leather supports of 1x2 cm² sized pieces with cyanoacrylate glue. After injecting warm pre-gel solution, asymmetric membrane layers were overlapped and the pre-gel solution was left for gelation at room temperature for 1 hour. The lap shear strength of the adhesives was then measured under the tensile

stress at a rate of 1 mm/min using a mechanical testing device (Univert, CellScale, Canada). The ultimate stress was reported as the shear strength of the bioadhesives ($n \geq 3$).

2.2.14 Scanning Electron Microscope Analysis of Hydrogels

For structural characterization, the swollen hydrogels were dehydrated through a graded series of ethanol solutions (70, 85, 95, 100%), and air dried in a flow chamber at room temperature. Dried samples were then sputter-coated with gold (thickness approximately 200 Å) prior to examination (Woerly et al. 2001). The analysis was performed with Quanta 400F Field Emission SEM (Hillsboro, Oregon, United States) in BIOMATEN, Turkey.

2.2.15 Scanning Electron Microscopy Analysis of Membranes

Surface properties of PCL and PCL-DOP membranes were analyzed by a FEI Nova Nano SEM 430 microscope after gold-coating the samples with a Quorum SC7640 high-resolution (HR) sputter coater.

2.2.16 Porosity Analysis of Hydrogels

Porosities of HECS:kC hydrogels were measured by liquid displacement method in which, the initial weights and geometric volumes of the lyophilized hydrogels were measured (W and V , respectively). Afterwards, the gels were immersed in absolute ethanol (with the density ρ) for 24 hours until complete saturation and weighed again (W'). The porosity was calculated using the equation (Qin et al., 2018):

$$\text{Porosity (\%)} = [(W' - W) / (V \times \rho)] \times 100\%$$

Pore size distribution of the hydrogels was determined by mercury porosimeter (Quantachrome Corporation, Poremaster 60) in METU Central Laboratory-Turkey under low pressure (0 - 50 psia) with contact angle of 140° (Horák et al., 2011). True density and porosity of the hydrogels were measured in pycnometer (Gierszewska-Drużyńska et al., 2013).

2.2.17 Porosity Analysis of Membranes

The porosity of the membrane was measured by liquid displacement method in combination with the Archimedes' principle (Delgado-Rangel et al., 2020; Qin et al., 2018).

Firstly, a 10 mL glass pipette with the narrow tip cut and the other side sealed with a rubber cap was used, it was aligned and fixed vertically and filled up with absolute ethanol. Changes in the liquid level after immersing the membrane samples for 24 hours was recorded as the absolute volume of the membrane (V_A). Secondly, the membranes immersed in absolute ethanol for 24 hours were weighted after removing the residual ethanol on the surface of the membranes to determine their wet weights (m_w). The samples were additionally weighted after vacuum-drying to determine their dry weights (m_d). Pore volumes (V_P) were determined by the following equation;

$$V_P = \frac{m_w - m_d}{\rho_e}$$

where ρ_e is the density of ethanol. The porosity of the membrane samples (n=3) was calculated according to the following equation:

$$\text{Porosity (\%)} = \frac{V_P}{V_P + V_A} \times 100$$

2.2.18 Water Contact Angle Analysis of Asymmetric PCL-DOP Membranes

Water contact angle was determined by goniometer (Attension, Biolin Scientific, Sweden) at 25 °C. dH₂O was chosen as testing liquid and droplets were set to 7 μ L. Contact angles were calculated using Young-Laplace equation (Taylor et al., 2007);

$$\gamma_{sv} = \gamma_{sl} + \gamma_{lv} \cos\theta$$

where γ_{sv} , γ_{sl} and γ_{lv} refer to solid-vapor, solid-liquid, and liquid-vapor interfacial tensions respectively, and $\cos\theta$ is the wetting angle (Türkkan et al., 2017).

2.2.19 Storax Release from HECS:kC Hydrogels

Storax loaded (1 mg/mL) hydrogels (300 μ L) were incubated at 37°C in 600 μ L of PBS at different pH (6.4, 7.4 and 8.4) for 10 days. 200 μ L aliquots were taken from the release medium at different time intervals (hours 0, 2, 6, 24 and days 3, 6, 10). After drying the samples with lyophilization, 200 μ L of absolute ethanol was added

and vortexed to dissolve the released storax. Then, the samples were centrifuged to remove any hydrogel degradation products and the absorbance of the supernatant was measured at 353 nm (Ehterami et al., 2019). The amount of storax released was determined using the calibration curve constructed with different concentrations of storax in ethanol (0.02-10% w/v) (**Appendix D Figure 1**). Percent release of storax was determined according to the following equation.

$$\text{Cumulative storax release (\%)} = (\text{Amount of released storax} / \text{Total storax}) \times 100$$

Obtained release profile was finally fitted in the Korsmeyer-Peppas kinetic model, which describes drug release from a polymeric system, to determine storax release mechanism from the hydrogels (Paarakh et al., 2018). According to the Korsmeyer-Peppas kinetic model:

$$M_t/M_\infty = K t^n$$

Where M_t/M_∞ is fraction of drug released at time t , K is the rate constant (having units of t^n). n is the release exponent indicative of the mechanism of transport of drug through the polymer (B. Singh et al., 2021a). When $n < 0.45$ release occurs by pseudo-Fickian diffusion, $n > 0.85$ is characterized by Non-Fickian diffusion whereas $n = 0.5$ means the diffusion has Fickian behavior.

2.2.20 Dose Dependent Cytotoxicity Analysis of Storax

Dose dependent cytotoxicity of storax was analyzed by MTT (3-(4,5-dimethylthiazol-2-yl)-2,5-diphenyltetrazoliumbromide) cell viability assay. Firstly,

1x10⁴ L929 mouse fibroblasts were allowed to adhere on 96-well plate in 199 μL of DMEM for 5 hours. Then, 1 μL of storax solution, dissolved in DMSO, was added onto the wells to achieve the following final storax concentrations; 50 μg/mL, 5 μg/mL, 0.5 μg/mL and 0 μg/mL. After incubation at 37 °C for 24 hours MTT solution was added onto each well to achieve 0.5 mg/mL of MTT in the wells. Cells were then incubated at 37°C for 3 hours, and formed formazan crystals were dissolved with DMSO after removal of MTT solution and washing steps. Afterwards, the absorbance of each well was measured with a microplate spectrophotometer (SpectraMax iD3, Molecular Devices, USA) at 570 nm and 630 nm as reference and relative cell viability was calculated based on the equation below:

$$Relative\ cell\ viability\ (\%) = \frac{Abs_{test\ (570\ nm)} - Abs_{test\ (630\ nm)}}{Abs_{control\ (570\ nm)} - Abs_{control\ (630\ nm)}} \times 100$$

Where $Ab_{S_{control}}$ is the absorbance obtained from the group with 0 μg/mL storax and $Ab_{S_{test}}$ is the the absorbance obtained from the test groups with storax concentrations of 50 μg/mL, 5 μg/mL and 0.5 μg/mL.

2.2.21 Effect of HECS:kC Hydrogels Loaded with Storax on L929 Fibroblasts

Effect of leachable fractions and degradation products of storax loaded and blank hydrogels on the viability of cells was analyzed with indirect elution test using MTT (3-(4,5-dimethylthiazol-2-yl)-2,5-diphenyltetrazoliumbromide) cell viability assay (J. Guo et al., 2016). The storax loaded and blank hydrogels (0.3 g) were incubated in 3 mL of PBS (pH 7.4) at 37 °C for 24 h. Next, the aliquots were diluted at different folds: 1X, 2X, 5X, 10X, 25X, 50X and 100X (1X was the solution of leached

products with no dilution; 2X means 2 times dilution of the 1X solution by PBS). In each well of a 96-well cell culture plate, 1×10^4 L929 mouse fibroblast cells in 180 μL were seeded and allowed to adhere for 5 hours and then, 20 μL of aliquots of different dilutions was added and the cells were incubated for 24 h. At the end of 24h viability of cells was determined by MTT assay as previously described.

2.2.22 Antimicrobial Activity of Storax Loaded HECS:kC Hydrogels

Antimicrobial activity of storax loaded hydrogels against *S. aureus* was analyzed according to a previously reported method (Z. Zheng et al., 2020). Due to its hydrophobic property, storax concentrations higher than 1 mg/mL noticeably impeded the gelation process. Therefore, a pre-gel solution was prepared with the storax concentration of 1 mg/mL and 300 μL of this pre-gel solution was added into the wells of 48-well plate and left to form hydrogels. Afterwards, 10 μL of bacterial suspension ($1 \times 10^8 \text{ CFU mL}^{-1}$) was added onto the hydrogel surfaces. The control group had PBS instead of hydrogel. Following incubation at 37 °C for 3 hours, 300 μL of PBS was added onto each hydrogel sample to re-suspend surviving bacteria and 100 μL of this bacterial suspension was spread on a solid agar plate. After incubation at 37 °C for 24 hours the colony-forming units were counted. Bacterial survival was calculated using the following equation:

$$\text{Bacterial survival (\%)} = \frac{N_{\text{hydrogel}}}{N_{\text{control}}} \times 100$$

Where N_{hydrogel} is the number of colony-forming units counted from the test samples (hydrogels) and N_{control} is the number of colony-forming units counted from the control group (PBS).

2.2.23 Antioxidant Activity of Storax Loaded HECS:kC Hydrogels

Antioxidant activities of the storax loaded and blank hydrogels were tested by L929 fibroblast exposed to oxidative stress by hydrogen peroxide (H_2O_2) (Isik et al., 2020). In order to cause oxidative damage to the cells, H_2O_2 with a concentration of 250 μ M was chosen as similar previous reports (Isik et al., 2020; Maity et al., 2022).

5000 cells/well were seeded 96-well plate in a cell growth medium of DMEM supplemented with 10% fetal bovine serum and 1% penicillin-streptomycin and incubated at 37°C in 5% CO_2 atmosphere for 5 hours until the cells adhered to tissue-culture polystyrene. Afterwards, the growth medium was changed with storax leachates from HECS:kC (1:1) hydrogel or only hydrogel leachates (0.22 μ m filter-sterilized), which were obtained after 24 hours of incubation in a release medium (DMEM) and H_2O_2 was directly added to have a final concentration of 250 μ M. After 24 hours of incubation, the medium was replaced by a fresh DMEM (without phenol red) with AlamarBlue (Invitrogen). After 3 hours of incubation, optical density of the AlamarBlue solutions were measured with a microplate reader (SpectraMax ID3 Instrument, Molecular Devices) at 570 nm (test wavelength) and 600 nm (reference wavelength) and relative cell viability of the test groups were compared to the cells grown without H_2O_2 treatment (positive control group) and cells grown with H_2O_2 treatment (negative control group). AlamarBlue test was repeated on day 4, 7 and 14.

Morphology of the cells were also examined with inverted phase contrast microscope (Eclipse TS100, Nikon Corp., USA) on day 7 and confocal laser scanning microscope Zeiss Cell Observer SD (Zeiss, Germany) on day 14. To prepare the cells for confocal laser scanning microscopy, the cells were washed with PBS and fixed

with paraformaldehyde solution (4% w/v) for 15 minutes at 37°C. Afterwards, the cells were permeabilized with Triton X-100 (0.1% v/v) for 5 minutes in ambient temperature. Prior to staining, the cells were blocked with bovine serum albumin (BSA) solution (1% w/v, prepared in PBS) for 1 hour at 37°C. The cells were then actin-stained with Alexa Fluor 488 (1:200, prepared in 0.1% BSA in PBS) for 1 hour at 37°C, washed with PBS and nuclear-stained with DAPI (2 ug/mL, prepared in 0.1% BSA in PBS) for 10 minutes at 37°C. The cells were visualized under fluorescence of excitation at 488 nm for Alexa Fluor 488 (green) and at 350 nm for DAPI (blue). In order to assess the oxidative stress recovery, cell cytoplasmic spread areas ($n > 50$) in each group were quantitatively measured in μm^2 from confocal laser scanning microscopy images with Image J software (Lee et al., 2022).

2.2.24 *In Vivo* Wound Healing Study of HECS:kC-PCL Bilayer Wound Dressing

In vivo tests were conducted on male Sprague Dawley rats (250-290 g) by using only PBS, blank HECS:kC hydrogel, storax loaded HECS:kC hydrogel and Tegaderm™. The number of rats to be used in each group was determined as $n=7$ by power analysis formula as given below with following assumptions; 80% power and 1% significance level.

$$n=1+2C(SD/d)^2$$

where d , represents the difference the observer wants to examine; SD , represents the standard deviation obtained from similar studies previously conducted; C , represents the constant term (Ankaralı & Ankaralı, 2019).

2.2.24.1 Wound Model

Rats were anesthetized with 50mg/kg ketamine hydrochloride and to-be-wound areas were shaved and disinfected with iodide solution. Afterwards, a full-thickness skin section of 1.5 cm diameter was excised (Hoque et al., 2017; J. Wang et al., 2020).

Developed bilayer wound dressings and Tegaderm™ were placed to fully cover the wound area. Wounds in the control group were treated with only PBS and covered with traditional gauze (J. Wang et al., 2020). On the first, third, fifth, seventh and tenth days wound areas were drawn on acetate paper and measured digitally with Image J software and calculated as follows (Zhao et al., 2020):

$$\text{Wound area (\%)} = A_n / A_0 \times 100$$

A_0 is initial wound area, A_n is wound area on n'th day.

2.2.24.2 Histological Examination

Rats were euthanized with ketamine hydrochloride on the fifth and tenth days and skin tissues from the wound area were collected and fixed with 10% phosphate buffered formaldehyde at room temperature for 24 hours. After thorough washing, the samples were dehydrated in consecutively increasing concentrations of ethanol and embedded in paraffin wax.

Samples of 5 μm thickness were removed from paraffin, rehydrated and dyed with hematoxylin-eosin and Masson's trichrome. Samples were examined under the light microscope (Nikon Eclipse 50i, Japan) with camera system (Leica DFC295, Germany) and evaluated based on the following parameters; epithelization, inflammation, fibroplasy, neovascularization, collagen fiber density and thickness and order (Z. Guo et al., 2021)(Cong et al., 2019)(Gangwar et al., 2013)(Rashtbar et al., 2018). Following numerical categories were used for histological scoring:

1. Epithelialization: 1—present, 2—partially present, 3—absent.
2. Inflammation: 1—resembling normal skin, 2—mild, 3—moderate, 4—severe.
3. Fibroplasia: 1—resembling normal skin, 2—mild, 3—moderate, 4—severe.
4. Neovascularization: 1—resembling normal skin , 2—mild, 3—moderate, 4—severe.
5. Collagen fiber density: 1—denser, 2—dense, 3—less dense.
6. Collagen fiber thickness: 1—thicker, 2—thick, 3—thin.
7. Collagen fiber arrangement: 1—best arranged, 2—better arranged, 3—badly arranged, 4—worst arranged.

2.2.25 Statistical Analysis

All experiments were conducted in at least triplicates. In comparing three or more groups for a single parameter One-way Analysis of Variance (ANOVA) test was done with Tukey's Multiple Comparison Test for the post-hoc pairwise comparisons, two groups were compared by student's t test using SPSS-9 Software Programme (SPSS Inc., USA).

CHAPTER 3

RESULTS AND DISCUSSION

3.1 Chemical Characterizations

3.1.1 Modification of Chitosan to Hydroxyethyl Chitosan

In contrast to the solubility of CS in acid environments, HECS can be dissolved in water in neutral pH. Therefore, hydroxyethylation increases the interaction of CS with water across a wider pH range for easier dissolution as a polymer. Moreover, it enables easier and pH-adaptable hydrogel preparation without the need for large volumes of acid. HECS was synthesized by accessing hydroxyethyl group to the C6 of chitosan and hydroxyethylation was achieved with chloroethanol and potassium hydroxide in alkaline alcohol water mixed phase. Temperature and pH were key factors to the reaction. The final HECS product was white with good water-solubility and moisture retention. The FTIR spectra of HECS and chitosan are shown in **Figure 3.1**. In the FTIR spectra, four absorption peaks centered at 1150 cm^{-1} , 1060 cm^{-1} , 1024 cm^{-1} , and 894 cm^{-1} were assigned to the characteristic peaks of the saccharide structure. Compared to those of chitosan, a new absorption peak appeared at 1105 cm^{-1} , which was ascribed to the symmetric C–O–C stretching vibration absorption (Shao et al., 2015b). Moreover, the new peak at 1448 cm^{-1} was assigned to the methylene bending vibration, and the absorption peak located at 2924 cm^{-1} corresponded to the methylene stretching vibration, which increased after hydroxyethylation. Moreover, a broad absorption peak appeared at 3290 cm^{-1} that become stronger which was ascribed to the stretching vibration of –OH. ^1H NMR analysis of CS and HECS were shown in **Appendix A Figure 2** and **Appendix A Figure 3**, respectively. As compared to CS, ^1H NMR spectrum of HECS showed a

new peak at $\delta = 3.9$ ppm and $\delta = 4.1$ ppm, which were assigned to the proton environments in two methylene groups in HECS.

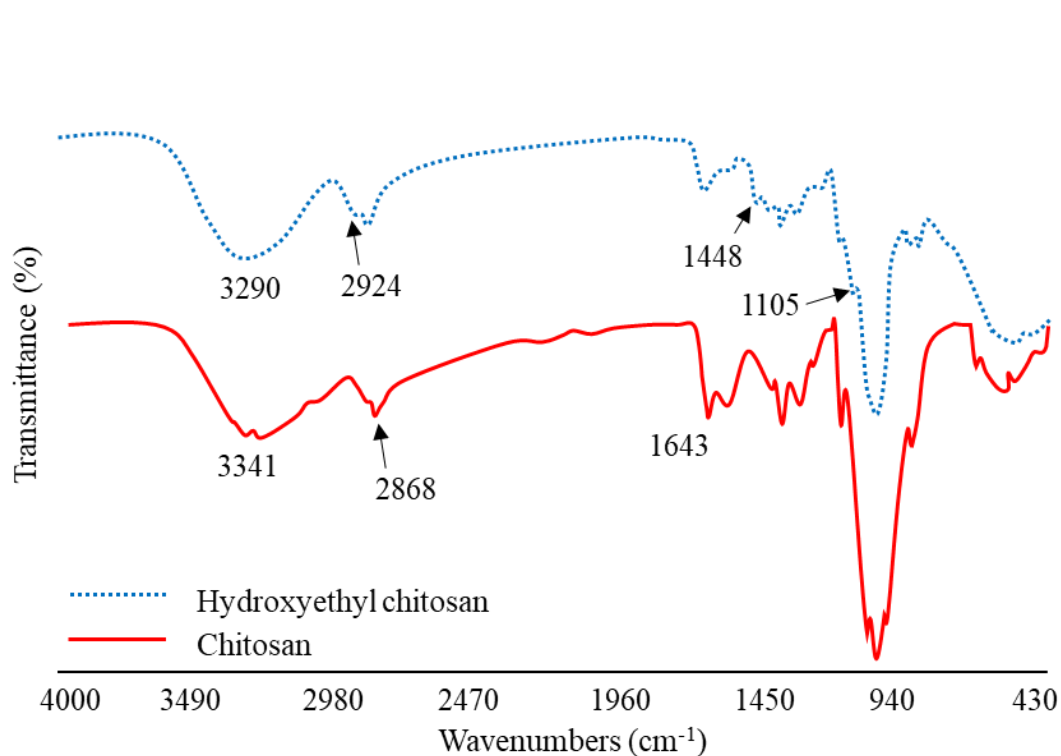


Figure 3.1. FTIR spectra of CS and HECS.

XRD pattern of CS exhibited a characteristic diffraction peak at $2\theta=20^\circ$. This indicates that CS acquired high crystallinity because the hydrogen bonds formed by the hydroxyl and amino groups in its molecular chain increased the regularity of the molecular structure; this is also the reason CS was acid-soluble only. By contrast, the diffraction peak of the HECS was significantly reduced, similar to the previous reports (**Figure 3.2**)(H. Li et al., 2010).

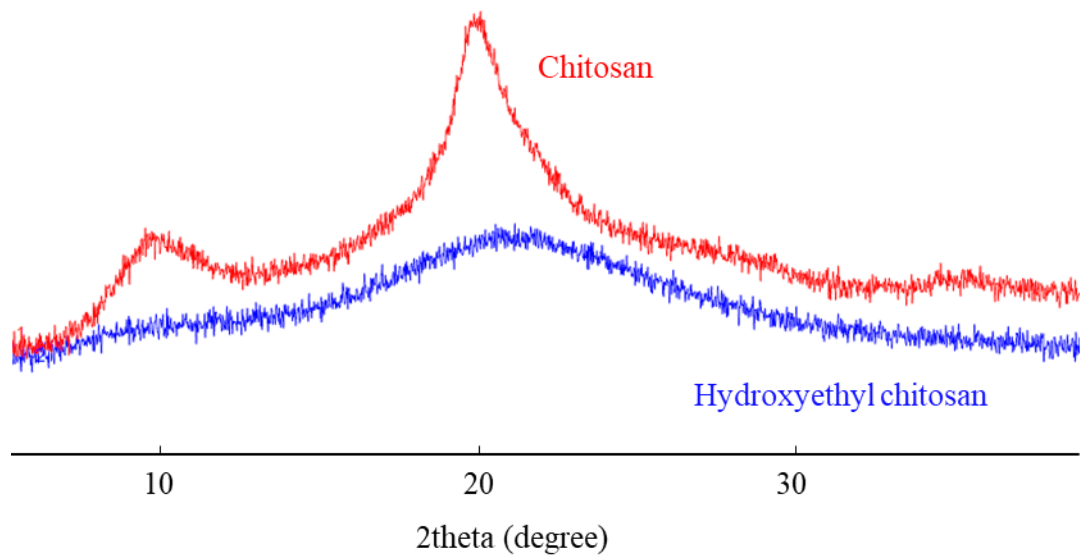


Figure 3.2. XRD analysis for CS and HECS.

3.2 Characterization of HECS-kC Hydrogels

3.2.1 Porosity and Pore Size Distribution of the HECS-kC Hydrogels

The pore size distribution for the HECS-kC hydrogels was measured by mercury porosimetry. Hydrogels with 2:1 ratio demonstrated pore diameter in the range of 50-200 μm (**Appendix B Figure 1a**). The hydrogels with HECS-kC ratio 1:1 showed multi modal peaks with pore diameters of 30-200 μm (**Appendix B Figure 1b**) whereas the hydrogel with 1:2 ratio showed pore diameters in the range of 10-100 μm (**Appendix B Figure 1c**). These observations confirmed that the prepared hydrogels are favorable for tissue regeneration applications, which requires a porous structure with interconnected pores and acceptable pore size (Swain et al., 2015).

Since a wound dressing must enable a proper mass transfer to and from a wound site (oxygen, nutrients, moisture and wound exudates), porosity has a critical importance, not only in facilitating the healing process but in terms of mechanical properties of the dressing as well (Bargavi et al., 2020).

Figure 3.3 shows the porosity analysis for HECS-kC hydrogels. Hydrogels with 2:1 ratio demonstrated porosity of 90.4% (± 4.4). The hydrogels with HECS-kC ratio 1:1 showed porosity of 80.0% (± 5.2) whereas the hydrogel with 1:2 ratio showed porosity of 62.2% (± 4.9). Decreasing porosity with increased kC content might suggest that kC can form denser interactions with HECS. In comparable studies; a chitosan/ β -glycerophosphate based hydrogel developed as a wound dressing showed porosities in the range of 80-90% (Qin et al., 2018), psyllium-keratin based hydrogel in the range of 76-82% porosity (Ponrasu et al., 2018).

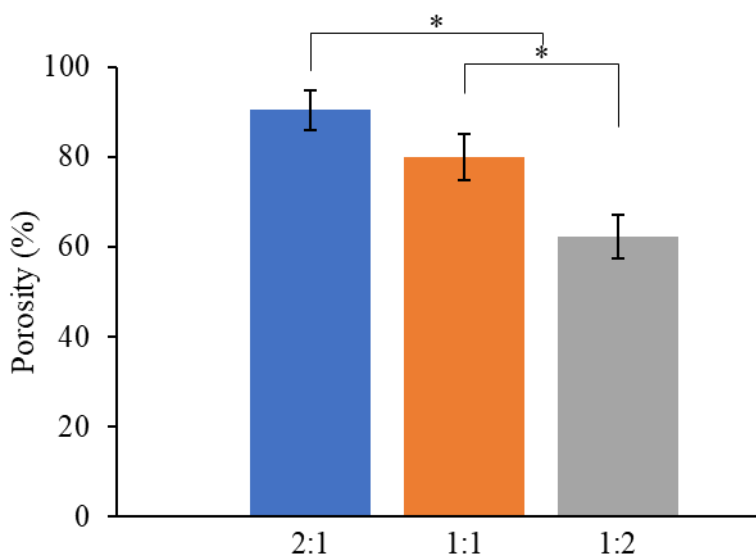


Figure 3.3. Porosity of hydrogel of different HECS:kC ratios (2:1, 1:1, 1:2). * denotes significant difference between groups ($p < 0.05$, $n=3$).

In correlation with the mercury porosimetry results, SEM micrographs revealed that the hydrogel compositions had open and interconnected porous structure with irregular pore sizes (**Figure 3.4**).

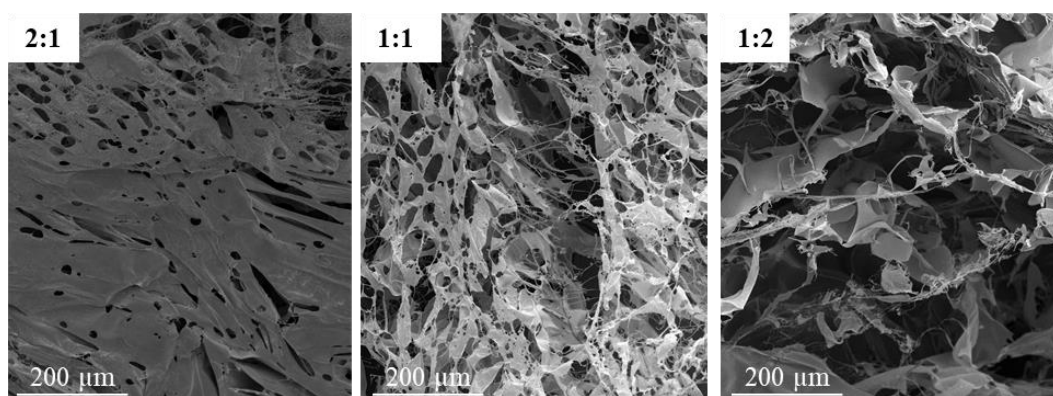


Figure 3.4. Scanning electron micrographs of hydrogels with HECS:kC ratios of 2:1, 1:1, 1:2 (w/w).

3.2.2 Water Uptake of HECS-kC Hydrogels in Acidic, Neutral and Basic pH Media

The water uptake capacity is an important parameter for any wound dressing as it allows the absorption of wound exudates. Since the pH of a wound site can vary from alkali to acidic, it is important to test whether the water uptake capacity of the hydrogels changes in media at different pH. Therefore, the water uptake capacity tests of the hydrogel compositions have been conducted in PBS with varying pH values 8.4, 7.4 and 6.4 in 37°C (Zepon et al., 2019b)(**Figure 3.5**). Hydrogel with HECS:kC ratio 2:1 reached ~1500% of the initial dry weight within 30 minutes in buffer environments at pH 6.4, pH 8.4 and ~2500% at pH 7.4. The hydrogels in pH 6.4 media showed a sharp decrease in the wet weight and disintegration related mass loss in 24 hours. (**Figure 3.5a**). This indicates that the 2:1 composition cannot yield

a stable polyelectrolyte complexation and it appears that only the decreasing solubility of HECS at pH 7.4 and pH 8.4 can hold the hydrogel by increased hydrophobic interactions and interlocking of HECS chains. Hydrogel with HECS:kC ratio 1:1 showed better stability and swells between 2000% to 3000% of the initial dry weight in 24 hours (**Figure 3.5b**). HECS:kC 1:2 swelled up to ~4000% in 24 hours at pH 7.4 (**Figure 3.5c**). As the ratio of kC was increased, the maximum water holding capacity (swelling) increased regardless of the pH. On the other hand, the maximum swelling ratio decreased as the pH was increased from 6.4 to 8.4. Since the pK_a of the amino groups on HECS is approximately 6.5 (Yoon et al., 2014), the solubility of HECS decreases as the pH of the media rises beyond pH 6.5. In other words, this phenomenon can be explained by the fact that in mildly acidic environments, both HECS and kC possess electrostatically charged groups, which allow better interaction with water molecules for absorption and eventual swelling. However, in alkali environments HECS molecular chains favor hydrophobic interactions and interlock HECS and kC molecular chains to interfere with water absorption depending on the ratio of HECS (**Figure 3.5d**).

A similar study was conducted with tannin-containing hydroxypropyl chitin hydrogel where the hydrogel samples were incubated in five different media with pH ranging from 3.0 to 9.0 (M. Ma et al., 2020). The hydrogel groups were reported to reach 115% swelling within 10 hours, followed by gradual decrease to 95% in 70 hours. (Zepon et al. 2018) studied the swelling equilibrium of silver nanoparticles containing kC hydrogels in pH 7.4 and pH 8.5. The hydrogels were swollen up to 2.5 to 3 folds of their initial weight in 100 minutes.

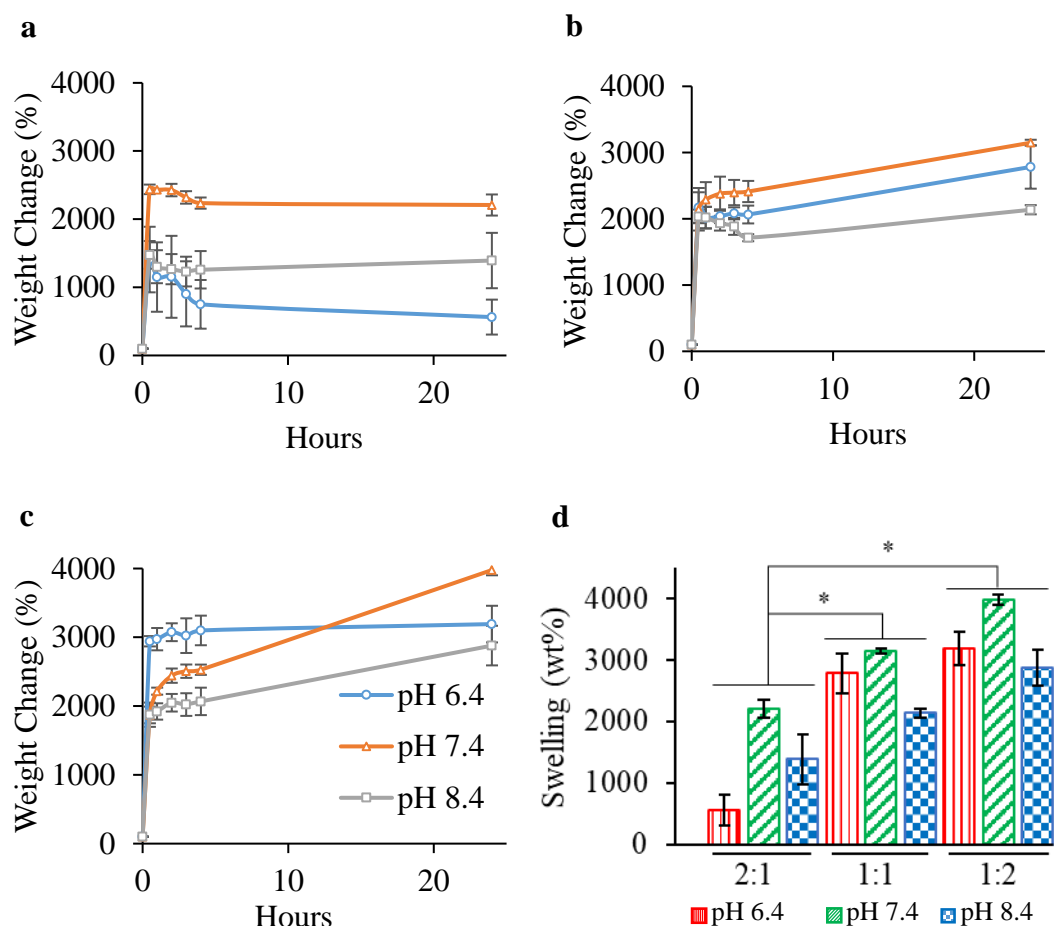


Figure 3.5. Swelling equilibria of HECS:kC hydrogels with 2:1 (a) 1:1 (b) 1:2 (c) ratio in 37°C at different pH (n=3). (d) Swelling ratios of the hydrogels after 24 hours of incubation at 37°C. * denotes significant difference between the groups ($p < 0.05$, $n=3$).

3.2.3 *In Vitro* Degradation of HECS-kC Hydrogel in Acidic, Neutral and Basic pH Media

In vitro degradation studies of HECS-kC hydrogels were conducted in PBS at pH 6.4, pH 7.4 and pH 8.4 to test whether the hydrogels are suitable for application in wound sites with varying pH levels. Hydrogels with HECS-kC ratio 2:1 incubated

in pH 7.4 and 8.4 showed a steady weight loss in 14 days to reach 60% and 77% of the initial weights, respectively (**Appendix C Figure 1a**). The hydrogels (2:1) incubated at pH 6.4 dissolved within 1 day and they are not shown in the graph. During the same period, hydrogels with 1:1 HECS-kC ratio yielded almost no weight loss at pH 8.4. In contrast to the hydrogels with 2:1 ratio, the ratio 1:1 proved to have a stable structure and 78% and 60% of the hydrogels remained when incubated in PBS at pH 7.4 and pH 6.4, respectively (**Appendix C Figure 1b**). The hydrogels with 1:2 ratio showed very similar results to the 1:1 ratio (**Appendix C Figure 1c**). Since polyelectrolyte complexes are formed by the interaction of oppositely charged groups, the strength of the polymer network relies primarily on the ratio of amino groups in HECS and sulfate groups in kC. Since the total polymer concentrations are constant throughout the study, it can be seen that the HECS-kC ratio of 1:1 and 1:2 enabled more electrostatic interactions to occur compared to the ratio of 2:1. In addition to the electrostatic interactions, hydrophobic interaction within the polymer network play an important role in the degradation profiles (Shou et al., 2020); the hydrogels in all groups showed significantly less weight loss in pH 8.4 media (**Appendix C Figure 2**). This can be attributed to the decrease in the solubility of HECS above neutral pH. The interlocking of kC chains by HECS chains prevents the polymers from being un-entangled and packs the polymer network; delaying both the initial swelling and the eventual dissolution of the hydrogels in basic media. The phenomenon was visually observed as the hydrogel samples swollen in basic media turned opaque while, in acid, they remained transparent (not shown). Throughout the *in vitro* degradation study in PBS with varying pH, the hydrogels did not change the pH of the media (**Appendix C Figure 3**). In addition, final dry weights correlate with the *in vitro* degradation profiles (**Figure 3.6**).

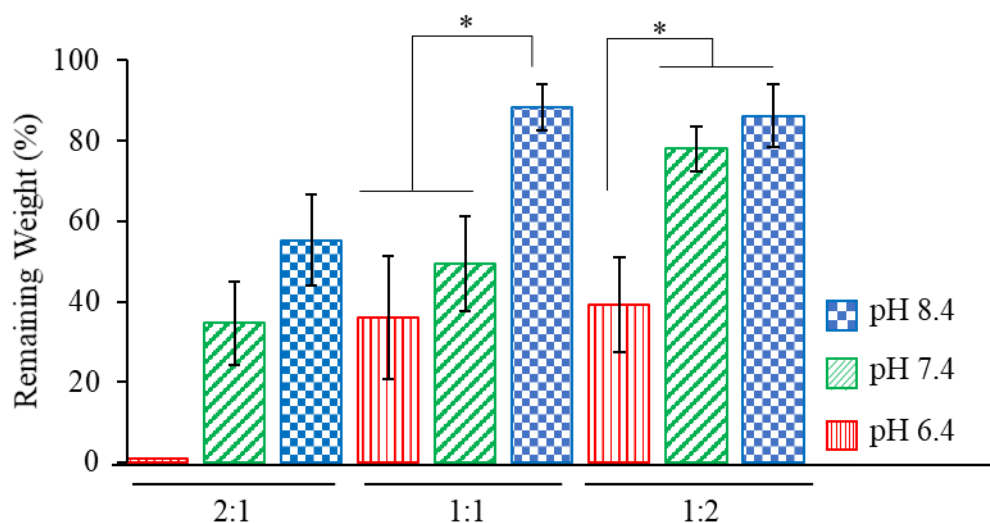


Figure 3.6. Remaining dry weights after 14 days with respect to the initial dry weights of incubation in PBS with varying pH. Significant differences between the groups are shown by * ($p < 0.05$, $n=3$).

3.2.4 Oxygen Permeability of HECS-kC Hydrogels

Experimental conditions of water-dissolved oxygen permeability assay for HECS-kC hydrogels were the same as it has been mentioned in the section 3.2.8. After the assay was conducted, open flasks, closed flasks and the test samples with HECS:kC ratio of 1:1 and 1:2 were found to have $5.45 (\pm 0.1)$ ppm, $0.86 (\pm 0.02)$ ppm, $5.19 (\pm 0.06)$ ppm and $5.20 (\pm 0.19)$ ppm dissolved oxygen, respectively (**Figure 3.7**). In accordance with the water vapor permeability results, these results indicate that changing ratios of HECS and kC without changing the total polymer concentration has no significant effect on the oxygen permeability of the hydrogels.

Recently, a hydrogel composed of tragacanth gum and alginate has been evaluated for dissolved oxygen permeability (B. Singh et al., 2021b). The tragacanth gum-

alginate hydrogel was able reach 81.6% dissolved oxygen saturation. In comparison to the open flask, HECS:kC hydrogels were able to reach 95% dissolved oxygen saturation.

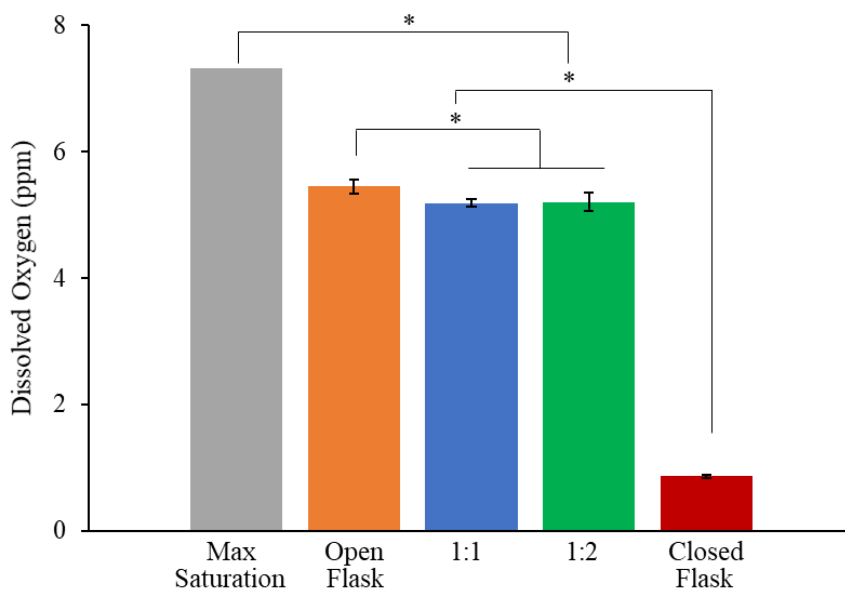


Figure 3.7. Oxygen permeability of HECS-kC hydrogels. * denotes significant difference between the groups ($p < 0.05$, $n=3$).

3.2.5 Water Vapor Transmission Rate of HECS-kC Hydrogels

The water vapor transmission rate (WVTR) across the surface of a wound dressing is an important parameter in healing process. WVTR depends on the structural properties such as porosity and thickness, chemical characteristics of the material as well as the ambient humidity and temperature (Morgado et al., 2014b). An ideal wound dressing would not allow rapid water loss that leads to the dehydration of the wound site while allowing sufficient vapor transfer to prevent exudate and pressure build up (Morgado et al., 2015). It has been reported that the WVTRs for normal

skin, first degree burns, and granulating wounds are 204 ± 12 , 279 ± 26 , and 5138 ± 202 g/m² day, respectively. In addition, it was recommended that wound dressings have WVTRs in the range of 2000–2500 g/m² day (Y. Chen et al., 2011).

All hydrogel compositions showed ~ 2250 g/m² day, while the positive control was measured to have WVTR ~ 1400 g/m² day. The difference between the obtained WVTR and the stated optimal WVTR in the literature may be attributed to the fact that the experiment was conducted in 50% relative humidity and 35°C temperature where only the open capped bottle (positive control) had WVTR in the range of 2000–2500 g/m² day (**Figure 3.8**). Nevertheless, the hydrogels show better WVTR when compared to the commercially available wound dressings such as Comfeels®, Dermiflexs®, Tegaderms®, and OpSites® with WVTRs about 285, 76, 491 and 792 g/m² day.

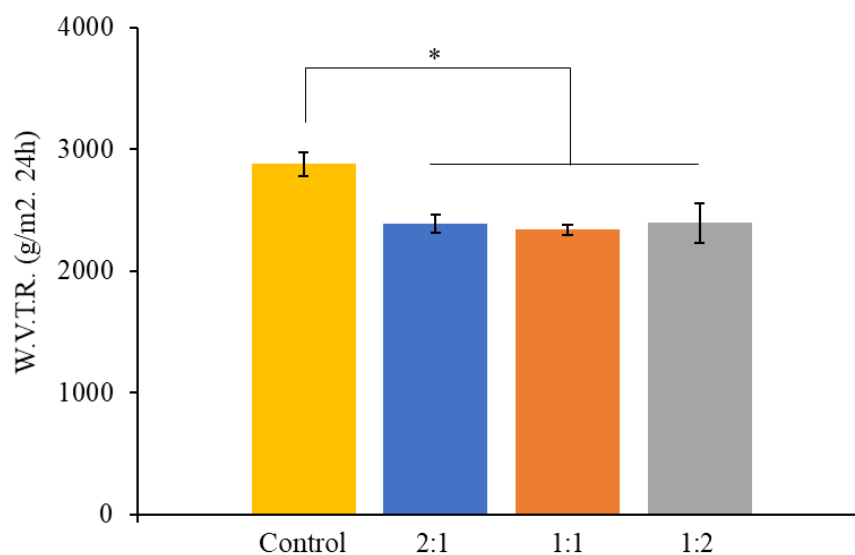


Figure 3.8. Water vapor transmission rate of the HECS-kC hydrogels. No significant difference was observed between the hydrogel groups. * denotes significant difference between the control and hydrogel groups ($p < 0.05$, $n=3$).

3.2.6 Mechanical Properties of HECS-kC Hydrogels

Unconfined uniaxial compression test was conducted with the HECS-kC hydrogels with ratios of 1:1 and 1:2. The hydrogel with 2:1 ratio did not yield a stable hydrogel and therefore it was not tested. Stress-strain curves are shown in **Figure 3.9** and the compressive moduli calculated from the stress-strain curves are shown in **Figure 3.10**. The Young's modulus calculated from the 35% to 45% strain. The hydrogels did not show a significant increase in stress till 30% strain and this may be attributed to the fact that the intermolecular and intramolecular interactions between HECS and kC polymer chains are based on non-covalent secondary interactions and physical polymer chain entanglements (Xiang et al., 2016). This enables the polymers chains to possess a mobility within the dynamic polymer network of the swollen hydrogel system, which allows the hydrogel to shrink up to 30% with relatively small force.

In addition, the hydrogels did not break in 90% strain and maintained their structural integrity while being deformed (data not shown). Hyaluronic acid and poly(l-lysine) were used to obtain polyelectrolyte hydrogels, which had comparable compressive moduli (Yamanlar et al., 2011). Schiff base and calcium ion double crosslinked gellan gum and chitosan developed as a wound dressing had comparable results (Zhang et al., 2020).

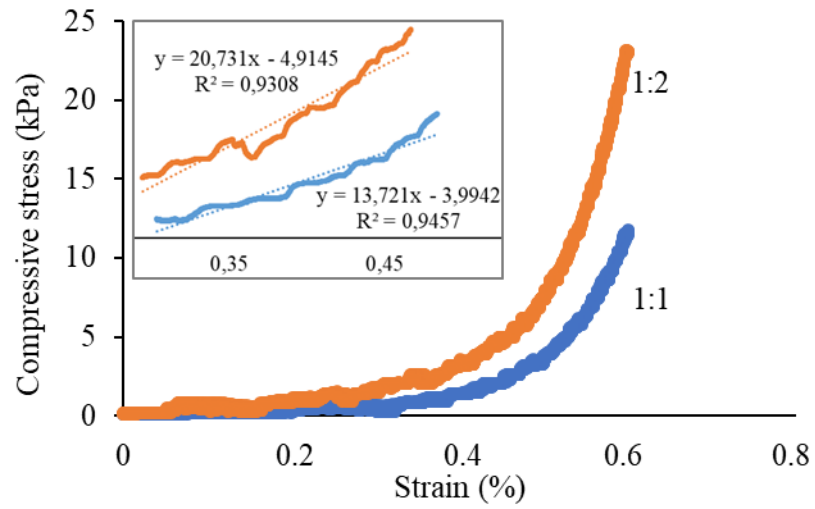


Figure 3.9. Typical compressive stress-strain curves of HECS-kC hydrogels with ratios of 1:1 and 1:2. Inset figure show trendlines for calculation of Young's modulus.

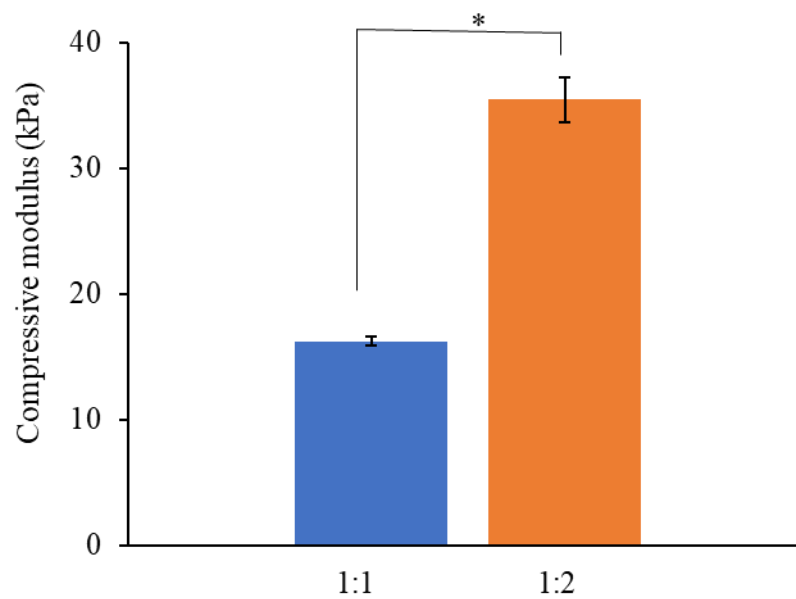


Figure 3.10. Compressive moduli of HECS-kC hydrogels with ratios 1:1 and 1:2. * denotes significant differences between the groups ($p < 0.05$, $n = 3$).

The representative stress-strain curve elastic moduli and tensile strength for HECS-kC hydrogels are shown in **Figure 3.11** and **Figure 3.12**, respectively. The test samples were prepared to have the dumbbell shape according to ASTM D638 Type IV. During the tensile test, no sample was broken and the tensile strengths were recorded at 140% strain. Despite having low elastic moduli, the hydrogels were moldable, extensively stretchable yet very resistant to breakages unlike the brittle carrageenan-divalent ion-based hydrogels (Tavakoli et al., 2020b).

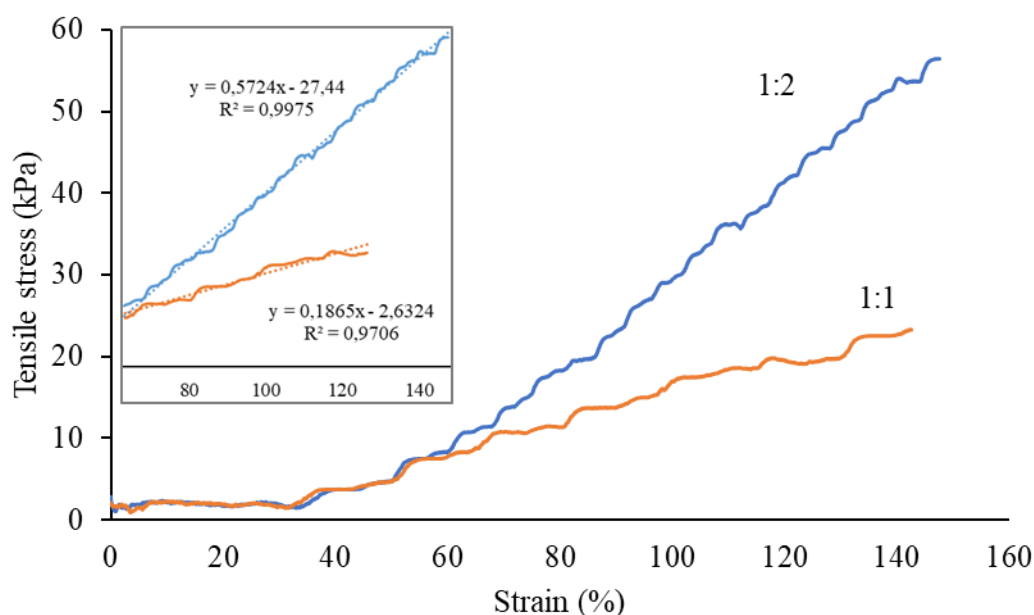


Figure 3.11. Typical tensile stress-strain curves of HECS-kC hydrogels with ratios of 1:1 and 1:2. Inset figure show trendlines for calculation of Young's modulus.

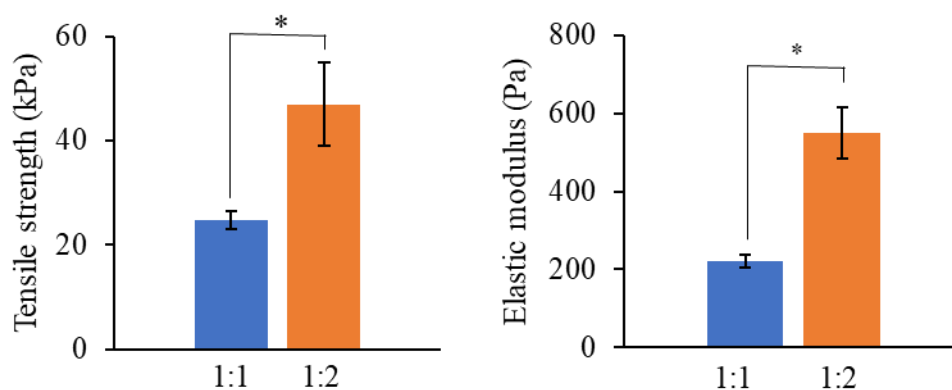


Figure 3.12. Elastic moduli (right) and tensile strength at 140% strain (left) for HECS-kC hydrogels with ratios 1:1 and 1:2. * denotes significant differences between the groups ($p < 0.05$, $n = 3$).

3.2.7 Rheological Analysis of HECS-kC Hydrogels

Analyses were conducted to characterize the rheological properties of HECS:kC hydrogels (ratios of 2:1, 1:1 and 1:2). The storage (G') and loss moduli (G'') of the hydrogels were measured at angular frequencies between 1-100 rad/s using 0.1% oscillatory shear strain. The results indicated that all hydrogels with different polymer ratios showed storage modulus higher than loss modulus which means that the hydrogels have complete network structure with dominant elastic response (J. Yang, Chen, et al., 2020). Moreover, the hydrogels showed a similar behavior under changing angular frequency. The increase of G' with increasing angular frequency showed that the hydrogels have a solid-like behavior and they can maintain structural integrity at a wide range of angular frequency (Zuidema et al., 2014). At 10 rad/s, hydrogels with HECS:kC ratio of 2:1, 1:1 and 1:2 exhibited G' of 15.96 kPa, 22.91 kPa, 27.19 kPa and G''/G' ratios of 0.15, 0.1 and 0.09, respectively (**Figure 3.13**). Consistent with the mechanical test results, these rheological findings indicated that the hydrogel with HECS:kC ratio of 1:1 and 1:2 showed a strong viscoelastic behavior (Alghooneh et al., 2019). Another study reported a G' value of 5.3 kPa at

10 rad/s for a silver nanoparticle incorporating hydrogel obtained via polyelectrolyte complexation of chitosan and carboxymethyl chitosan at 2:4 ratio (J. Yang, Chen, et al., 2020). The fact that our hydrogel demonstrated a higher G' value could be due to the stronger electrostatic interaction between anionic kC polymer chains and cationic HECS polymers chains, which contributed to the formation of a polymeric network with higher elastomer behavior.

To further characterize rheological properties of the hydrogels, G' and G'' were analyzed over a temperature range of 20-60 °C. The results showed that for all hydrogel groups, G' and G'' values decreased with increasing temperature and especially after 40°C, a steeper decrease in storage modulus was observed which indicates weakening elastomer behavior. However, sol-gel transition, which is the point where G'' starts becoming higher than G' , was not observed throughout the temperature range (**Figure 3.13**).

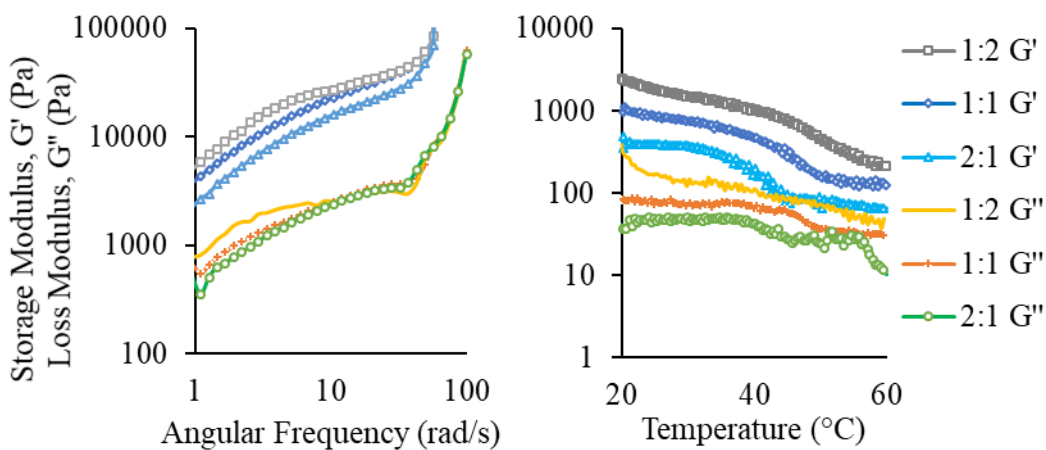


Figure 3.13. Rheological properties of hydrogels with HECS:kC ratios of 2:1, 1:1 and 1:2 in terms of storage and loss moduli versus angular frequency (left), temperature effect on G' & G'' of the hydrogels between 20-60 °C (right).

Viscosity of hydrogels as a function of temperature was also analyzed (**Figure 3.14**). In agreement with the previous findings, HECS:kC hydrogel (2:1) demonstrated a considerably lower viscosity as compared to the other hydrogel groups. This result further shows that HECS:kC at 2:1 ratio does not yield a strong gelation.

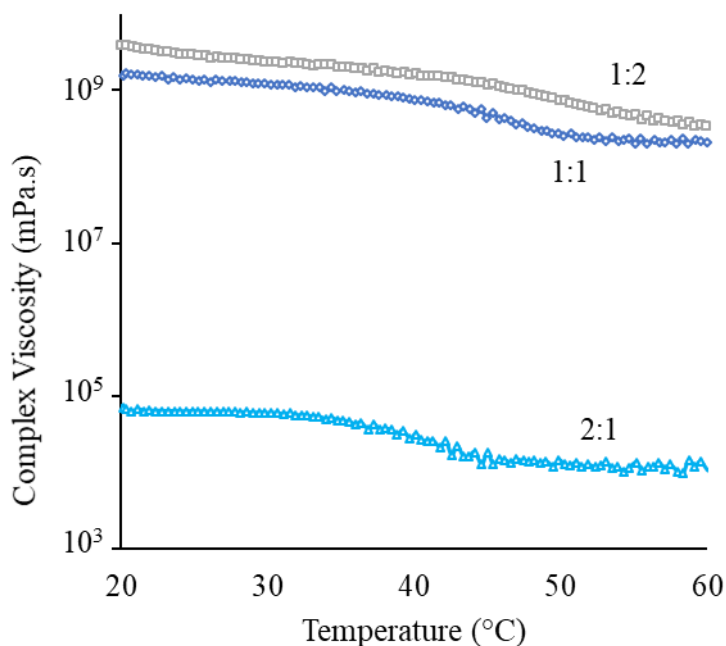


Figure 3.14. Temperature effect on the viscosity of the hydrogels with HECS:kC ratios of 2:1, 1:1 and 1:2 between 20-60 °C.

3.2.8 *Ex Vivo* Adhesion Strength of HECS-kC Hydrogels

A hydrogel based wound dressing should be able to adhere to the wound site to seal the wound and facilitate healing (He et al., 2020). On the other hand, an excessively strong adhesion may prevent on-demand removal of the wound dressing by causing secondary injuries on removal (Nam & Mooney, 2021). To investigate the adhesive strength of HECS:kC hydrogels, lap shear strength tests were conducted by applying

the hydrogel samples to sheep and chicken dermal tissues. According to the tests, HECS:kC hydrogel groups with ratios of 1:1 and 1:2 exhibited an adhesive strength of 10.65 kPa and 10.48 kPa on chicken skin and 3.49 kPa and 5.61 kPa on sheep skin, respectively (**Figure 3.15**). Higher adhesive strength on chicken skin might suggest the hydrogel can interact (topologically) better with thinner and flexible chicken skin-like dermal tissues as compared to thicker and relatively harder sheep skin-like dermal tissues. On the same type of dermal tissue, the hydrogels with different HECS:kC ratios yielded similar results. This adhesion performance might be due to the electrostatic interactions between negatively (sulfate groups) or positively charged groups on HECS:kC (amine groups) with the groups of opposite charges on dermal tissues and hydrogen bonds (Khaliq et al., 2022). It was also reported that chitosan can interact with the phospholipid molecules on the cell membranes via hydrophobic interactions which also contribute to the adhesion (Felippe J. Pavinatto et al., 2007). Chitosan based adhesive hydrogels reported in other studies demonstrated similar adhesive strength on porcine skin (Qu et al., 2018) (He et al., 2020).

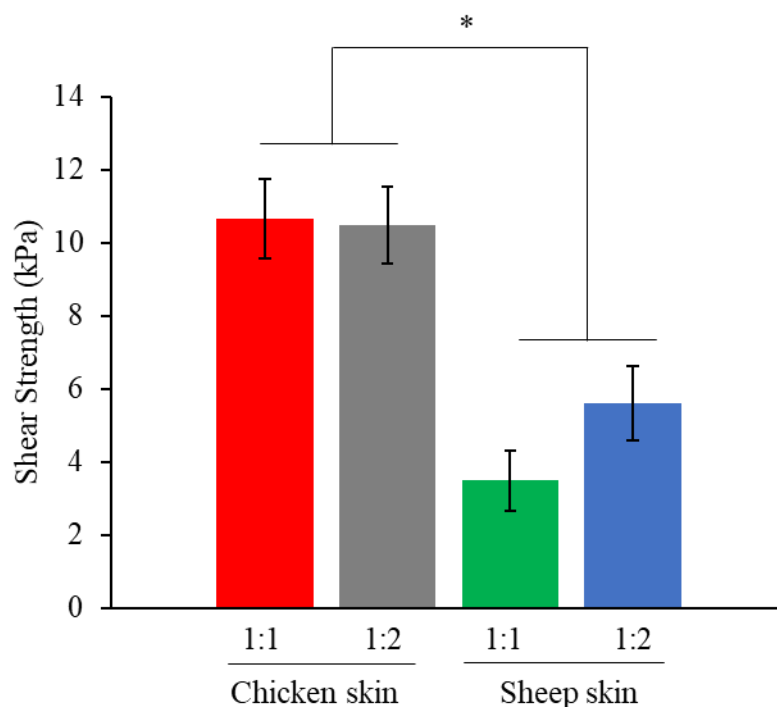


Figure 3.15. *Ex vivo* adhesion strength of hydrogels with HECS:kC ratios of 1:1 and 1:2. * denotes significant difference between the groups ($p < 0.05$, $n \geq 3$).

3.2.9 Antimicrobial Activity of Storax Loaded HECS-kC Hydrogels

Storax obtained from *Liquidambar orientalis* Mill, a tree endemic to Muğla province of Turkey, has been used traditionally by the locals for centuries for its topical antiseptic and paraciticide effects (Karadeniz et al., 2013). Minimum inhibitory concentration of storax on various microorganisms were reported previously (Okmen et al., 2014). Herein, we report the antimicrobial activity of storax loaded HECS:kC hydrogels against *S. aureus*.

Due to its hydrophobic property, storax concentrations higher than 1 mg/mL noticeably impeded the gelation process. To test the surface antimicrobial activity of

storax loaded hydrogels (1 mg/mL) and blank hydrogels, *S. aureus* suspensions with 10^8 CFU/mL were added onto the hydrogels for 3 hours of incubation followed by spread-plating for CFU counting (**Figure 3.16**). As compared to the control group treated with PBS, the lowest bacterial survival of 10.4% was observed with the storax loaded hydrogel with the HECS:kC ratio of 2:1 whereas the highest bacterial survival of 86.3% was observed with the blank hydrogel with the HECS:kC ratio of 1:2 (**Figure 3.17**). Increasing the ratio of HECS in the blank hydrogels from 33% to 66% has increased antimicrobial activity by 56.2% which demonstrated the antimicrobial activity of chitosan and its derivatives as ubiquitously reported in the literature (J. Li & Zhuang, 2020). The results also showed that the incorporation of storax in the hydrogels had a significant effect to further enhance the antimicrobial activity; for the hydrogel with the HECS:kC ratio of 1:2, the mean difference between the storax loaded hydrogels and blank hydrogels was 29.2% in terms of their bacterial survival ratios. This result agrees with the previous studies that demonstrated the antimicrobial activity of storax (10%) against Gram-positive and Gram-negative bacteria through an inhibition zone test (Sağdıç, Özkan, Özcan, Özçelik, et al., 2005).

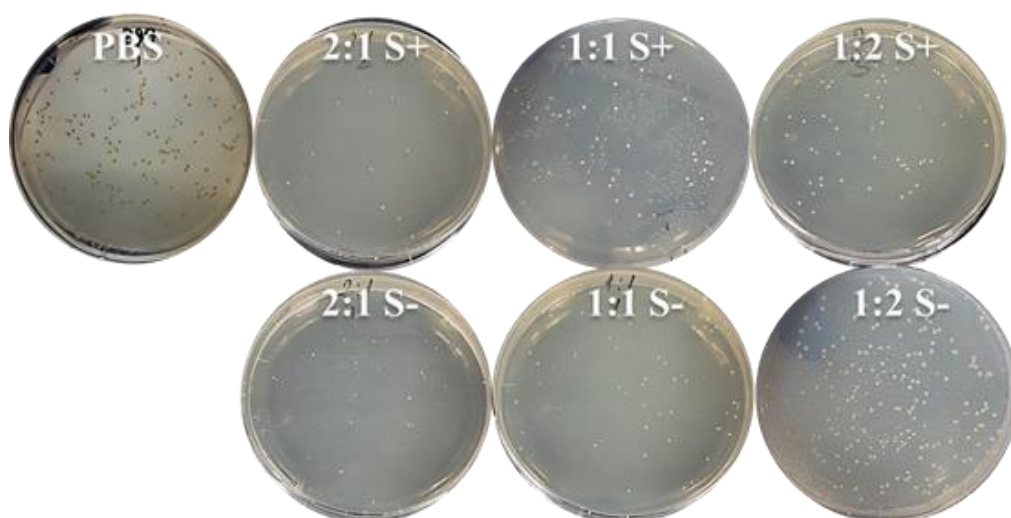


Figure 3.16. Representative images of *S. aureus* agar-plates treated with blank and storax loaded hydrogels with different HECS:kC ratios. 2:1, 1:1 and 1:2 represents

the HECS:kC ratio in the hydrogels and S+ represents the hydrogels loaded with storax (1 mg/mL) while S- represents the blank hydrogels.

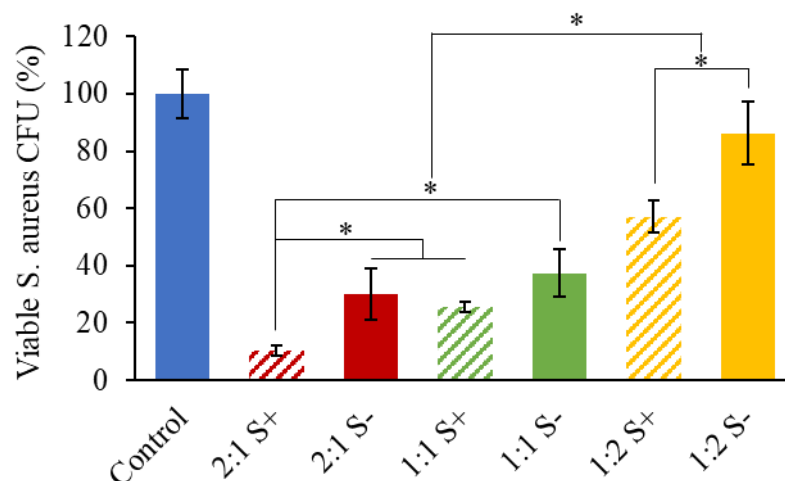


Figure 3.17. Antimicrobial activity of blank and storax loaded hydrogels with different HECS:kC ratios against *S. aureus*. 2:1, 1:1 and 1:2 represents the HECS:kC ratio in the hydrogels and S+ represents the hydrogels loaded with storax (1 mg/mL) while S- represents the blank hydrogels (*p < 0.05, n=3).

3.3 Characterization of PCL-DOP Asymmetric Membranes

3.3.1 FTIR Analysis of PCL-DOP Asymmetric Membranes

The characteristic FTIR peaks for PCL can be seen at 2949 cm^{-1} (asymmetric $-\text{CH}_2$ stretching), 2868 cm^{-1} (symmetric $-\text{CH}_2$ stretching), 1726 cm^{-1} (carbonyl stretching), 1294 cm^{-1} (C–O and C–C stretching), 1239 cm^{-1} (asymmetric C–O–C stretching), and 1169 cm^{-1} (symmetric C–O–C stretching) (Tayebi et al., 2021). After the polydopamine coating of the PCL membranes, the stretching vibration of -OH at

3350 cm^{-1} and N-H bending peak at 1600 cm^{-1} were ascribed to the polydopamine coating of PCL membrane (PCL-DOP) (**Figure 3.18**) (Zuppolini et al., 2020).

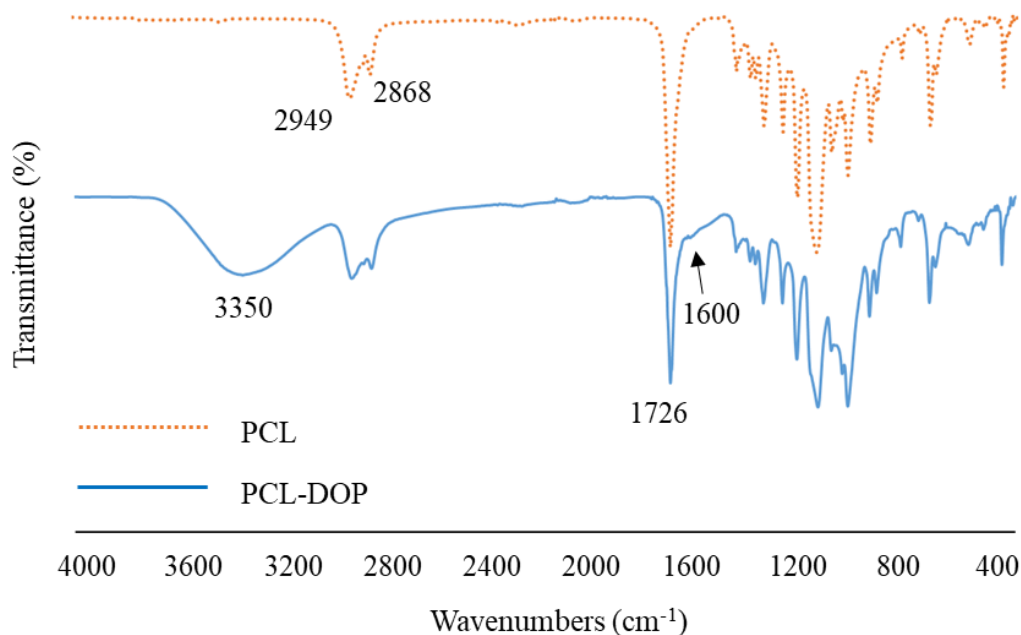


Figure 3.18. FTIR spectra of PCL and PCL-DOP.

3.3.2 Water Vapor Transmission Rate of PCL-DOP Membrane

The water vapor transmission rate (WVTR) across the surface of a wound dressing is an important parameter in healing process. WVTR depends on the structural properties such as porosity and thickness, chemical characteristics of the material as well as the ambient humidity and temperature (Morgado et al., 2014a). An ideal wound dressing would not allow rapid water loss that leads to the dehydration of the wound site while allowing sufficient vapor transfer to prevent exudate and pressure build up (Morgado et al., 2015). It has been reported that the WVTRs for normal skin, first degree burns, and granulating wounds are 204 ± 12 , 279 ± 26 , and $5138 \pm$

202 g/m² day, respectively. In addition, it was recommended that wound dressings have WVTRs in the range of 2000–2500 g/m² day (Y. Chen et al., 2011).

PCL-DOP (7,5%) allowed a water vapor transmission at 2130 (±240) g/m² day (**Figure 3.19**). Furthermore, a WVTR of 2188 (±239) g/m² day of the PCL (7.5%) membrane with no polydopamine coating (blank) indicates that the polydopamine coating of the membranes did not yield a significant change in terms of WVTR. On the other hand, PCL (10%) membrane's WVTR was measured to have 1560 (±80) g/m² day, which is below the ideal range for wound dressings and therefore it was not chosen for further testing. Therefore, PCL-DOP abbreviation will be used for PCL-DOP (7.5%) in the following sections. Ultimately, PCL-DOP (7.5%) membrane showed better WVTR when compared to the commercially available wound dressings such as Comfeels®, Dermiflexs®, Tegaderms®, and OpSites® with WVTRs about 285, 76, 491 and 792 g/m² day.

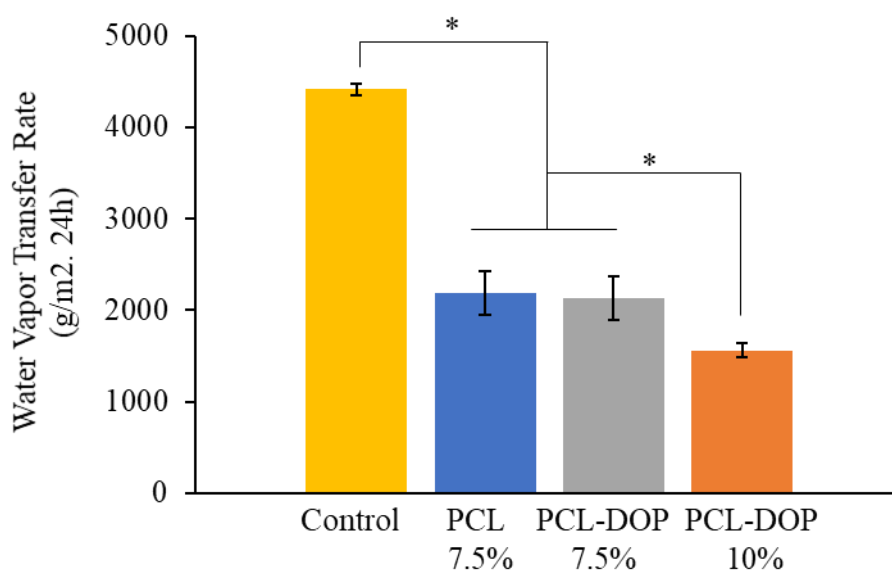


Figure 3.19. Water vapor transmission rate of asymmetric PCL membranes (*p < 0.05, n=6).

3.3.3 Oxygen Permeability of Asymmetric PCL-DOP Membrane

Oxygen permeability is an important parameter for wound dressings since hampered oxygen transfer rates delays the healing process (Shafique et al., 2021). The solubility of oxygen in water depends on crucially on-air pressure, temperature and the salinity of water (Xing et al., 2014). The test was conducted at 932 m altitude which corresponds to 0.89 atm air pressure and 25°C temperature. The salinity of the water sample has a direct relationship with its conductivity and the specific conductance of the water sample was 43 $\mu\text{S}/\text{cm}$. According to DOTABLES software (U.S. Geological Survey) (<https://www.usgs.gov/software/dotables>) an oxygen-saturated water sample in the above-mentioned conditions would have 7.32 ppm dissolved oxygen.

Prior to the test, all the water samples were first boiled for 10 minutes to remove any already-dissolved oxygen (B. Singh et al., 2013). Afterwards, positive control samples (open flask), test samples and negative control samples (closed flask) were covered with nothing, PCL-DOP membranes and plastic bottle cap, respectively. Afterwards the samples were mixed at 600 rpm in 125 mL Erlenmeyer flasks (3.14 cm^2 of test area) at 25°C. After 24 hours, water samples were taken from the flasks to fill 10 mL volumetric flasks for the Winkler's dissolved oxygen assay. After the assay was conducted, open flasks, closed flasks and PCL-DOP (7.5%) were found to have 5.45 (± 0.1) ppm, 0.86 (± 0.02) ppm and 5.05 (± 0.12) ppm dissolved oxygen, respectively (**Figure 3.20**).

A similar test was conducted with acacia gum-carbopol based hydrogel and 5.63 (± 0.06) ppm dissolved oxygen with %79 saturation with respect to open flask (B. Singh et al., 2013). The results indicate that the PCL-DOP membranes allow water-

dissolved oxygen permeability of %92 in comparison to an open flask. The porous structure of the membranes allowed high water-dissolved oxygen permeability (Rakhshaei & Namazi, 2017).

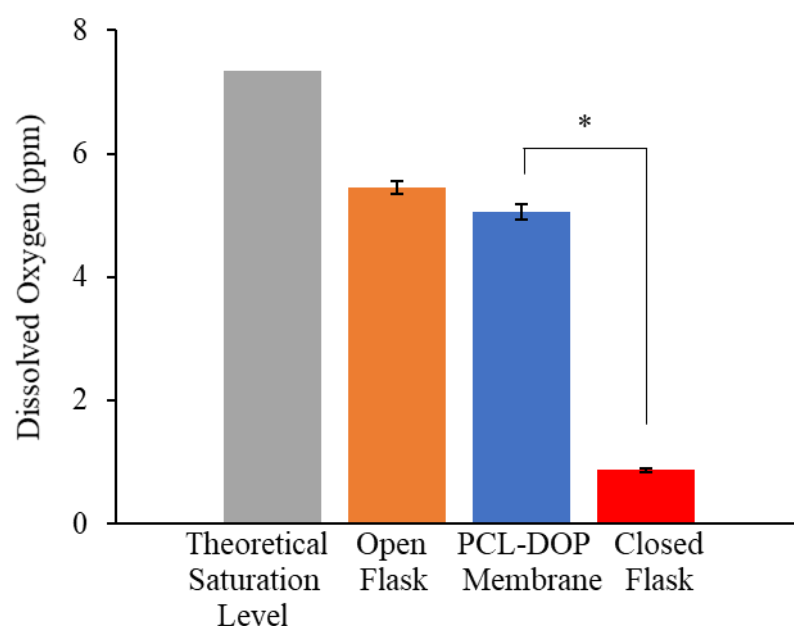


Figure 3.20. Oxygen permeability of asymmetric PCL-DOP membrane (* $p < 0.05$, $n=3$).

3.3.4 Mechanical Properties of Asymmetric PCL-DOP Membrane

The top layer of the wound dressing has been sought to increase the mechanical strength of the overall structure against tensile forces. **Figure 3.21** shows the tensile characteristics of the PCL-DOP membranes. The membrane exhibited a tensile modulus of ~76 kPa and a tensile strength of 805kPa at 100% strain. There is a scarcity of studies using the same fabrication method and polymer in the literature for comparison however the ideal tensile strength range for wound dressing and skin cell culture is 0.8–18 MPa (Eskandarinia et al., 2020).

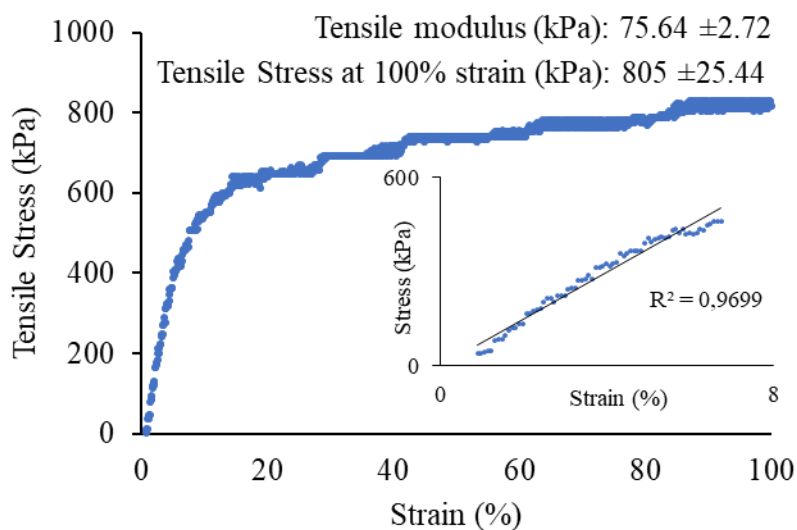


Figure 3.21. Representative tensile stress-strain curve of PCL-DOP membrane. The inset figure shows the representative stress-strain curve used to compute the elastic modulus.

3.3.5 Adhesion Strength of Asymmetric PCL-DOP Membrane

The purpose of the top layer of the bilayered wound dressing is to provide the underlying hydrogel a mechanical support while allowing optimum exchange of air and preventing bacterial penetration. To achieve this objective, asymmetric PCL-DOP membrane should be able to adhere to the HECS:kC hydrogel however this adhesion should not be excessively strong so that upon necessity, poorly degradable asymmetric PCL-DOP membrane can be easily removed on-demand. To test the adhesion strength between the hydrogel and the asymmetric membrane lap shear tests were conducted. According to the tests, there was no significant difference between the two hydrogel groups. However, there was a significant difference between asymmetric PCL membranes and asymmetric PCL-DOP membranes. Adhesion strength was ~22,5 kPa for PCL and ~31 kPa for PCL-DOP (**Figure 3.22**). This adhesion strength might be due to the hydrophobic interactions between PCL

and HECS as well as electrostatic interactions between the carbonyl groups of PCL and amine groups HECS. In addition to the chemical interactions, topological adhesion and mechanical interlocking could be in effect due to the highly porous nature of the asymmetric membranes (J. Yang, Bai, et al., 2020). Study of the adhesion between asymmetric PCL membrane and a hydrogel is an innovation and there is not any study in the literature to compare our results.

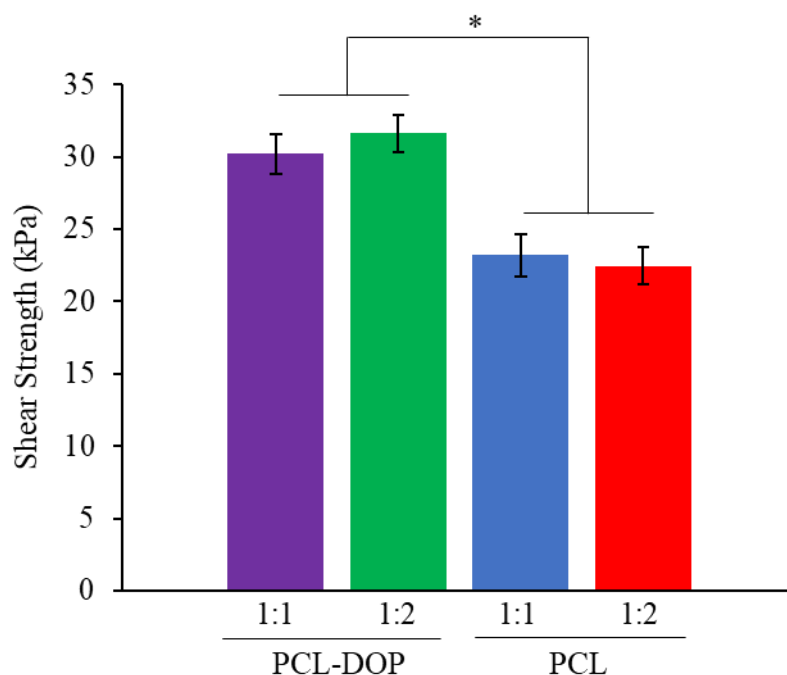


Figure 3.22. *In vitro* adhesion strength of asymmetric PCL and PCL-DOP membranes on hydrogels with HECS:kC ratios of 1:1 and 1:2. * denotes significant differences ($p < 0.05$, $n \geq 3$).

3.3.6 Microbial Penetration Tests of Asymmetric PCL-DOP Membrane

The ability of a wound dressing to prevent bacterial penetration into wound site while allowing sufficient aeration has a focal importance for wound healing process. To

conduct the test, sterile nutrient broth filled tubes were left open as the positive control, the negative control tubes were closed with cotton gauze and the test tubes were covered with PCL-DOP membranes. After 7 days at $\sim 25^{\circ}\text{C}$, the samples were measured in a spectrophotometer at 600 nm for absorbance and the results were normalized with the initial sterile nutrient broth's optical density. The results showed that there was no significant difference between the closed tubes and test tubes, indicating that PCL-DOP membranes effectively prevent microbial penetration (**Figure 3.23**). The same method was used to test sericin-collagen based wound dressing film with similar results (Akturk et al., 2011).

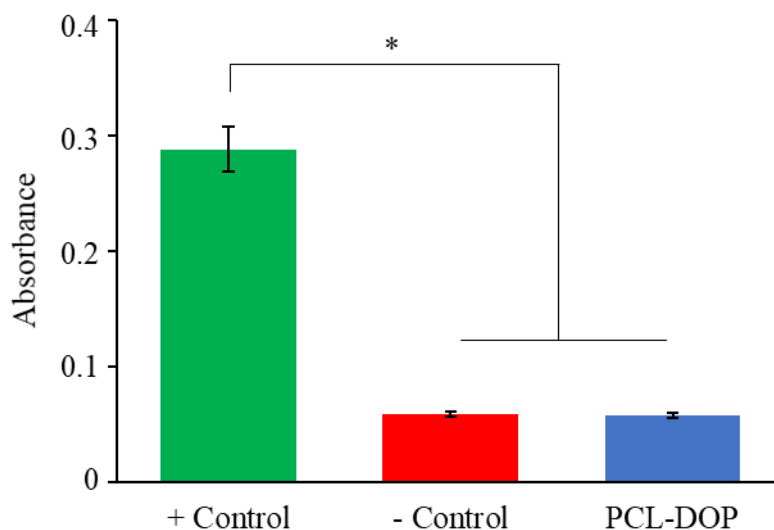


Figure 3.23. Microbial penetration from PCL-DOP membrane.* denotes significant difference between the groups ($p < 0.05$, $n=3$).

3.3.7 Water Contact Angle Analysis of Asymmetric PCL-DOP Membrane

Water contact angle assay reflects the hydrophilicity of PDA coated PCL membranes (PCL-DOP). PDA coating enables mussel-inspired (catechol-based) adhesion of materials onto wet surfaces, such as hydrogels (Zuppolini et al., 2020). Information on the underlying chemical interactions of catechol-based adhesion can be found elsewhere (Saiz-Poseu et al., 2019).

Figure 3.24 shows the difference between PCL and PCL-DOP membranes before and after dopamine treatment in terms of their water contact angles. While the contact angle for PCL was $76.5^\circ (\pm 10)$, PCL-DOP was able to achieve significant hydrophilicity by $48.2^\circ (\pm 4.2)$. In comparison to our study, the blank electrospun PCL meshes demonstrated higher hydrophobicity by 107.9° while PDA coated PCL showed 27.7° (M. Liu et al., 2017).

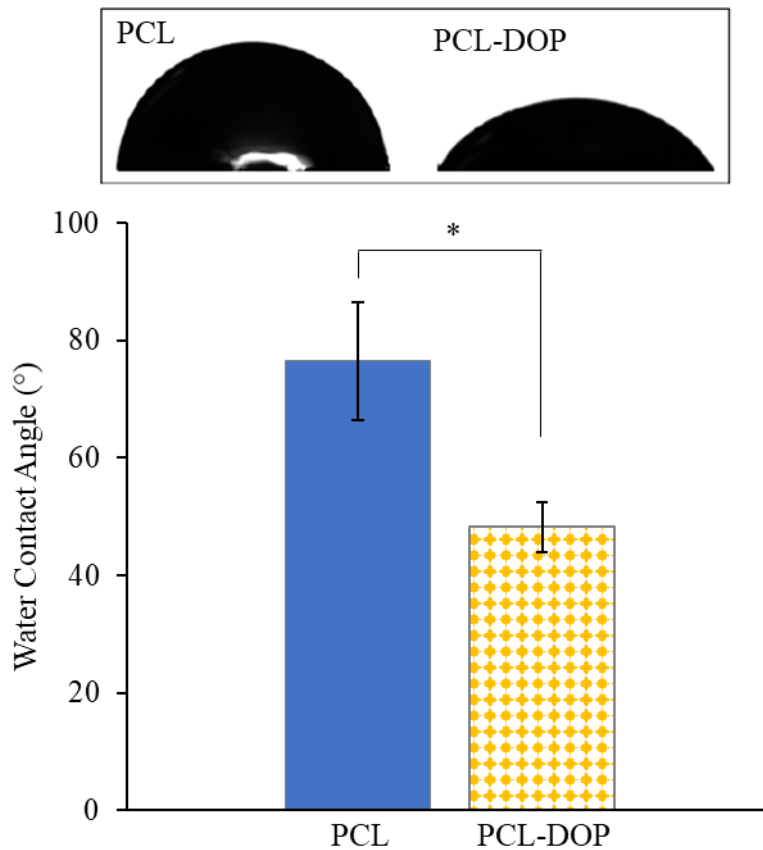


Figure 3.24. Water contact angle analysis for PCL and PCL-DOP membranes. Inset figure shows representative contact angles (* $p < 0.05$, $n=3$).

3.3.8 Porosity and Scanning Electron Microscopy Analysis of Asymmetric PCL-DOP Membrane

Porosity as well as thickness of membranes can theoretically have an effect on mass transfer rates through the membrane which is crucial in fulfilling its designed function the bilayered wound dressing. The uncoated PCL membrane was measured to have 72% porosity which is significantly higher than the polydopamine-coated PCL membrane with 40% porosity (**Figure 3.25**). As it can be confirmed from the scanning electron microscopy images, the polydopamine has covered the surface of

the membranes and the walls of the interfacial microvoids formed during non-solvent induced phase separation. Scanning electron microscopy images also demonstrate how the coating affected the surface characteristics of the membrane, yielding a smoother surface by filling the crevices on the membrane and visibly decreasing the pore sizes (**Figure 3.26**). PCL membranes prepared with the same principal method in other studies reported comparable results in terms of surface morphology and porosity (Sohn et al., 2015; Yen et al., 2009).

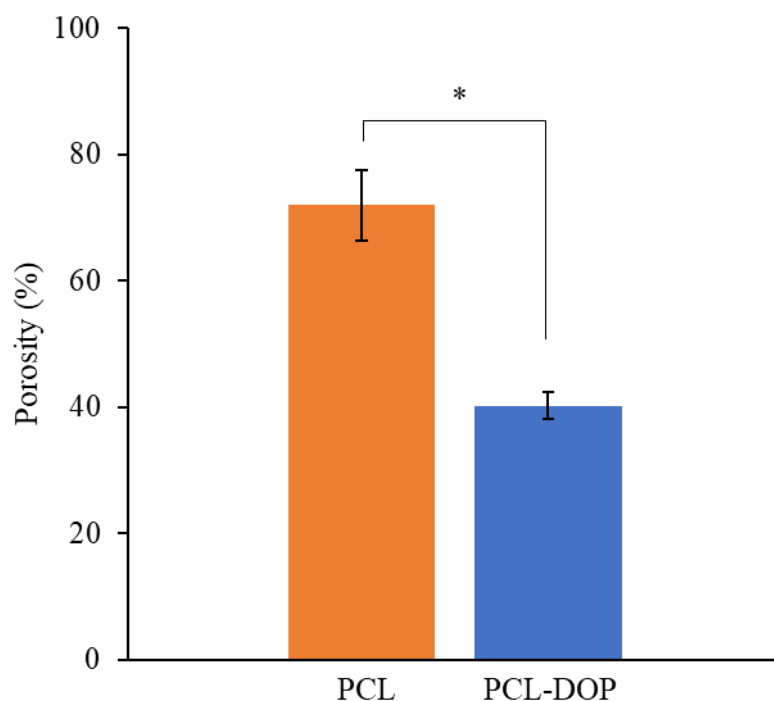


Figure 3.25. Porosity of PCL and PCL-DOP membranes. * denotes significant difference between the groups ($p < 0.05$, $n=3$).

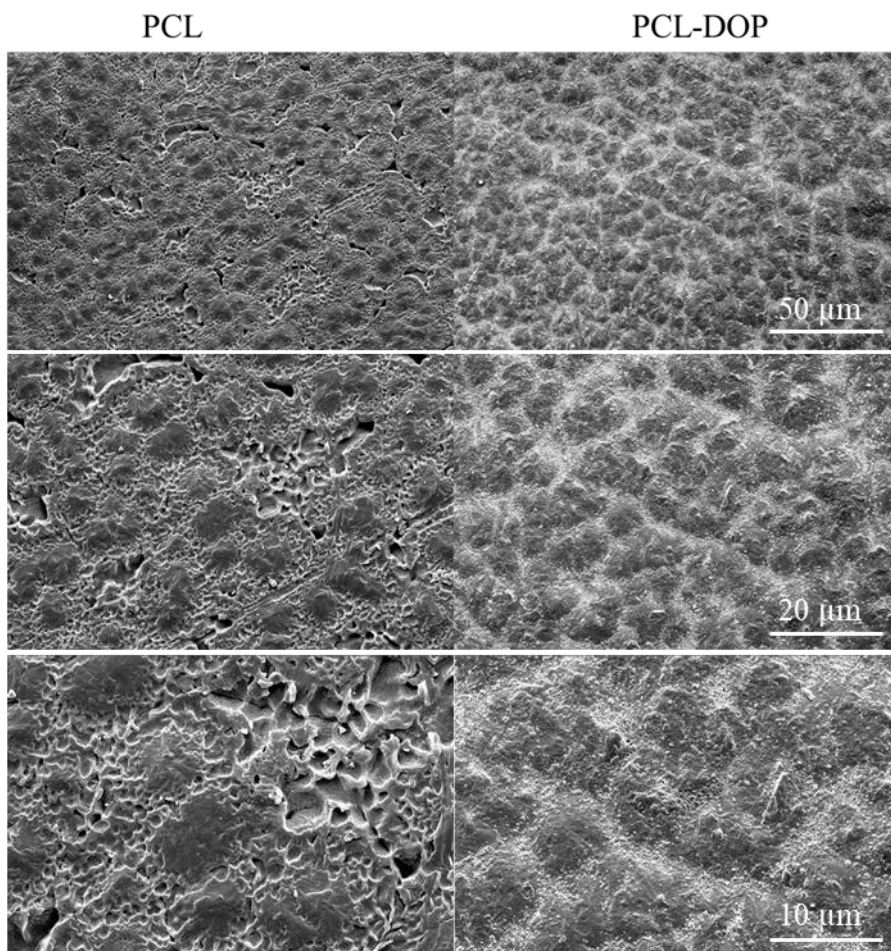


Figure 3.26. Scanning electron microscopy images of PCL and PCL-DOP membranes.

3.4 *In vitro* Cytocompatibility and Antioxidant Analyses

3.4.1 Dose Dependent Cytotoxicity of *Liquidambar orientalis* Mill. Storax

Dose dependent cytotoxicity of storax was tested on L929 mouse fibroblast cells by MTT analysis. After 24 hours of incubation the results showed 89%, 73% and 30% cell viability for the storax concentrations of 0.5 µg/mL, 5 µg/mL and 50 µg/mL,

respectively (**Figure 3.27**). Similarly, a previous study reported that viability of human lymphocytes was above 75% after 24 hours incubation with different storax concentrations between 0.4 $\mu\text{g/mL}$ and 4 $\mu\text{g/mL}$ (Karadeniz et al., 2013).

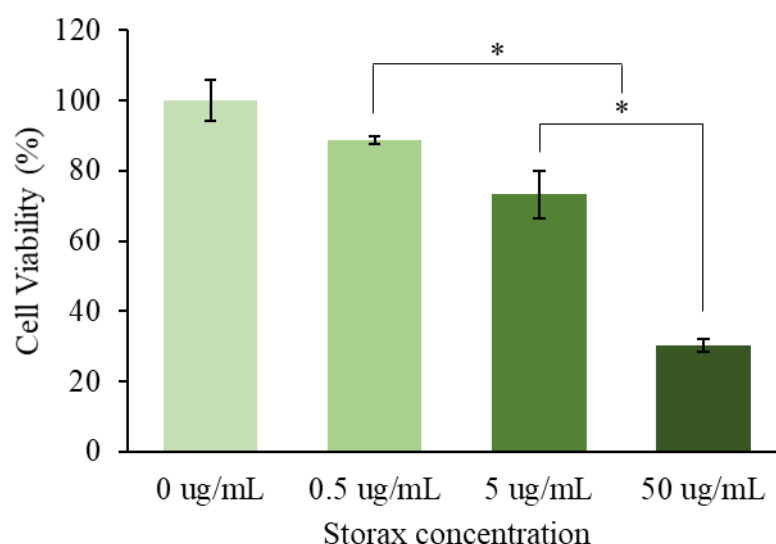


Figure 3.27. Cytocompatibility of storax on L929 mouse fibroblast cells. * denotes significant difference between the groups ($p < 0.05$, $n=3$).

3.4.2 Cytocompatibility of Blank and Storax Loaded HECS-kC Hydrogels

In order to evaluate the cytocompatibility of hydrogels, 1 mg/mL storax loaded hydrogels with HECS:kC ratios of 1:1 and 1:2 were prepared. Hydrogels with the same HECS:kC ratios were also prepared without storax (blank hydrogels). Leachable fractions of these hydrogels were collected after 24 hours and diluted 2, 5, 10, 25, 50 and 100 times prior to the cell viability test.

The results showed that all groups showed above 80% cell viability with overall mean of 112 ± 16 % and the highest cell viability of 133 ± 7 % was observed with the blank hydrogel with HECS:kC ratio of 1:1 (x2 dilution) (**Figure 3.28**). Despite the decreasing trend in the means of the hydrogel groups of the same dilution group, these differences were mostly insignificant. This indicates that neither the changing hydrogel ratios (HECS:kC ratio of 1:1 or 1:2) nor the initial presence or absence of storax (1 mg/mL) have a significant effect on the viability of the L929 cells. However, a significant difference can be seen across the dilution groups as the mean viability from the undiluted leachate group (x1) to the x100 dilution group shows a small decrease. This may be attributed to the antioxidant activity of kappa-carrageenan (Sun et al., 2010) which decreases the oxidative stress on the cells to enhance cell viability and proliferation. In fact, there are many studies reported kappa-carrageenan based hydrogels with excellent cytocompatibility (El-Aassar et al., 2015)(Fernández-Ferreiro et al., 2015)(Patel, Sant, et al., 2020)(Pettinelli et al., 2020)(Özbaş et al., 2021)(Tavakoli et al., 2020c).

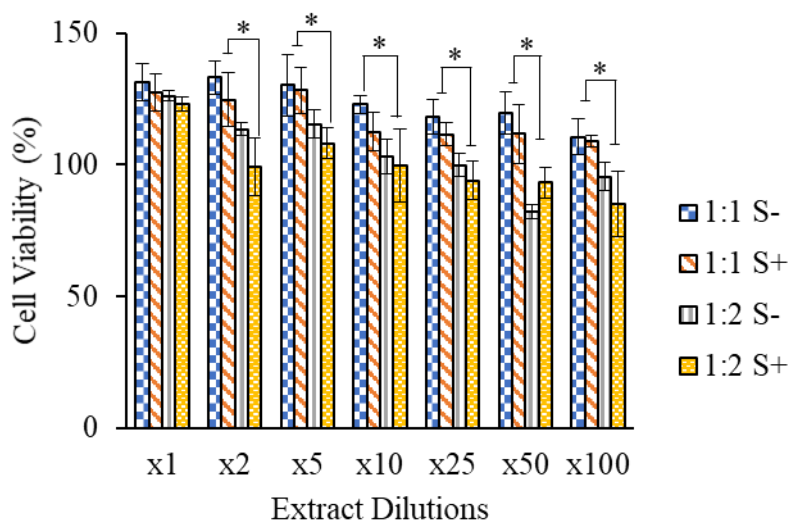


Figure 3.28. Cytocompatibility of blank and storax loaded HECS:kC hydrogels. * denotes significant difference between the groups ($p < 0.05$, $n=3$).

3.4.3 Antioxidant Activity of Storax Loaded HECS-kC Hydrogels

Elevated reactive oxygen species (ROS) in wounds can significantly impair healing processes by causing protein, nucleic acid, and lipid damages in cells and even cell death (Dunnill et al., 2017). Therefore, prevention of excessive ROS levels may enable quicker wound healing. In order to assess whether HECS:kC hydrogels or storax have the ability to rescue cells from oxidative damage, L929 fibroblasts were exposed to H₂O₂ concurrently with HECS:kC leachate and HECS:kC+storax leachate. After H₂O₂ exposure, cell viability of test groups (HECS:kC and HECS:kC +Storax) and control groups (0 μM H₂O₂ and 250 μM H₂O₂) were assayed on days 1, 4, 7 and 14. On days 1 and 4, no significant difference was observed between the groups however, from day 7 onwards, HECS:kC +Storax group demonstrated significantly higher cell viability compared to the control groups. Although HECS:kC group showed higher cellular viability compared to the control groups as well, the mean difference to the 0 μM H₂O₂ group was not significant. Similar results were also observed on day 14, with wider mean differences between the significant groups (**Figure 3.29**).

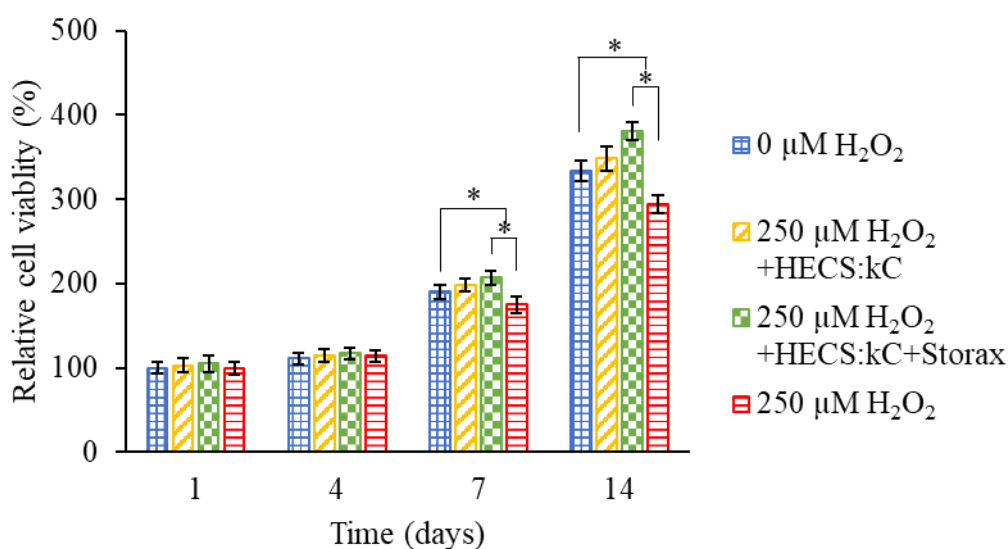


Figure 3.29. Relative cell viability of L929 fibroblasts treated with H₂O₂ in the presence of HECS:kC and HECS:kC+Storax. * denotes significant difference between the groups ($p < 0.05$, $n=5$).

Increased ROS levels can damage cell components, change size and morphology of cells (Duan et al., 2017; S. Tan et al., 1998). Morphological changes on the cells were observed with inverted phase contrast microscopy and confocal laser scanning microscopy (**Figure 3.30**). Analysis on the ability of HECS:kC and HECS:kC+Storax to rescue cells from oxidative damage demonstrated that while the cells treated with only H₂O₂ (**Figure 3.30a,e**) showed drastic morphological change with higher frequency of cells with globular shape, HECS:kC+Storax treated group (**Figure 3.30c,g**) showed less number of affected cells and resembled the cells grown in normal growth conditions (**Figure 3.30d,h**). Cells treated with only HECS:kC, on the other hand, did not demonstrate a similarly potent effect as HECS:kC+Storax did, but decreased the number of globular cells only slightly (**Figure 3.30b,f**).

Oxidative stress can cause breaks on actin filaments and disorganize the microfilament network, which prevents cell spreading (Huot et al., 1997; Y. Ma et al., 2021). When extensive damage occurs, actin filaments collapse around the nucleus to form concentrated actin patches (Rouyère et al., 2022). Therefore, quantitative analysis on cell spread areas can provide a valuable information on the extent HECS:kC and HECS:kC+Storax rescued the cells from oxidative damage. Cells grown in normal growth conditions showed a mean cell spread area of $1003 \pm 328 \mu\text{m}^2$. On the other hand, cells treated only with H₂O₂ showed $540 \pm 254 \mu\text{m}^2$. Treatment of both HECS:kC and HECS:kC+Storax together with H₂O₂ enabled better average cell spreading up to $586 \pm 307 \mu\text{m}^2$ and $860 \pm 330 \mu\text{m}^2$, respectively. Results demonstrated that HECS:kC+Storax can significantly relieve the cells from oxidative damage caused by 250 μM H₂O₂ (**Figure 3.31**).

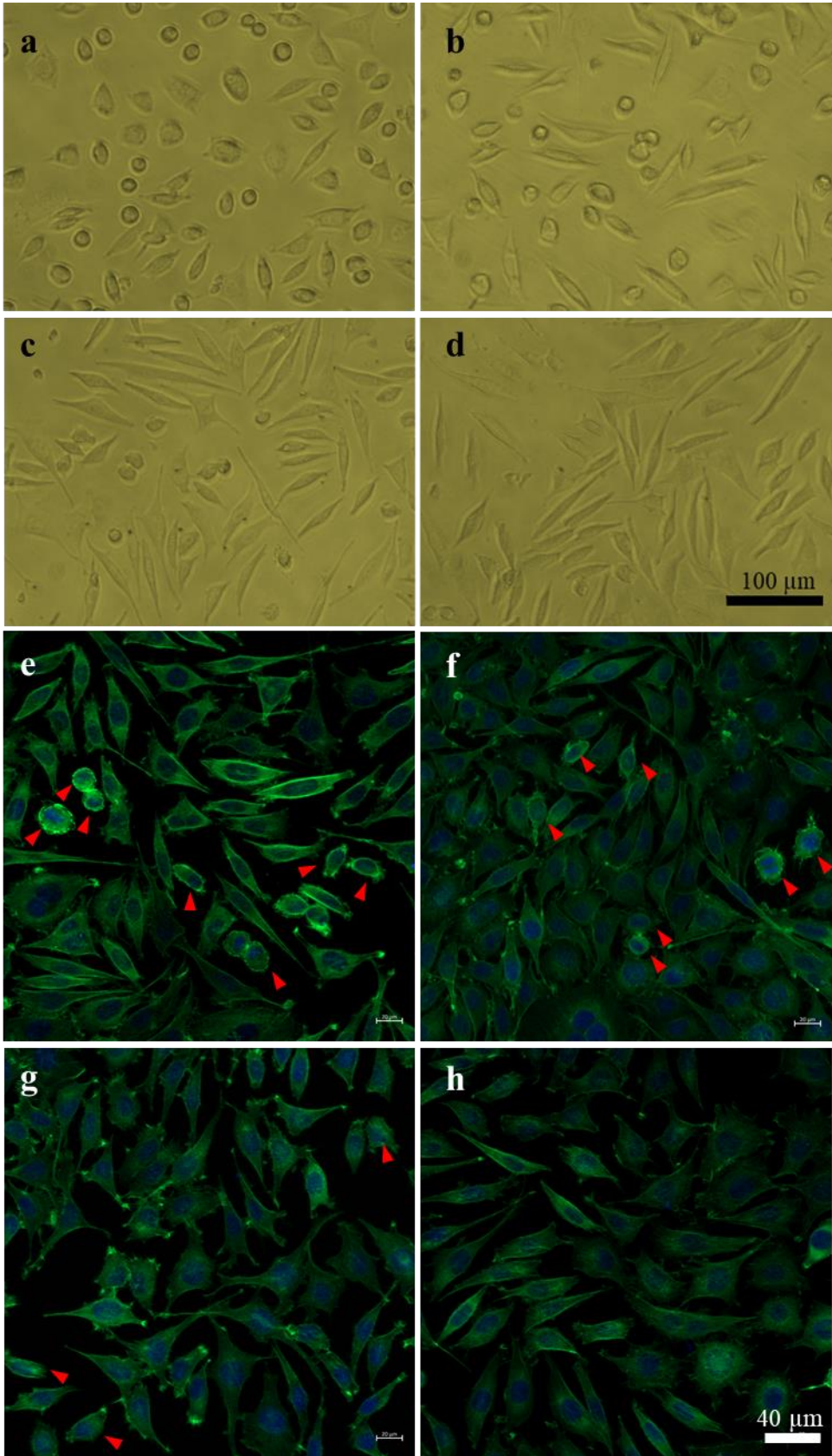


Figure 3.30. Morphological analysis of L929 fibroblasts L929 fibroblasts treated with H₂O₂ in the presence of HECS:kC and HECS:kC+Storax. (a-d) Inverted phase contrast microscopy images obtained on day 7; (e-h) confocal laser scanning microscopy images obtained on day 14. Cells treated with; only 250 μM H₂O₂ (a, e), 250 μM H₂O₂ and HECS:kC (b, f), 250 μM H₂O₂ and HECS:kC+Storax (c, g) and 0 μM H₂O₂ (d, h). Red arrow heads show globular cells under excessive oxidative stress.

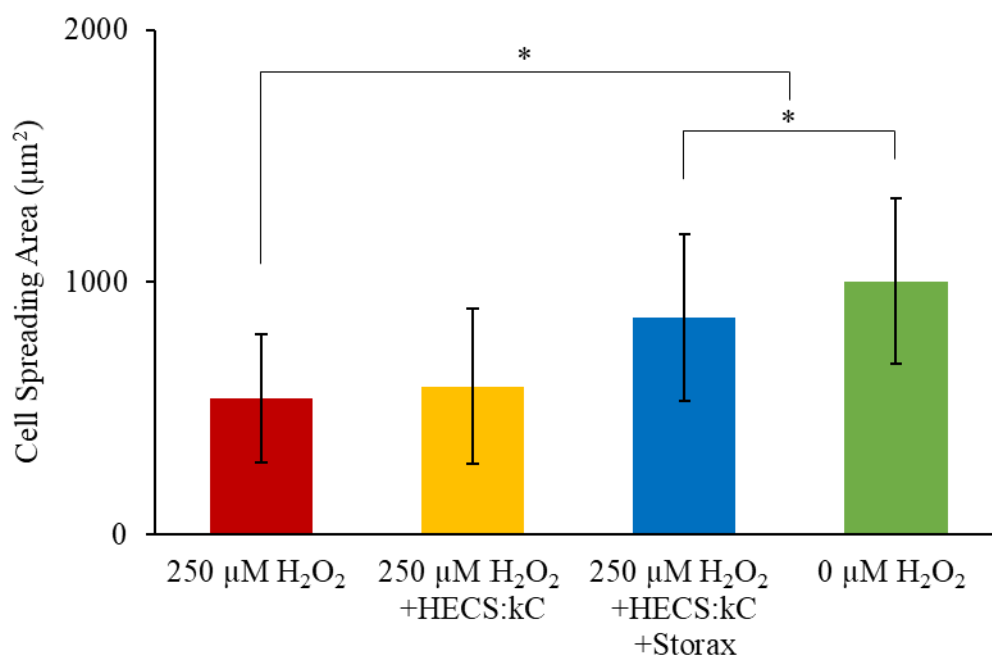


Figure 3.31. Cell spreading areas of L929 fibroblasts treated with H₂O₂ in the presence of HECS:kC and HECS:kC+Storax. * denotes significant difference between the groups ($p < 0.05$, $n > 50$).

Antioxidant activity of storax (balsam of *Liquidambar orientalis* Mill.) were previously reported to reduce inducible nitric oxide synthase, a marker for oxidative stress as well (Nalbantsoy et al., 2016; Okmen et al., 2014). In fact, gas

chromatography and mass spectrometry analyses showed that storax is consisted of a variety of phenol-rich compounds such as styrene, phenyl-propyl alcohol, cinnamyl alcohol, cinnamic acid, phenylpropyl cinnamate, styracin and some unidentified components (Hafizoğlu, 1982). Therefore, potent antioxidant activity of storax demonstrated in this study by oxidative stress-rescue experiment could be attributed to the synergistic effect of consisting phenolic compounds, which are well-known for their antioxidant activities (J. Chen et al., 2020; Rice-Evans et al., 1997; Zeb, 2020; W. Zheng & Wang, 2001).

3.5 Storax Release from HECS-kC Hydrogels

Storax release profiles from the hydrogels were examined in environments with different pH 6.4, 7.4 and 8.4. Both HECS:kC hydrogels (1:1, 1:2) demonstrated a similar biphasic release profile in different pH environments. Korsmeyer-Peppas fitting on both drug release profiles with $R^2 > 0.99$ yielded n values below 0.45 for all pH environments, which indicates that storax is released from the hydrogels with pseudo-Fickian diffusion, and lower K values indicate faster release (**Table 3.1**). Pseudo-Fickian diffusion implies that the release curve of storax resembled Fickian diffusion, however equilibrium state was reached considerably slower (Shu et al., 2023). This might be due to the fact that storax is hydrophobic and remains trapped in the hydrogel for a longer time. A similar phenomenon was also observed with *Piper crocatum* extract release from a polyvinyl alcohol-based hydrogel (Edikresnha et al., 2021).

The burst release during the first 24 hours might be due to the storax present on the surface of the hydrogels. In first 6 hours of the experiment, a release of 19.9%, 22.8% and 22.2% was observed in pH 8.4, 7.4 and 6.4, respectively for the hydrogel with HECS:kC ratio of 1:1. Other hydrogel group with HECS:kC ratio of 1:2 showed

a similar release of 20.2%, 23.3% and 22.3% in pH 8.4, 7.4 and 6.4, respectively. The slower release after 24 hours could be related with degradation of the hydrogels (~10% in pH 8.4, ~20% in pH 7.4 and ~40% in pH 6.4 environment) in the sense that the highest release was observed in acidic environment and slowest release was observed in basic environment. Considering the fact that storax has a hydrophobic nature, it has a limited solubility in the release medium and it can be released in parallel with hydrogel degradation. After the burst release in 24 hours, there was a slower release where hydrogels with HECS:kC ratios of 1:1 and 1:2 showed ~80% and ~77% release in acidic environment, 55% and 50% release in physiological pH, 46% and 43% release in basic environment in 10 days, respectively (**Figure 3.32**). The initial burst release of storax can facilitate the initial stabilization of the wound site while the slower release in the following days can provide a long-term antibacterial effect to wound. Comparable to our findings, a recently developed kC and PEG based hydrogel loaded with thyme oil as antibacterial agent demonstrated a similar release profile with ~37% release in 50 hours (P. Singh et al., 2022). Scanning electron microscopy images after 10 days of storax release from hydrogels with HECS:kC ratio of 1:1 also shows storax droplets embedded in the hydrogel structure which further supports the suggestion that the release of storax takes places in parallel with hydrogel degradation (**Figure 3.33**).

Table 3.1 Korsmeyer-Peppas values of hydrogels with HECS:kC ratios of 1:1 and 1:2 for different pH environments.

| | HECS:kC (1:1) | | | HECS:kC (1:2) | | |
|----------------------|---------------|--------|--------|---------------|--------|--------|
| | pH 6.4 | pH 7.4 | pH 8.4 | pH 6.4 | pH 7.4 | pH 8.4 |
| K | 8.983 | 14.257 | 14.894 | 9.230 | 14.697 | 15.737 |
| n | 0.431 | 0.249 | 0.211 | 0.410 | 0.229 | 0.190 |
| R² | 0.998 | 0.997 | 0.996 | 0.995 | 0.994 | 0.997 |

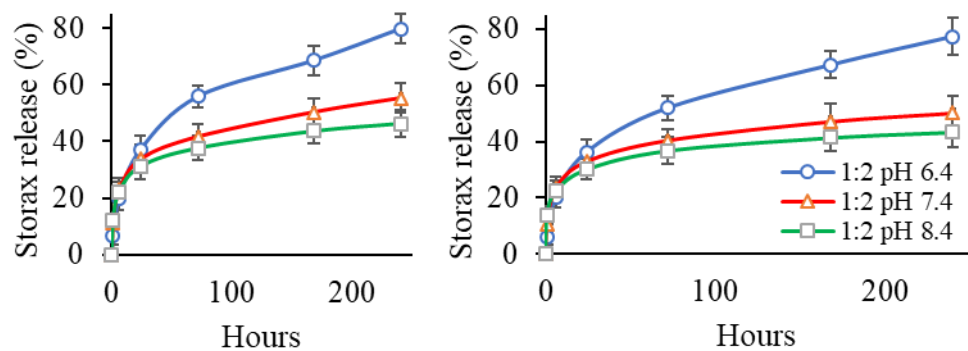


Figure 3.32. Storax release profiles from the hydrogels with HECS:kC ratios; 1:1 (left) and 1:2 (right) in different pH environment ($n \geq 3$).

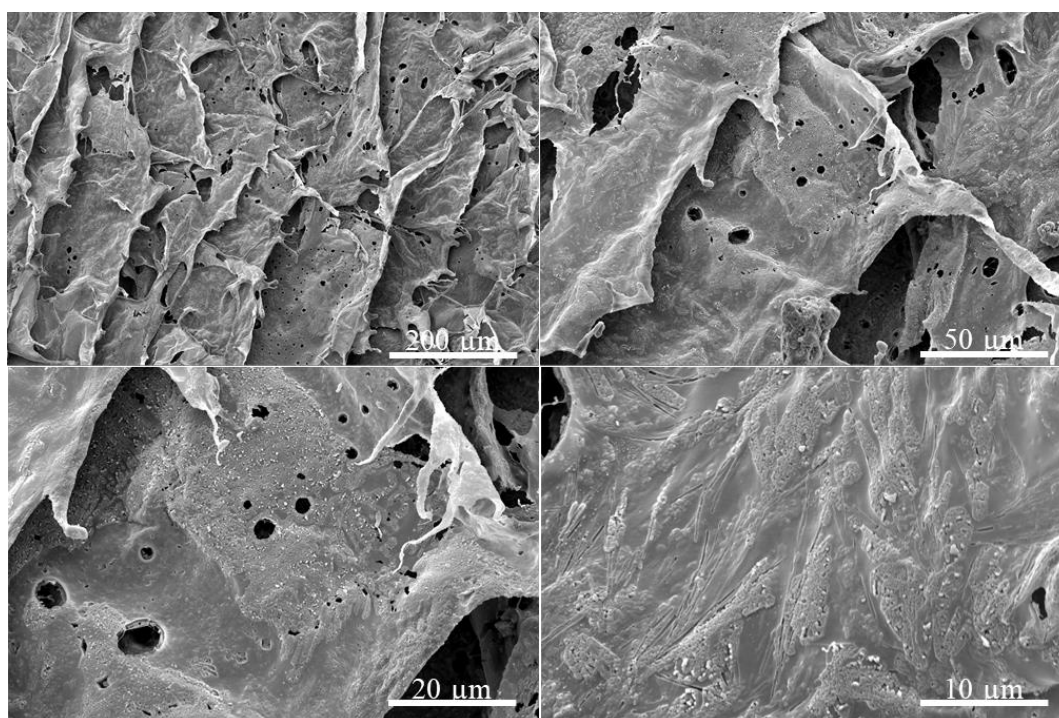


Figure 3.33. Scanning electron microscopy images of storax loaded hydrogels (HECS:kC ratio of 1:1) after 10 days of storax release in PBS at 37°C.

3.6 *In Vivo* Wound Healing Study of HECS-kC/PCL-DOP Bilayer Wound Dressing

3.6.1 Wound Closure

Full-thickness skin defect model on rats was used to determine *in vivo* effectiveness of blank HECS:kC hydrogel (1:1)-PCL-DOP asymmetric membrane and storax loaded HECS:kC hydrogel (1:1)-PCL-DOP asymmetric membrane in comparison to a commercial product TegadermTM and control (no treatment group) (**Figure 3.34**). Throughout 10 days, wounds areas were photographed and measured (**Figure 3.35**). In terms of remaining wound area, statistically significant differences between HECS:kC hydrogels (~55±15%) and Tegaderm (~75±6%) were observed as early as day 3. A similar result was observed on day 5, however it was evident that the group treated with storax loaded HECS:kC hydrogel (32±8%) began to further distinguish itself from all other groups although statistically significant differences were not yet observed as compared to the group treated with blank HECS:kC hydrogels (40±16%). By day 7, the group treated with Tegaderm remained at 32±4.4% whereas the group treated with blank HECS:kC hydrogels had only 15±2.6% of the initial wound area. On the 10th day of the experiment the remaining wound areas of the test groups were as follows: control, 15±4.5%; blank HECS:kC hydrogels 10±3.6%; storax loaded HECS:kC hydrogel 5±2.6%; Tegaderm 11±3% (**Figure 3.36**). These results indicated that storax loaded HECS:kC hydrogel had excellent wound healing effect and the fact that storax loaded hydrogel having almost half of the wound area of blank hydrogel by day 10 strongly emphasizes the effect of storax in quicker wound closure.

Although scarcely, naturally occurring compounds or their extracts were tested in hydrogels developed for wound healing in the literature. Polysaccharide isolated from Egyptian *Avena sativa* L. grains were incorporated in hydroxyethylcellulose

hydrogel and *in vivo* full-thickness rat skin defect models showed wound closure of 99% in 10 days (el Hosary et al., 2020).

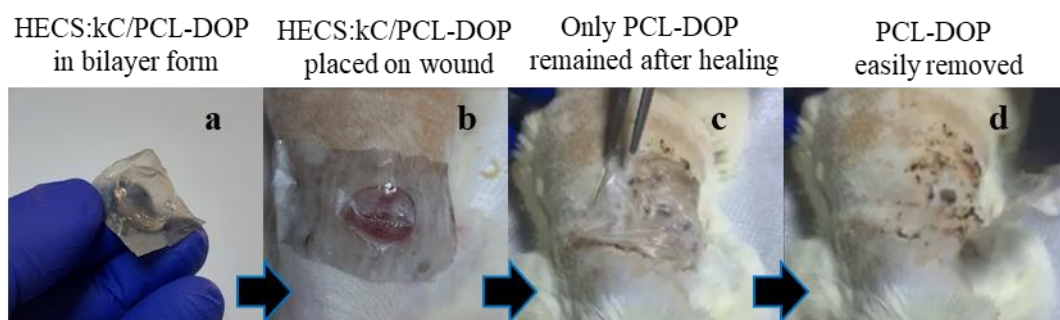


Figure 3.34. Application of HECS:kC/PCL-DOP bilayer wound dressing on rat full-thickness skin defect model. Photographs were taken on day 0 (a, b) and day 10 (c, d).

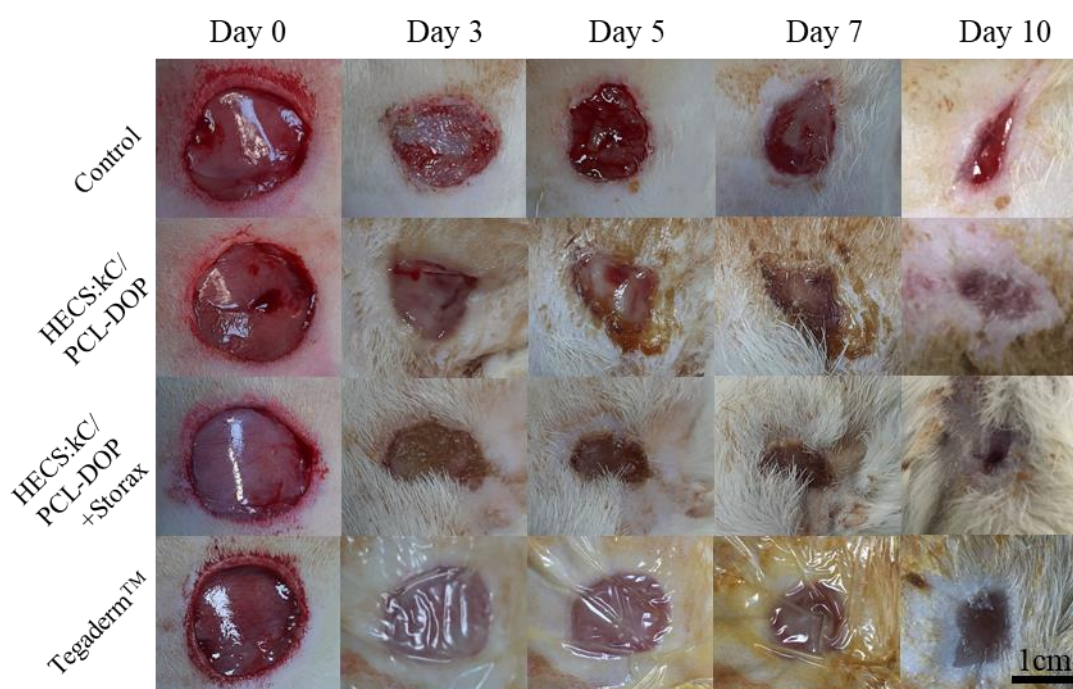


Figure 3.35. Representative images of the gross appearance of full-thickness skin defects over 10 days.

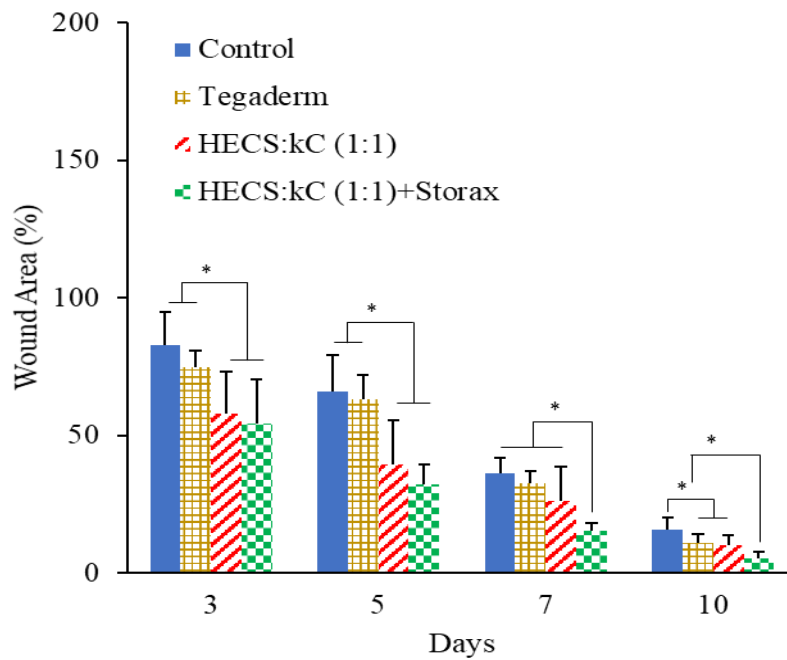


Figure 3.36. Wound closure rate at different periods of post wounding. * denotes significant difference between the groups ($p < 0.05$, $n=7$).

3.6.2 Histological Examination

Histological examination of rat full-thickness skin defect models was conducted on 5th and 10th days postoperative. Tissue samples of the test groups were stained with Masson's trichrome and hematoxylin-eosin and systematically evaluated based on several criteria after light-microscopy inspection. Tissues samples obtained from healthy skin were also stained and visualized as a reference (**Appendix E Figure 1** and **Appendix E Figure 2**). Masson's trichrome staining on day 5 showed a thick scab formation in the control group and absence of epithelialization at the center of the defect, unlike other groups. Rats treated with Tegaderm showed initial epithelialization and a thick granulation tissue. HECS:kC hydrogel treated group showed similarly thick granulation and partial epithelialization whereas storax

loaded HECS:kC hydrogel had clear epithelialization and epithelial thickening (Figure 3.37).

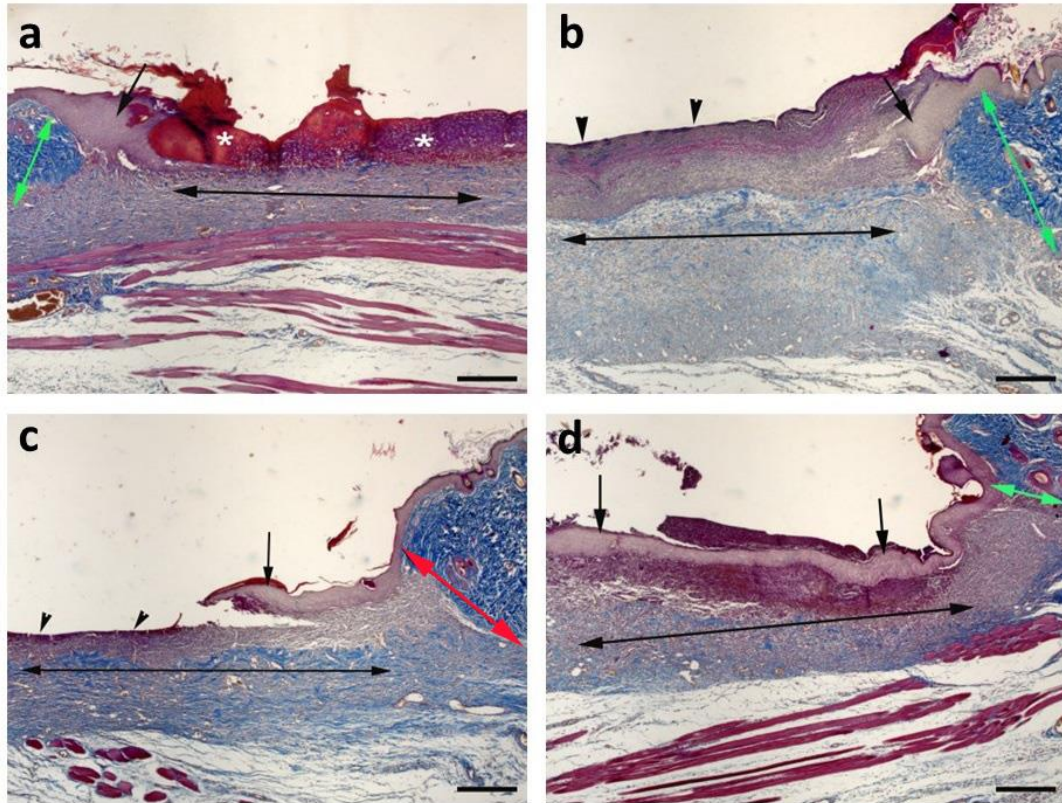


Figure 3.37. Histological evaluation of Masson's trichrome stained full-thickness skin defect representative tissue samples on day 5. **(a)** Control, **(b)** Tegaderm, **(c)** HECS:kC hydrogel, **(d)** Storax loaded HECS:kC hydrogel. Scale bar: 250 μ m. **(a)** Granulation tissue in defect area (double headed black arrow), normal skin tissue-defect border (double headed green arrow), epidermal thickening on defect edge (black arrow), scab formation (white asterisk). **(b)** Granulation tissue in defect area (double headed black arrow), normal skin tissue-defect border (double headed green arrow), epidermal thickening on defect edge (black arrow), insufficient epithelialization (arrow head). **(c)** Granulation tissue in defect area (double headed black arrow), normal skin tissue-defect border (double headed red arrow), partial epithelialization and epidermal thickening (black arrow), insufficient

epithelialization at the center of the defect (arrow head). **(d)** Granulation tissue in defect area (double headed black arrow), normal skin tissue-defect border (double headed green arrow), sufficient epithelialization on defect area and subsequent epidermal thickening (black arrow).

On day 10, neovascularization could be seen in all groups. Control group could develop thick granulation tissue by day 10 and showed insufficient epithelialization at the center. HECS:kC hydrogel group and Tegaderm group showed similar healing although Tegaderm showed partial epithelialization and weak epidermal thickening. Group treated with storax loaded HECS:kC hydrogel, on the other hand, developed epidermis and epithelialization similar to normal skin as well as the dermis layer which had closely resembled normal skin **Figure 3.38**.

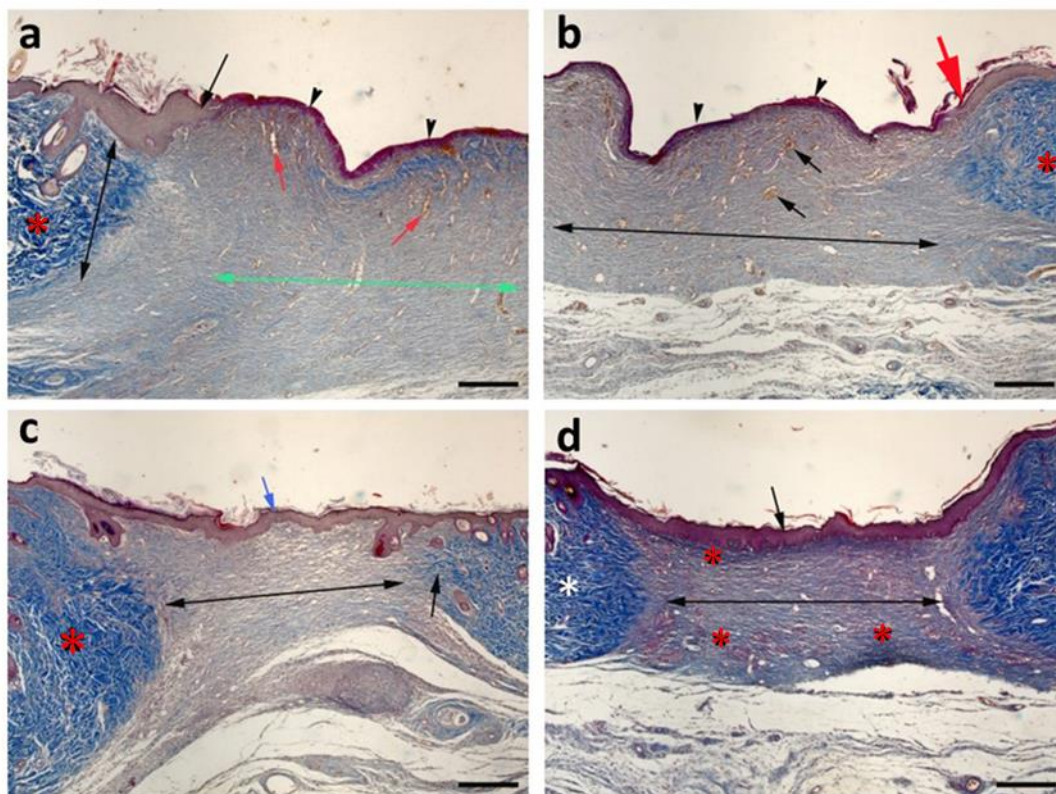


Figure 3.38. Histological evaluation of Masson's trichrome stained full-thickness skin defect representative tissue samples on day 10. **(a)** Control, **(b)** Tegaderm, **(c)** HECS:kC hydrogel, **(d)** Storax loaded HECS:kC hydrogel. Scale bar: 250 μ m. **(a)** Thick granulation tissue (double headed green arrow), normal skin-defect border (double headed black arrow), partial epithelialization and epidermal thickening (black arrow), insufficient epithelialization at the center of the defect (arrow head), neovascularization (red arrows), normal skin (red asterix). **(b)** Granulation tissue in defect area (double headed black arrow), normal skin (red asterix), insufficient epithelialization and epidermal thickening (red arrow), insufficient epithelialization at the center of the defect (arrow head), neovascularization (black arrow). **(c)** Granulation tissue in defect area (double headed black arrow), normal skin (red asterix), type-1 collagen remodeling areas (black arrow), epidermis and epithelialization similar to normal skin (blue arrow). **(d)** Granulation tissue in defect area (double headed black arrow), type-1 collagen remodeling in granulation tissue (red asterix), normal skin (white asterix), epidermis and epithelialization similar to normal skin (black arrow).

Hematoxylin-eosin staining of the samples obtained from control group on day 5 also demonstrated a large scab formation, very weak epithelialization and rare neovascularization (**Figure 3.39a**). In addition, large number of neutrophil granulocyte and macrophage infiltration was observed (**Figure 3.39b**). Tegaderm treated group on day 5 postoperative exhibited scab formation with partial epithelialization on a thick granulation tissue (**Figure 3.40a**). Moderate neovascularization was accompanied by large infiltration of neutrophil granulocytes and macrophages (**Figure 3.40b**).

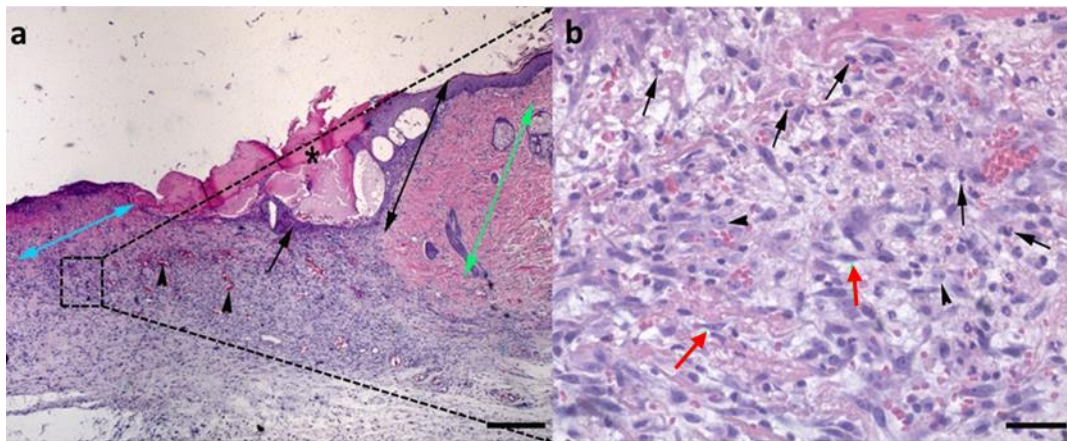


Figure 3.39. Control group, day 5. Hematoxylin-eosin stained full-thickness skin defect representative tissue samples. Scale bar: (a) 250 μm , (b) 50 μm . **(a)** Normal skin-defect border (double headed black arrow), normal skin (double headed green arrow), scab formation (asterix), insufficient epithelialization (black arrow), neovascularization (arrow head). **(b)** 40X view the marked section; neutrophil granulocytes (black arrow), macrophages (arrow head), dermal fibroblasts (red arrow).

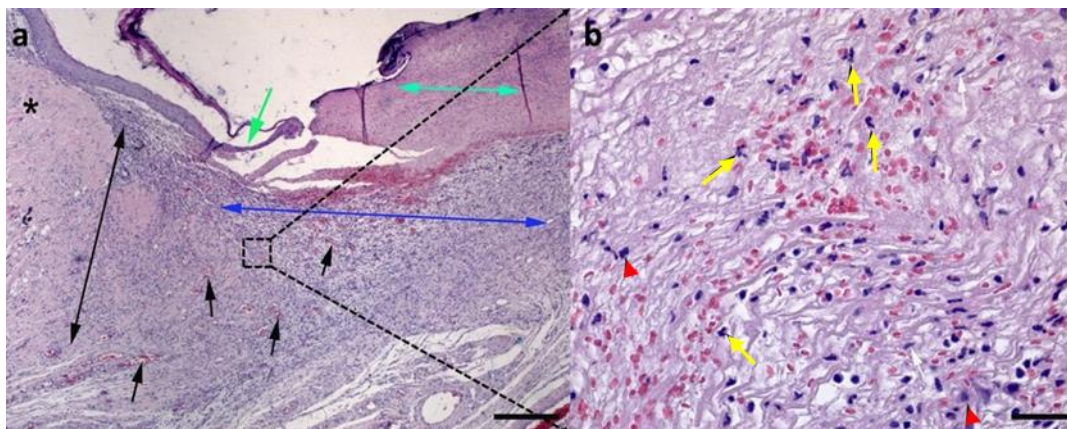


Figure 3.40. Tegaderm group, day 5. Hematoxylin-eosin stained full-thickness skin defect representative tissue samples. Scale bar: (a) 250 μm , (b) 50 μm . **(a)** Normal skin-defect border (double headed black arrow), scab formation (double headed green arrow), normal skin (asterix), partial epithelialization (green arrow), granulation tissue (double headed blue arrow), neovascularization (black arrow). **(b)**

40X view the marked section; neutrophil granulocytes (yellow arrow), macrophages (red arrow head).

HECS:kC hydrogel group on day 5 showed a wide granulation tissue and a lack of epithelialization (**Figure 3.41a**). As compared to the control group, more neovascularization and less immune cell infiltration were observed (**Figure 3.41b**). Storax loaded HECS:kC hydrogel group exhibited a superficial scab formation and partial epithelialization and epidermal thickening on a thicker granulation tissue on day 5 (**Figure 3.42a**). Moreover, number of infiltrating immunity cells were minimal and fibroblast migration could be seen (**Figure 3.42b**).

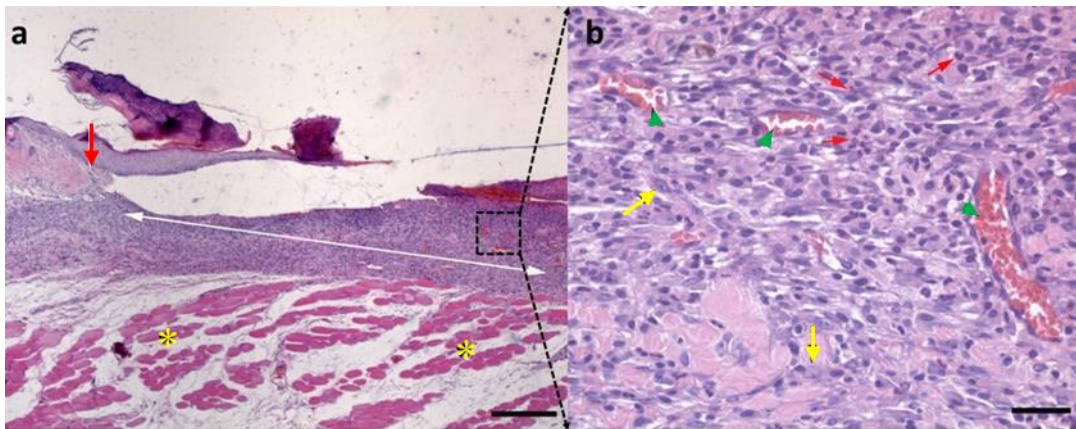


Figure 3.41. HECS:kC hydrogel group, day 5. Hematoxylin-eosin stained full-thickness skin defect representative tissue samples. Scale bar: (a) 250 μm , (b) 50 μm . (a) Normal skin-defect border (red arrow), granulation tissue (double headed white arrow), muscle tissue (yellow asterix). (b) 40X view the marked section; neutrophil granulocytes (red arrow), macrophages (yellow arrow), neovascularization (green arrow head).

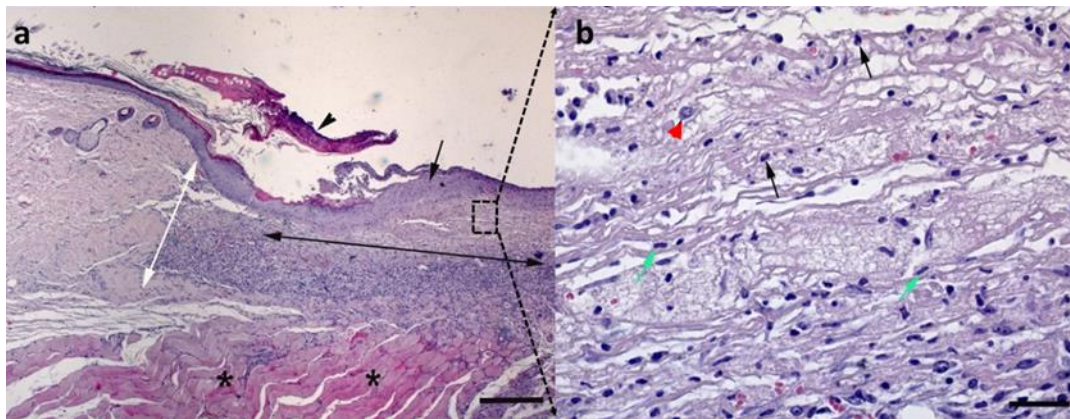


Figure 3.42. Storax loaded HECS:kC hydrogel group, day 5. Hematoxylin-eosin stained full-thickness skin defect representative tissue samples. Scale bar: (a) 250 μm , (b) 50 μm . **(a)** Normal skin-defect border (white arrow), granulation tissue (double headed black arrow), scab formation (arrow head), partial epithelialization and epidermal thickening (black arrow), muscle tissue (asterix). **(b)** 40X view the marked section; neutrophil granulocytes (black arrow), macrophages (arrow head), dermal fibroblasts (green arrow).

Samples obtained on day 10 showed better regeneration, especially those of HECS:kC hydrogel groups. Control group still showed weak epithelialization and epidermal thickening, especially at the center (**Figure 3.43a**). Neovascularization was more evident and mild infiltration was still present (**Figure 3.43b**). Group treated with Tegaderm showed continuous, however, thin epithelialization above a large granulation tissue (**Figure 3.44a**). In addition, rich neovascularization and abundant fibroblast presence was observed with only few infiltrating immunity cells (**Figure 3.44b**).

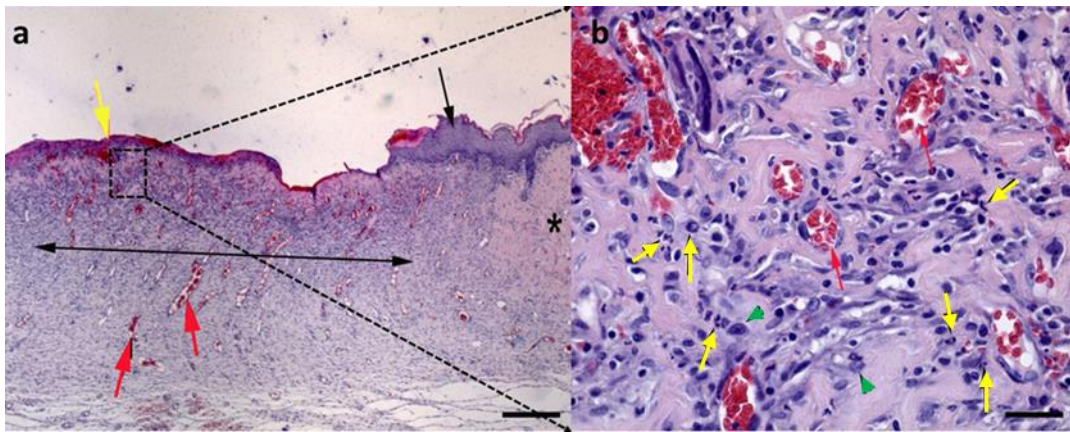


Figure 3.43. Control group, day 10. Hematoxylin-eosin stained full-thickness skin defect representative tissue samples. Scale bar: (a) 250 μm , (b) 50 μm . **(a)** Normal skin (asterix), partial epithelialization and epidermal thickening (black arrow), insufficient epithelialization at the center of the defect (yellow arrow), neovascularization (red arrow). **(b)** 40X view the marked section; neutrophil granulocytes (yellow arrow), macrophages (green arrow head), neovascularization (red arrow).

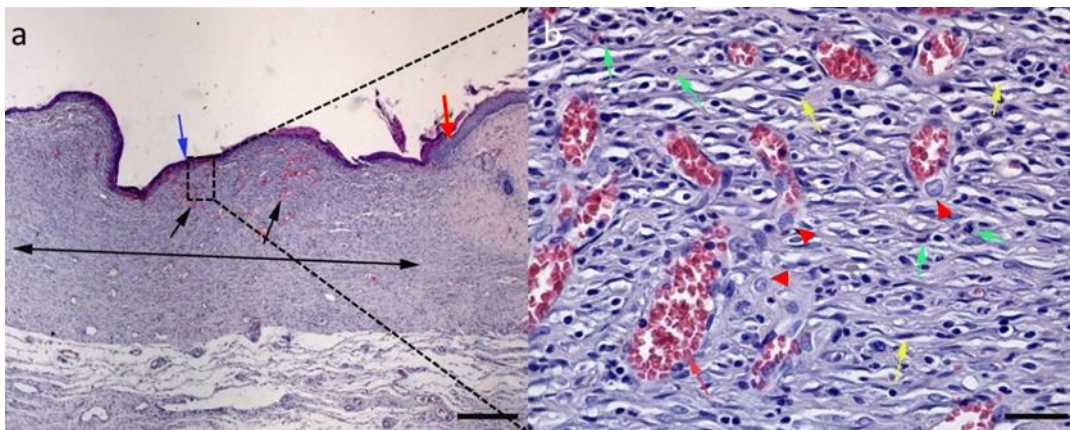


Figure 3.44. Tegaderm group, day 10. Hematoxylin-eosin stained full-thickness skin defect representative tissue samples. Scale bar: (a) 250 μm , (b) 50 μm . **(a)** Normal skin-defect border (red arrow), partial epithelialization (blue arrow), granulation tissue (double headed black arrow), neovascularization (black arrow). **(b)** 40X view

the marked section; neutrophil granulocytes (green arrow), macrophages (red arrow head), dermal fibroblasts (yellow arrow).

HECS:kC hydrogel treated groups on day 10 showed only a section of granulation tissue at the center while edges outer areas of the defect achieving completely normal skin morphology with well defined epidermal layer (**Figure 3.45a**), although a light inflammation was still present (**Figure 3.45b**). A continuous layer of regenerated epidermis was more emphasized with storax loaded HECS:kC hydrogel with hair follicle growth (**Figure 3.46a**). No inflammation was observed (**Figure 3.46b**). **Figure 3.47** shows scoring on histological evaluation of the test groups based on 7 criteria, namely; epithelialization, inflammation, fibroplasia, neovascularization, collagen density, collagen thickness and collagen arrangement. Storax loaded HECS:kC group was significantly better than control group and Tegaderm group in epithelialization and inflammation from day 5 onward. By day 10, storax loaded HECS:kC group achieved significantly better results as compared to other 3 groups in terms of fibroplasia and neovascularization. Significant differences were also present between storax loaded HECS:kC group and Tegaderm group at day 10 in terms of collagen density, collagen thickness and collagen arrangement. Taken together, results indicate storax loaded HECS:kC group facilitated wound healing in rat full-thickness skin defect model better than a commercial product. Furthermore, positive effects of storax on wound healing was further proven as both histological data and wound area measurements show statistically significant differences in the favor of storax incorporating group.

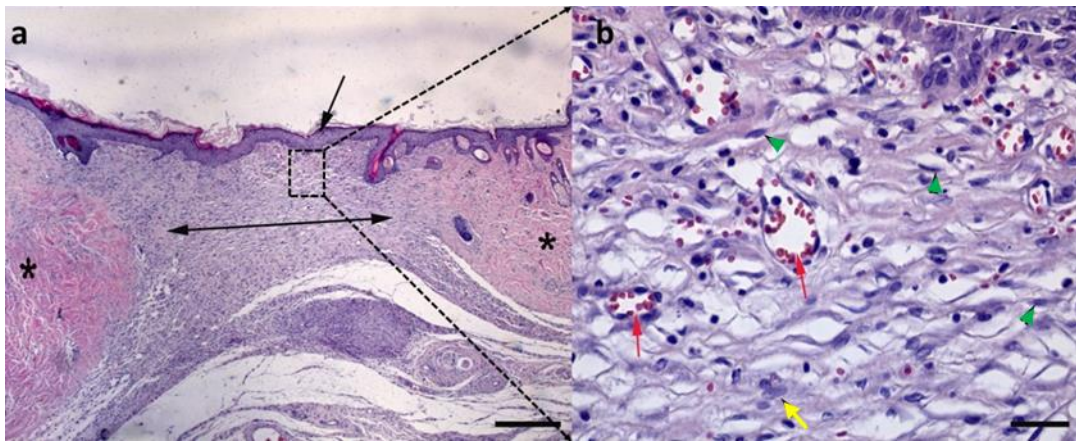


Figure 3.45. HECS:kC hydrogel group, day 10. Hematoxylin-eosin stained full-thickness skin defect representative tissue samples. Scale bar: (a) 250 μm , (b) 50 μm . **(a)** Normal skin (asterix), granulation tissue (double headed black arrow), sufficient epithelialization (black arrow). **(b)** 40X view the marked section; macrophages (yellow arrow), neovascularization (red arrow), dermal fibroblasts (green arrow head).

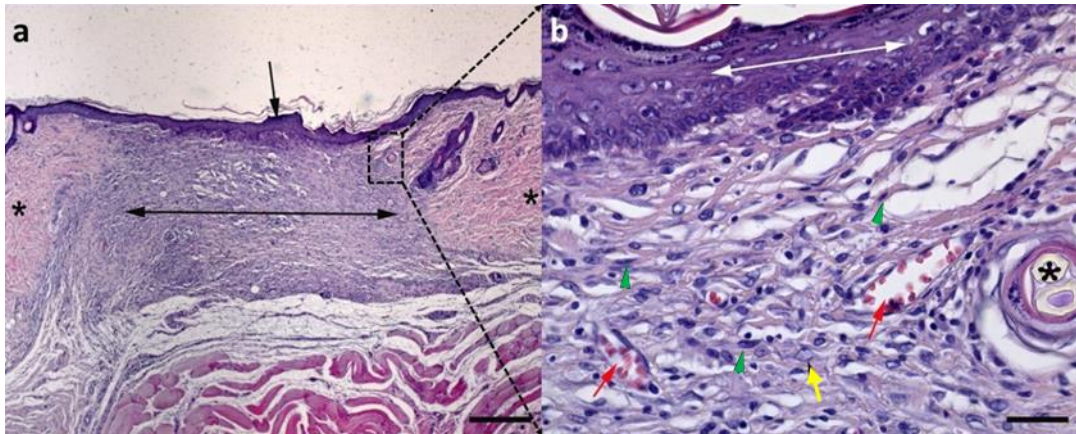


Figure 3.46. Storax loaded HECS:kC hydrogel group, day 10. Hematoxylin-eosin stained full-thickness skin defect representative tissue samples. Scale bar: (a) 250 μm , (b) 50 μm . **(a)** Normal skin (asterix), granulation tissue (double headed black arrow), sufficient epithelialization (black arrow). **(b)** 40X view the marked section; macrophages (yellow arrow), neovascularization (red arrow), dermal fibroblasts (green arrow head), hair follicles (asterix), normal skin appearance of epidermis as a result re-epithelialization (double headed white arrow).

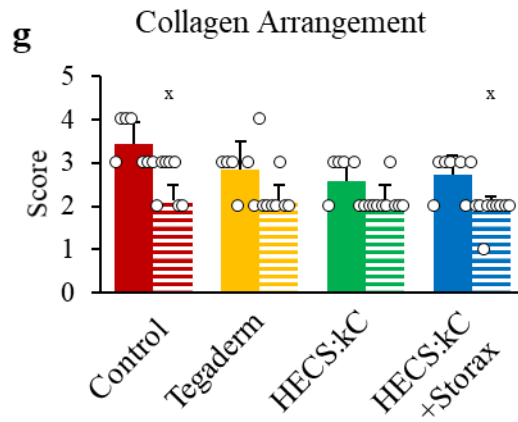
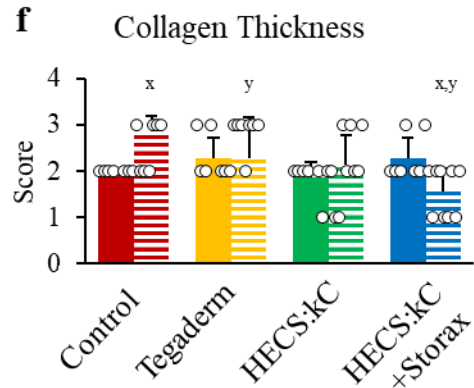
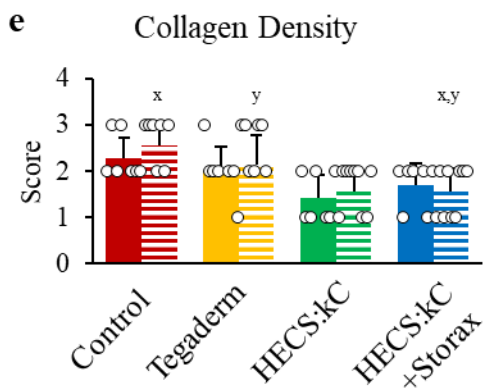
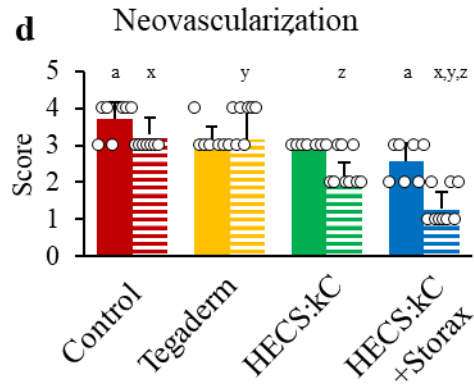
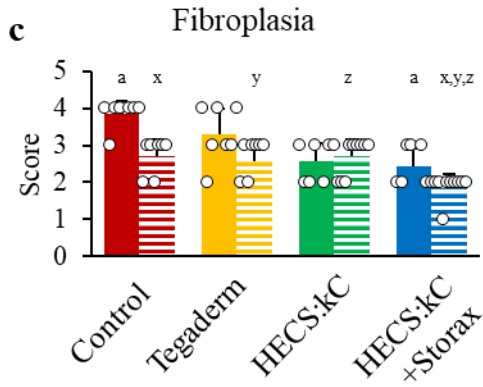
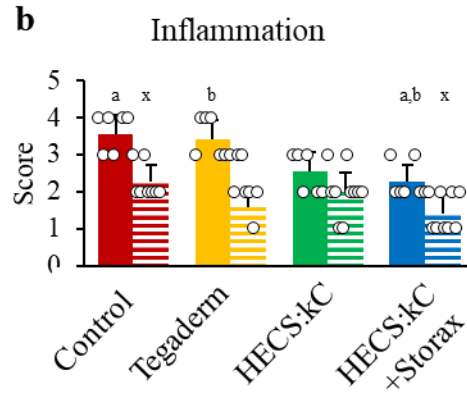
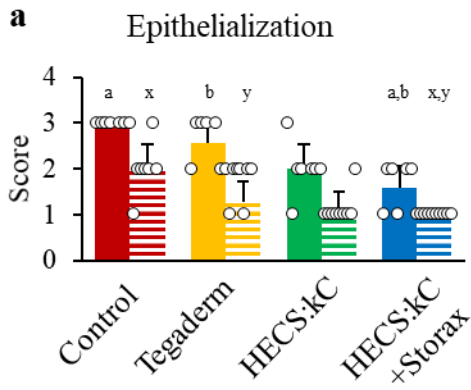


Figure 3.47. Histological scoring of tissue samples based on **(a)** epithelialization, **(b)** inflammation, **(c)** fibroplasia, **(d)** neovascularization, **(e)** collagen density, **(f)** collagen thickness, **(g)** collagen arrangement. Lower scores indicate better outcomes. Solid colored bars indicate parameters obtained on day 5. Horizontally striped bars indicate parameters obtained on day 10. White dots on bars are individual data points, same letters show significant differences ($p < 0.05$).

CHAPTER 4

CONCLUSION

In this study, we developed a multifunctional bilayered wound dressing composed of storax (*Liquidambar orientalis* Mill.) loaded hydroxyethyl chitosan/kappa-carrageenan hydrogel (HECS:kC) and dopamine coated asymmetric polycaprolactone membrane (PCL-DOP). The bottom layer hydrogel were prepared by exploiting the electrostatic charges of the two comprising polymers (HECS:kC) to achieve gelation through polyelectrolyte complexation. Afterwards, storax was also loaded to the hydrogel. The top layer asymmetric membrane was prepared via non-solvent induced phase separation followed by dopamine coating to obtain PCL-DOP.

Among *in vitro* tested groups, the hydrogel with HECS:kC ratio of 1:1 demonstrated pH-sensitive water uptake capacity (~3000% in pH 7.4 and ~2000% in pH 8.4) and degradation (~15% in pH 8.4 and ~65% in pH 6.4 in 14 days). The hydrogel showed high oxygen permeability (5.19 ppm) and optimal water vapor transmission rate (~2250 g/m² day). The hydrogel demonstrated immense versatility in mechanical tests and maintained integrity at compressive strain up to 90% and tensile strain more than %140. Rheological evaluation indicated the hydrogels can maintain structural integrity at a wide range of angular frequency and temperature. Furthermore, *ex vivo* tests on chicken and sheep skin demonstrated a mild adhesion with a shear strength of ~11 kPa and ~4 kPa, respectively. Cytocompatibility and antimicrobial effect of storax was evident as storax loaded HECS:kC (1:1) reduced viable *S. aureus* colony forming units by ~75% without causing any cytotoxicity to L929 fibroblast cells, with or without HECS:kC. Furthermore, quantitative cell viability and morphology analyses demonstrated potent antioxidant activity of storax. Storax release from

HECS:kC demonstrated a similar pattern to the HECS:kC *in vitro* degradation, suggesting that the release was degradation (thus, pH) dependent.

In vitro assessment of PCL-DOP also showed highly promising results. Porous structure (~40%) of PCL allowed good water vapor transmission (~2130 g/m² day) and oxygen permability (5.05 ppm) results and indicated that the membrane enables optimal gas exchange while preventing excessive moisture loss. More importantly, PCL-DOP, was able to effectively prevent microbial penetration. Despite its thickness (200 µm) PCL-DOP was immensely stretchable (>100%), suggesting its suitability for dynamic wounds where wound dressing should be able to withstand tensile forces without breaking. In addition, *in vitro* adhesion tests revealed that PCL-DOP mildly adheres (~31 kPa) to HECS:kC however, it can be removed on-demand for adaptability to healing rate of wound.

In vivo wound closure effectiveness of HECS:kC/PCL-DOP bilayer wound dressing assessed on rat full-thickness skin defect model exhibited highly promising results. Groups treated with HECS:kC showed significantly better healing compared to a commercial wound dressing as early as day 3. By day 10, the group treated with storax loaded HECS:kC had remaining wound area half of the group treated with the commercial product. Histological evaluation further confirmed the effectiveness of the bilayered wound dressing as compared to commercial wound care product.

Overall, the developed bilayer wound dressing showed a great promise for the betterment of contemporary wound treatment.

REFERENCES

- Ageitos, J. M., Sánchez-Pérez, A., Calo-Mata, P., & Villa, T. G. (2017). Antimicrobial peptides (AMPs): Ancient compounds that represent novel weapons in the fight against bacteria. *Biochemical Pharmacology*, *133*, 117–138. <https://doi.org/10.1016/J.BCP.2016.09.018>
- Aktürk, Ö., & Keskin, D. (2016). Collagen/PEO/gold nanofibrous matrices for skin tissue engineering. *Turkish Journal of Biology*, *40*(2), 380–398. <https://doi.org/10.3906/biy-1502-49>
- Akturk, O., Tezcaner, A., Bilgili, H., Deveci, M. S., Gecit, M. R., & Keskin, D. (2011). Evaluation of sericin/collagen membranes as prospective wound dressing biomaterial. *Journal of Bioscience and Bioengineering*, *112*(3), 279–288. <https://doi.org/10.1016/j.jbiosc.2011.05.014>
- Alghooneh, A., Razavi, S. M. A., & Kasapis, S. (2019). Classification of hydrocolloids based on small amplitude oscillatory shear, large amplitude oscillatory shear, and textural properties. *Journal of Texture Studies*, *50*(6), 520–538. <https://doi.org/10.1111/JTXS.12459>
- Ankaralı, H., & Ankaralı, S. (2019). Experimental Designs and Number of Animal to Increase Efficiency in Animal Experiments. *Anadolu Kliniği Tıp Bilimleri Dergisi*, *24*(3), 248–258. <https://doi.org/10.21673/anadoluklin.556640>
- Annabi, N., Rana, D., Shirzaei Sani, E., Portillo-Lara, R., Gifford, J. L., Fares, M. M., Mithieux, S. M., & Weiss, A. S. (2017). Engineering a sprayable and elastic hydrogel adhesive with antimicrobial properties for wound healing. *Biomaterials*, *139*, 229–243. <https://doi.org/10.1016/j.biomaterials.2017.05.011>
- Balcioglu, S., Noma, S. A. A., Ulu, A., Karaaslan-Tunc, M. G., Ozhan, O., Koytepe, S., Parlakpınar, H., Vardi, N., Colak, M. C., & Ates, B. (2022). Fast Curing

- Multifunctional Tissue Adhesives of Sericin-Based Polyurethane-Acrylates for Sternal Closure. *ACS Applied Materials and Interfaces*, *14*, 41819–41833. <https://doi.org/10.1021/ACSAMI.2C14078>
- Bal-Ozturk, A., Cecen, B., Avci-Adali, M., Topkaya, S. N., Alarcin, E., Yasayan, G., Li, Y. C. E., Bulkurcuoglu, B., Akpek, A., Avci, H., Shi, K., Shin, S. R., & Hassan, S. (2021). Tissue adhesives: From research to clinical translation. *Nano Today*, *36*, 101049. <https://doi.org/10.1016/J.NANTOD.2020.101049>
- Bargavi, P., Ramya, R., Chitra, S., Vijayakumari, S., Riju Chandran, R., Durgalakshmi, D., Rajashree, P., & Balakumar, S. (2020). Bioactive, degradable and multi-functional three-dimensional membranous scaffolds of bioglass and alginate composites for tissue regenerative applications. *Biomaterials Science*, *8*(14), 4003–4025. <https://doi.org/10.1039/d0bm00714e>
- Berg, I., Rizzo, R., Lee, M., Ren, Q., Broguiere, N., & Zenobi-Wong, M. (2021). Factor XIII Cross-Linked Adhesive Chitosan Hydrogels. *ACS Biomaterials Science & Engineering*, *7*(6), 2198–2203. <https://doi.org/10.1021/ACSBIOMATERIALS.1C00298>
- Boda, S. K., Fischer, N. G., Ye, Z., & Aparicio, C. (2020). Dual Oral Tissue Adhesive Nanofiber Membranes for pH-Responsive Delivery of Antimicrobial Peptides. *Biomacromolecules*, *21*(12), 4945–4961. <https://doi.org/10.1021/acs.biomac.0c01163>
- Chen, J., Yang, J., Ma, L., Li, J., Shahzad, N., & Kim, C. K. (2020). Structure-antioxidant activity relationship of methoxy, phenolic hydroxyl, and carboxylic acid groups of phenolic acids. *Scientific Reports 2020 10:1*, *10*(1), 1–9. <https://doi.org/10.1038/s41598-020-59451-z>
- Chen, Y., Wang, D., Mensaha, A., Wang, Q., Cai, Y., & Wei, Q. (2022). Ultrafast gelation of multifunctional hydrogel/composite based on self-catalytic Fe³⁺/Tannic acid-cellulose nanofibers. *Journal of Colloid and Interface Science*, *606*, 1457–1468. <https://doi.org/10.1016/J.JCIS.2021.08.104>

- Chen, Y., Yan, L., Yuan, T., Zhang, Q., & Fan, H. (2011). Asymmetric polyurethane membrane with in situ-generated nano-TiO₂ as wound dressing. *Journal of Applied Polymer Science*, *119*(3), 1532–1541. <https://doi.org/10.1002/app.32813>
- Coccolini, F., Improta, M., Cicuttin, E., Catena, F., Sartelli, M., Bova, R., de' Angelis, N., Gitto, S., Tartaglia, D., Cremonini, C., Ordonez, C., Baiocchi, G. L., & Chiarugi, M. (2021). Surgical site infection prevention and management in immunocompromised patients: a systematic review of the literature. *World Journal of Emergency Surgery*, *16*(1), 1–13. <https://doi.org/10.1186/S13017-021-00375-Y/TABLES/2>
- Cong, H., Zhou, L., Meng, Q., Zhang, Y., Yu, B., Shen, Y., & Hu, H. (2019). Preparation and evaluation of PAMAM dendrimer-based polymer gels physically cross-linked by hydrogen bonding. *Biomaterials Science*, *7*(9), 3918–3925. <https://doi.org/10.1039/C9BM00960D>
- Contardi, M., Russo, D., Suarato, G., Heredia-Guerrero, J. A., Ceseracciu, L., Penna, I., Margaroli, N., Summa, M., Spanò, R., Tassistro, G., Vezzulli, L., Bandiera, T., Bertorelli, R., Athanassiou, A., & Bayer, I. S. (2019). Polyvinylpyrrolidone/hyaluronic acid-based bilayer constructs for sequential delivery of cutaneous antiseptic and antibiotic. *Chemical Engineering Journal*, *358*, 912–923. <https://doi.org/10.1016/j.cej.2018.10.048>
- Costa-Almeida, R., Gasperini, L., Borges, J., Babo, P. S., Rodrigues, M. T., Mano, J. F., Reis, R. L., & Gomes, M. E. (2017). Microengineered Multicomponent Hydrogel Fibers: Combining Polyelectrolyte Complexation and Microfluidics. *ACS Biomaterials Science and Engineering*, *3*(7), 1322–1331. <https://doi.org/10.1021/acsbiomaterials.6b00331>
- Cutionco, M. F. A., Choo, R. K. T., Shen, N. J. X., Chua, B. M. X., Sju, E., Choo, A. W. L., Le Visage, C., & Yim, E. K. F. (2015). Composite scaffold of poly(vinyl alcohol) and interfacial polyelectrolyte complexation fibers for

- controlled biomolecule delivery. *Frontiers in Bioengineering and Biotechnology*, 3(FEB). <https://doi.org/10.3389/fbioe.2015.00003>
- Daeschlein, G., Dr, Priv.-D., & Daeschlein, . G. (2013). *Antimicrobial and antiseptic strategies in wound management*. 9–14. <https://doi.org/10.1111/IWJ.12175>
- Darmayanti, M. G., Radiman, C. L., & Sudarma, I. M. (2016). Kappa-Carrageenan as an attractive green substitute for polyacrylamide in enhanced oil recovery applications. *International Journal of Technology*, 7(3), 431–437. <https://doi.org/10.14716/IJTECH.V7I3.2869>
- Delgado-Rangel, L. H., Huerta-Saquero, A., Eufrazio-García, N., Meza-Villezcás, A., Mota-Morales, J. D., & González-Campos, J. B. (2020). Deep eutectic solvent-assisted phase separation in chitosan solutions for the production of 3D monoliths and films with tailored porosities. *International Journal of Biological Macromolecules*, 164, 4084–4094. <https://doi.org/10.1016/j.ijbiomac.2020.08.254>
- di Filippo, M. F., Albertini, B., Dolci, L. S., Bonvicini, F., Bigi, A., Gentilomi, G. A., Passerini, N., & Panzavolta, S. (2021). Novel drug-loaded film forming patch based on gelatin and snail slime. *International Journal of Pharmaceutics*, 598, 120408. <https://doi.org/10.1016/J.IJPHARM.2021.120408>
- Ding, L., Shan, X., Zhao, X., Zha, H., Chen, X., Wang, J., Cai, C., Wang, X., Li, G., Hao, J., & Yu, G. (2017). Spongy bilayer dressing composed of chitosan–Ag nanoparticles and chitosan –Bletilla striata polysaccharide for wound healing applications. *Carbohydrate Polymers*, 157, 1538–1547. <https://doi.org/10.1016/j.carbpol.2016.11.040>
- Duan, X., Wan, J. M. F., & Mak, A. F. T. (2017). Oxidative Stress Alters the Morphological Responses of Myoblasts to Single-Site Membrane Photoporation. *Cellular and Molecular Bioengineering*, 10(4), 313–325. <https://doi.org/10.1007/S12195-017-0488-5/FIGURES/5>

- Dunnill, C., Patton, T., Brennan, J., Barrett, J., Dryden, M., Cooke, J., Leaper, D., & Georgopoulos, N. T. (2017). Reactive oxygen species (ROS) and wound healing: the functional role of ROS and emerging ROS-modulating technologies for augmentation of the healing process. *International Wound Journal*, *14*(1), 89–96. <https://doi.org/10.1111/IWJ.12557>
- Edikresnha, D., Suciati, T., Suprijadi, & Khairurrijal, K. (2021). Freeze-thawed hydrogel loaded by Piper crocatum extract with in-vitro antibacterial and release tests. *Journal of Materials Research and Technology*, *15*, 17–36. <https://doi.org/10.1016/J.JMRT.2021.07.151>
- Ehterami, A., Salehi, M., Farzamfar, S., Samadian, H., Vaez, A., Ghorbani, S., Ai, J., & Sahrapeyma, H. (2019). Chitosan/alginate hydrogels containing Alpha-tocopherol for wound healing in rat model. *Journal of Drug Delivery Science and Technology*, *51*, 204–213. <https://doi.org/10.1016/J.JDDST.2019.02.032>
- Ehterami, A., Salehi, M., Farzamfar, S., Vaez, A., Samadian, H., Sahrapeyma, H., Mirzaii, M., Ghorbani, S., & Goodarzi, A. (2018). In vitro and in vivo study of PCL/COLL wound dressing loaded with insulin-chitosan nanoparticles on cutaneous wound healing in rats model. *International Journal of Biological Macromolecules*, *117*, 601–609. <https://doi.org/10.1016/J.IJBIOMAC.2018.05.184>
- El-Aassar, M. R., El Fawal, G. F., Kamoun, E. A., & Fouda, M. M. G. (2015). Controlled drug release from cross-linked κ -carrageenan/hyaluronic acid membranes. *International Journal of Biological Macromolecules*, *77*, 322–329. <https://doi.org/10.1016/J.IJBIOMAC.2015.03.055>
- el Hosary, R., El-Mancy, S. M. S., el Deeb, K. S., Eid, H. H., el Tantawy, M. E., Shams, M. M., Samir, R., Assar, N. H., & Sleem, A. A. (2020). Efficient wound healing composite hydrogel using Egyptian Avena sativa L. polysaccharide containing β -glucan. *International Journal of Biological Macromolecules*, *149*, 1331–1338. <https://doi.org/10.1016/j.ijbiomac.2019.11.046>

- Eskandarinia, A., Kefayat, A., Agheb, M., Rafienia, M., Amini Baghbadorani, M., Navid, S., Ebrahimpour, K., Khodabakhshi, D., & Ghahremani, F. (2020). A Novel Bilayer Wound Dressing Composed of a Dense Polyurethane/Propolis Membrane and a Biodegradable Polycaprolactone/Gelatin Nanofibrous Scaffold. *Scientific Reports*, *10*(1), 3063. <https://doi.org/10.1038/s41598-020-59931-2>
- Fan, L., Wang, L., Gao, S., Wu, P., Li, M., Xie, W., Liu, S., & Wang, W. (2011). Synthesis, characterization and properties of carboxymethyl kappa carrageenan. *Carbohydrate Polymers*, *86*(3), 1167–1174. <https://doi.org/10.1016/j.carbpol.2011.06.010>
- Fathi- Achachelouei, M., Keskin, D., Bat, E., Vrana, N. E., & Tezcaner, A. (2020). Dual growth factor delivery using PLGA nanoparticles in silk fibroin/PEGDMA hydrogels for articular cartilage tissue engineering. *Journal of Biomedical Materials Research Part B: Applied Biomaterials*, *108*(5), 2041–2062. <https://doi.org/10.1002/jbm.b.34544>
- Felippe J. Pavinatto, †, Adriana Pavinatto, †, Luciano Caseli, *,†, David S. dos Santos, Jr. †, Thatyane M. Nobre, ‡, Maria E. D. Zaniquelli, ‡ and, & Osvaldo N. Oliveira, Jr. †. (2007). Interaction of Chitosan with Cell Membrane Models at the Air–Water Interface. *Biomacromolecules*, *8*(5), 1633–1640. <https://doi.org/10.1021/BM0701550>
- Fernández-Ferreiro, A., González Barcia, M., Gil-Martínez, M., Vieites-Prado, A., Lema, I., Argibay, B., Blanco Méndez, J., Lamas, M. J., & Otero-Espinar, F. J. (2015). In vitro and in vivo ocular safety and eye surface permanence determination by direct and Magnetic Resonance Imaging of ion-sensitive hydrogels based on gellan gum and kappa-carrageenan. *European Journal of Pharmaceutics and Biopharmaceutics*, *94*, 342–351. <https://doi.org/10.1016/J.EJPB.2015.06.003>

- Gangwar, A. K., Kumar, N., Sharma, A. K., Devi, K. S., Negi, M., Shrivastava, S., Mathew, D. D., Remya, V., Sonal, Arundeeep, P. S., Maiti, S. K., Kumar, V., Kaarthick, D. T., Kurade, N. P., & Singh, R. (2013). Bioengineered acellular dermal matrix for the repair of full thickness skin wounds in rats. *Trends in Biomaterials and Artificial Organs*, 27(2), 67–80.
- García, M. C., Aldana, A. A., Tártara, L. I., Alovero, F., Strumia, M. C., Manzo, R. H., Martinelli, M., & Jimenez-Kairuz, A. F. (2017). Bioadhesive and biocompatible films as wound dressing materials based on a novel dendronized chitosan loaded with ciprofloxacin. *Carbohydrate Polymers*, 175, 75–86. <https://doi.org/10.1016/j.carbpol.2017.07.053>
- Ge, L., & Chen, S. (2020). Recent Advances in Tissue Adhesives for Clinical Medicine. *Polymers* 2020, Vol. 12, Page 939, 12(4), 939. <https://doi.org/10.3390/POLYM12040939>
- Giano, M. C., Ibrahim, Z., Medina, S. H. S. H., Sarhane, K. A. K. A. K. A. K. A., Christensen, J. M. J. M., Yamada, Y., Brandacher, G., & Schneider, J. P. J. P. J. P. J. P. (2014). Injectable bioadhesive hydrogels with innate antibacterial properties. *Nature Communications*, 5(1), 1–9. <https://doi.org/10.1038/ncomms5095>
- Gierszewska-Drużyńska, M., Ostrowska-Czubenko, J., & Kwiatkowska, A. (2013). Effect of ionic crosslinking on density of hydrogel chitosan membranes. *Progress on Chemistry and Application of Chitin and Its Derivatives*, 18, 49–58.
- Gimeno, M., Pinczowski, P., Pérez, M., Giorello, A., Martínez, M. Á., Santamaría, J., Arruebo, M., & Luján, L. (2015). A controlled antibiotic release system to prevent orthopedic-implant associated infections: An in vitro study. *European Journal of Pharmaceutics and Biopharmaceutics*, 96, 264. <https://doi.org/10.1016/J.EJPB.2015.08.007>

- Glazer, B. T., Marsh, A. G., Stierhoff, K., & Luther, G. W. (2004). The dynamic response of optical oxygen sensors and voltammetric electrodes to temporal changes in dissolved oxygen concentrations. *Analytica Chimica Acta*, 518(1–2), 93–100. <https://doi.org/10.1016/J.ACA.2004.05.040>
- Guo, J., Wang, W., Hu, J., Xie, D., Gerhard, E., Nisic, M., Shan, D., Qian, G., Zheng, S., & Yang, J. (2016). Synthesis and characterization of anti-bacterial and anti-fungal citrate-based mussel-inspired bioadhesives. *Biomaterials*, 85, 204–217. <https://doi.org/10.1016/j.biomaterials.2016.01.069>
- Guo, Z., Zhang, Z., Zhang, N., Gao, W., Li, J., Pu, Y., He, B., & Xie, J. (2021). A Mg²⁺/polydopamine composite hydrogel for the acceleration of infected wound healing. *Bioactive Materials*. <https://doi.org/10.1016/J.BIOACTMAT.2021.11.036>
- Gupta, A., Keddie, D. J., Kannappan, V., Gibson, H., Khalil, I. R., Kowalczyk, M., Martin, C., Shuai, X., & Radecka, I. (2019). Production and characterisation of bacterial cellulose hydrogels loaded with curcumin encapsulated in cyclodextrins as wound dressings. *European Polymer Journal*. <https://doi.org/10.1016/j.eurpolymj.2019.06.018>
- Hafizoğlu, H. (1982). Analytical studies on the balsam of liquidambar orientalis mill by gas chromatography and mass spectrometry. In *Holzforschung* (Vol. 36, Issue 6, pp. 311–313). De Gruyter. <https://doi.org/10.1515/hfsg.1982.36.6.311>
- Hejazi, R., & Amiji, M. (2003). Chitosan-based gastrointestinal delivery systems. *Journal of Controlled Release: Official Journal of the Controlled Release Society*, 89(2), 151–165.
- He, J., Shi, M., Liang, Y., & Guo, B. (2020). Conductive adhesive self-healing nanocomposite hydrogel wound dressing for photothermal therapy of infected full-thickness skin wounds. *Chemical Engineering Journal*, 394, 124888. <https://doi.org/10.1016/j.cej.2020.124888>

- Hoffmann, R. A., Russell, A. L., & Cidley, M. J. (1996). *Gums and Stabilizers for the Food Industry B Phillips* (Vol. 137). eds fRL Press.
- Hoque, J., Prakash, R. G., Paramanandham, K., Shome, B. R., & Haldar, J. (2017). Biocompatible injectable hydrogel with potent wound healing and antibacterial properties. *Molecular Pharmaceutics*, *14*(4), 1218–1230. <https://doi.org/10.1021/acs.molpharmaceut.6b01104>
- Horák, D., Matulka, K., Hlídková, H., Lapčíková, M., Beneš, M. J., Jaroš, J., Hampl, A., & Dvořák, P. (2011). Pentapeptide-modified poly(N,N-diethylacrylamide) hydrogel scaffolds for tissue engineering. *Journal of Biomedical Materials Research Part B: Applied Biomaterials*, *98B*(1), 54–67. <https://doi.org/10.1002/jbm.b.31832>
- Huang, L., Zhu, Z., Wu, D., Gan, W., Zhu, S., Li, W., Tian, J., Li, L., Zhou, C., & Lu, L. (2019). Antibacterial poly (ethylene glycol) diacrylate/chitosan hydrogels enhance mechanical adhesiveness and promote skin regeneration. *Carbohydrate Polymers*, *225*, 115110. <https://doi.org/10.1016/j.carbpol.2019.115110>
- Huang, Y., Dan, N., Dan, W., Zhao, W., Bai, Z., Chen, Y., & Yang, C. (2019). Facile fabrication of gelatin and polycaprolactone based bilayered membranes via spin coating method with antibacterial and cyto-compatible properties. *International Journal of Biological Macromolecules*, *124*, 699–707. <https://doi.org/10.1016/j.ijbiomac.2018.11.262>
- Huot, J., Houle, F., Marceau, F., & Landry, J. (1997). Oxidative Stress-Induced Actin Reorganization Mediated by the p38 Mitogen-Activated Protein Kinase/Heat Shock Protein 27 Pathway in Vascular Endothelial Cells. *Circulation Research*, *80*(3), 383–392. <https://doi.org/10.1161/01.RES.80.3.383>
- Hurler, J., Berg, O. A., Skar, M., Conradi, A. H., Johnsen, P. J., & Škalko-Basnet, N. (2012). Improved burns therapy: Liposomes-in-hydrogel delivery system for

- mupirocin. *Journal of Pharmaceutical Sciences*, 101(10), 3906–3915. <https://doi.org/10.1002/jps.23260>
- Isik, G., Hasirci, N., Tezcaner, A., & Kiziltay, A. (2020). Multifunctional periodontal membrane for treatment and regeneration purposes. *Journal of Bioactive and Compatible Polymers*, 35(2), 117–138. <https://doi.org/10.1177/0883911520911659>
- Jia, Z., Lv, X., Hou, Y., Wang, K., Ren, F., Xu, D., Wang, Q., Fan, K., Xie, C., & Lu, X. (2021). Mussel-inspired nanozyme catalyzed conductive and self-setting hydrogel for adhesive and antibacterial bioelectronics. *Bioactive Materials*, 6(9), 2676–2687. <https://doi.org/10.1016/J.BIOACTMAT.2021.01.033>
- Kamel, R., & Abbas, H. A. (2013). Self-assembled carbohydrate hydrogels for prolonged pain management. *Pharmaceutical Development and Technology*, 18(5), 990–1004. <https://doi.org/10.3109/10837450.2011.609992>
- Karadeniz, B., Ulker, Z., & Alpsoy, L. (2013). Genotoxic and cytotoxic effects of storax in vitro. *Toxicology and Industrial Health*, 29(2), 181–186. <https://doi.org/10.1177/0748233711428642>
- Khalil, I. A., Saleh, B., Ibrahim, D. M., Jumelle, C., Yung, A., Dana, R., & Annabi, N. (2020). Ciprofloxacin-loaded bioadhesive hydrogels for ocular applications. *Biomaterials Science*, 8(18), 5196–5209. <https://doi.org/10.1039/d0bm00935k>
- Khaliq, T., Sohail, M., Minhas, M. U., Ahmed Shah, S., Jabeen, N., Khan, S., Hussain, Z., Mahmood, A., Kousar, M., & Rashid, H. (2022). Self-crosslinked chitosan/κ-carrageenan-based biomimetic membranes to combat diabetic burn wound infections. *International Journal of Biological Macromolecules*, 197, 157–168. <https://doi.org/10.1016/J.IJBIOMAC.2021.12.100>
- Koehler, J., Brandl, F. P., & Goepferich, A. M. (2018). Hydrogel wound dressings for bioactive treatment of acute and chronic wounds. *European Polymer Journal*, 100, 1–11. <https://doi.org/10.1016/J.EURPOLYMJ.2017.12.046>

- Kumar, K., Dhawan, N., & Sharma, H. (2014). Bioadhesive polymers: Novel tool for drug delivery. *Nanomedicine, and Biotechnology*, 42(4), 274–283. <https://doi.org/10.3109/21691401.2013.815194>
- Lalevée, G., David, L., Montembault, A., Blanchard, K., Meadows, J., Malaise, S., Crépet, A., Grillo, I., Morfin, I., Delair, T., & Sudre, G. (2017). Highly stretchable hydrogels from complex coacervation of natural polyelectrolytes. *Soft Matter*, 13(37), 6594–6605. <https://doi.org/10.1039/c7sm01215b>
- Lee, G. M., Kim, S. jeong, Kim, E. M., Kim, E., Lee, S., Lee, E., Park, H. H., & Shin, H. (2022). Free radical-scavenging composite gelatin methacryloyl hydrogels for cell encapsulation. *Acta Biomaterialia*, 149, 96–110. <https://doi.org/10.1016/J.ACTBIO.2022.06.043>
- Lefnaoui, S., & Moulai-Mostefa, N. (2015). Polyelectrolyte complex based on carboxymethyl-kappa-carrageenan and Eudragit RL 30D as prospective carriers for sustained drug delivery. *Chemical Engineering Research and Design*, 97, 165–174. <https://doi.org/10.1016/J.CHERD.2014.12.006>
- Lei, J., Sun, L. C., Huang, S., Zhu, C., Li, P., He, J., Mackey, V., Coy, D. H., & He, Q. Y. (2019). The antimicrobial peptides and their potential clinical applications. *American Journal of Translational Research*, 11(7), 3919. [/pmc/articles/PMC6684887/](https://pubmed.ncbi.nlm.nih.gov/36684887/)
- Liang, Y., Zhao, X., Ma, P. X., Guo, B., Du, Y., & Han, X. (2019). pH-responsive injectable hydrogels with mucosal adhesiveness based on chitosan-grafted-dihydrocaffeic acid and oxidized pullulan for localized drug delivery. *Journal of Colloid and Interface Science*, 536, 224–234. <https://doi.org/10.1016/j.jcis.2018.10.056>
- Li, B., & Webster, T. J. (2018). Bacteria antibiotic resistance: New challenges and opportunities for implant-associated orthopedic infections. *Journal of Orthopaedic Research*, 36(1), 22–32. <https://doi.org/10.1002/jor.23656>

- Li, H., Huo, M., Zhou, J., Dai, Y., Deng, Y., Shi, X., & Masoud, J. (2010). Enhanced Oral Absorption of Paclitaxel in N-Deoxycholic Acid-N, O-Hydroxyethyl Chitosan Micellar System. *Journal of Pharmaceutical Sciences*, 99(11), 4543–4553. <https://doi.org/10.1002/JPS.22159>
- Li, J., & Zhuang, S. (2020). Antibacterial activity of chitosan and its derivatives and their interaction mechanism with bacteria: Current state and perspectives. *European Polymer Journal*, 138, 109984. <https://doi.org/10.1016/J.EURPOLYMJ.2020.109984>
- Lingbeck, J. M., O'Bryan, C. A., Martin, E. M., Adams, J. P., & Crandall, P. G. (2015). Sweetgum: An ancient source of beneficial compounds with modern benefits. *Pharmacognosy Reviews*, 9(17), 1–11. <https://doi.org/10.4103/0973-7847.156307>
- Liu, M., Luo, G., Wang, Y., He, W., Liu, T., Zhou, D., Hu, X., Xing, M., & Wu, J. (2017). Optimization and integration of nanosilver on polycaprolactone nanofibrous mesh for bacterial inhibition and wound healing in vitro and in vivo. *International Journal of Nanomedicine*, 12, 6827–6840. <https://doi.org/10.2147/IJN.S140648>
- Liu, S., Liu, X., Ren, Y., Wang, P., Pu, Y., Yang, R., Wang, X., Tan, X., Ye, Z., Maurizot, V., & Chi, B. (2020). Mussel-Inspired Dual-Cross-linking Hyaluronic Acid/ ϵ -Polylysine Hydrogel with Self-Healing and Antibacterial Properties for Wound Healing. *ACS Applied Materials and Interfaces*, 12(25), 27876–27888. <https://doi.org/10.1021/acsami.0c00782>
- Li, Z., Mo, Z., Guo, R., Meng, S., Wang, R., Gao, H., & Niu, X. (2017). Electrochemical enantio-recognition of tryptophan enantiomers based on a multi-walled carbon nanotube–hydroxyethyl chitosan composite film. *Analytical Methods*, 9(35), 5149–5155. <https://doi.org/10.1039/C7AY01775H>
- Maity, B., Alam, S., Samanta, S., Prakash, R. G., & Govindaraju, T. (2022). Antioxidant Silk Fibroin Composite Hydrogel for Rapid Healing of Diabetic

- Wound. *Macromolecular Bioscience*, 22(9), 2200097.
<https://doi.org/10.1002/MABI.202200097>
- Ma, M., Zhong, Y., & Jiang, X. (2020). Thermosensitive and pH-responsive tannin-containing hydroxypropyl chitin hydrogel with long-lasting antibacterial activity for wound healing. *Carbohydrate Polymers*, 236, 116096.
<https://doi.org/10.1016/j.carbpol.2020.116096>
- Mandapalli, P. K., Labala, S., Bojja, J., & Venuganti, V. V. K. (2016). Effect of pirfenidone delivered using layer-by-layer thin film on excisional wound healing. *European Journal of Pharmaceutical Sciences*, 83, 166–174.
<https://doi.org/10.1016/j.ejps.2015.12.027>
- Mao, H., Zhao, S., He, Y., Feng, M., Wu, L., He, Y., & Gu, Z. (2022). Multifunctional polysaccharide hydrogels for skin wound healing prepared by photoinitiator-free crosslinking. *Carbohydrate Polymers*, 285, 119254.
<https://doi.org/10.1016/J.CARBPOL.2022.119254>
- Ma, Y., Li, P., Zhao, L., Liu, J., Yu, J., Huang, Y., Zhu, Y., Li, Z., Zhao, R., Hua, S., Zhu, Y., & Zhang, Z. (2021). <p>Size-Dependent Cytotoxicity and Reactive Oxygen Species of Cerium Oxide Nanoparticles in Human Retinal Pigment Epithelia Cells</p>. *International Journal of Nanomedicine*, 16, 5333–5341.
<https://doi.org/10.2147/IJN.S305676>
- Mejía, E. H., Contreras, H., Delgado, E., & Quintana, G. (2019). Effect of Experimental Parameters on the Formation of Hydrogels by Polyelectrolyte Complexation of Carboxymethylcellulose, Carboxymethyl Starch, and Alginate Acid with Chitosan. *International Journal of Chemical Engineering*, 2019.
<https://doi.org/10.1155/2019/3085691>
- Mercer, D. K., & O’Neil, D. A. (2020). Innate Inspiration: Antifungal Peptides and Other Immunotherapeutics From the Host Immune Response. *Frontiers in Immunology*, 0, 2177. <https://doi.org/10.3389/FIMMU.2020.02177>

- Miller, R. J., Chan, C. Y., Rastogi, A., Grant, A. M., White, C. M., Bette, N., Schaub, N. J., & Corey, J. M. (2018). Combining electrospun nanofibers with cell-encapsulating hydrogel fibers for neural tissue engineering. *Journal of Biomaterials Science, Polymer Edition*, 29(13), 1625–1642. <https://doi.org/10.1080/09205063.2018.1479084>
- Mogoşanu, G. D., & Grumezescu, A. M. (2014). Natural and synthetic polymers for wounds and burns dressing. *International Journal of Pharmaceutics*, 463(2), 127–136. <https://doi.org/10.1016/J.IJPHARM.2013.12.015>
- Morgado, P. I., Aguiar-Ricardo, A., & Correia, I. J. (2015). Asymmetric membranes as ideal wound dressings: An overview on production methods, structure, properties and performance relationship. In *Journal of Membrane Science* (Vol. 490, pp. 139–151). Elsevier. <https://doi.org/10.1016/j.memsci.2015.04.064>
- Morgado, P. I., Lisboa, P. F., Ribeiro, M. P., Miguel, S. P., Simões, P. C., Correia, I. J., & Aguiar-Ricardo, A. (2014a). Poly(vinyl alcohol)/chitosan asymmetrical membranes: Highly controlled morphology toward the ideal wound dressing. *Journal of Membrane Science*, 469, 262–271.
- Morgado, P. I., Lisboa, P. F., Ribeiro, M. P., Miguel, S. P., Simões, P. C., Correia, I. J., & Aguiar-Ricardo, A. (2014b). Poly(vinyl alcohol)/chitosan asymmetrical membranes: Highly controlled morphology toward the ideal wound dressing. *Journal of Membrane Science*, 469, 262–271. <https://doi.org/10.1016/J.MEMSCI.2014.06.035>
- Mou, J., Liu, Z., Liu, J., Lu, J., Zhu, W., & Pei, D. (2019). Hydrogel containing minocycline and zinc oxide-loaded serum albumin nanoparticle for periodontitis application: preparation, characterization and evaluation. *Drug Delivery*, 26(1), 179–187. <https://doi.org/10.1080/10717544.2019.1571121>
- Murakawa, K., King, D. R., Sun, T., Guo, H., Kurokawa, T., & Gong, J. P. (2019). Polyelectrolyte complexation via viscoelastic phase separation results in tough

and self-recovering porous hydrogels. *Journal of Materials Chemistry B*, 7(35), 5296–5305. <https://doi.org/10.1039/c9tb01376h>

Nalbantsoy, A., Karış, M., Karakaya, L., & Akgül, Y. (2016). Liquidambar orientalis Mill. reçine ekstraktlarının antioksidan, sitotoksik ve iNOS aktiviteleri. *Turkish Journal of Biochemistry*, 41(3), 198–205. <https://doi.org/10.1515/tjb-2016-0030>

Nam, S., & Mooney, D. (2021). Polymeric Tissue Adhesives. *Chemical Reviews*, 121(18), 11336–11384. <https://doi.org/10.1021/ACS.CHEMREV.0C00798>

Ocsel, H., Teke, Z., Sacar, M., Kabay, B., Duzcan, S. E., & Kara, I. G. (2012). Effects of oriental sweet gum storax on porcine wound healing. *Journal of Investigative Surgery*, 25(4), 262–270. <https://doi.org/10.3109/08941939.2011.639847>

Okmen, G., Turkcan, O., Ceylan, O., & Gork, G. (2014). The Antimicrobial Activity of Liquidambar Orientalis Mill. Against Food Pathogens and Antioxidant Capacity of Leaf Extracts. *African Journal of Traditional, Complementary, and Alternative Medicines*, 11(5), 28. <https://doi.org/10.4314/AJTAM.V11I5.4>

Özbaş, Z., Özkahraman, B., Bayrak, G., Kılıç Süloğlu, A., Perçin, I., Boran, F., & Tamahkar, E. (2021). Poly(vinyl alcohol)/(hyaluronic acid-g-kappa-carrageenan) hydrogel as antibiotic-releasing wound dressing. *Chemical Papers*, 75(12), 6591–6600. <https://doi.org/10.1007/S11696-021-01824-3/FIGURES/7>

Paarakh, M. P., Jose, P. A., Setty, C., & Peterchristoper, G. V. (2018). *Release Kinetics - Concepts and Applications*. International Journal of Pharmacy Research & Technology. <https://www.bibliomed.org/?mno=302643667>

Pagano, C., Ceccarini, M. R., Calarco, P., Scuota, S., Conte, C., Primavilla, S., Ricci, M., & Perioli, L. (2019). Bioadhesive polymeric films based on usnic acid for burn wound treatment: Antibacterial and cytotoxicity studies. *Colloids and Surfaces B: Biointerfaces*, 178(March), 488–499. <https://doi.org/10.1016/j.colsurfb.2019.03.001>

- Pagano, C., Marinozzi, M., Baiocchi, C., Beccari, T., Calarco, P., Ceccarini, M. R., Chielli, M., Orabona, C., Orecchini, E., Ortenzi, R., Ricci, M., Scuota, S., Tiralti, M. C., & Perioli, L. (2020). Bioadhesive Polymeric Films Based on Red Onion Skins Extract for Wound Treatment: An Innovative and Eco-Friendly Formulation. *Molecules*, 25(2), 318. <https://doi.org/10.3390/molecules25020318>
- Patel, A., Sant, V., Velankar, S., Dutta, M., Balasubramanian, V., Sane, P., Agrawal, V., Wilson, J., Rohan, L. C., & Sant, S. (2020). Self-assembly of multiscale anisotropic hydrogels through interfacial polyionic complexation. *Journal of Biomedical Materials Research Part A*, 108(12), 2504–2518. <https://doi.org/10.1002/JBM.A.37001>
- Patel, A., Zaky, S. H., Li, H., Schoedel, K., Almarza, A. J., Sfeir, C., Sant, V., & Sant, S. (2020). Bottom-Up Self-assembled Hydrogel-Mineral Composites Regenerate Rabbit Ulna Defect without Added Growth Factors. *ACS Applied Bio Materials*, 3(9), 5652–5663. <https://doi.org/10.1021/acsabm.0c00371>
- Permana, A. D., Utomo, E., Pratama, M. R., Amir, M. N., Anjani, Q. K., Mardikasari, S. A., Sumarheni, S., Himawan, A., Arjuna, A., Usmanengsi, U., & Donnelly, R. F. (2021). Bioadhesive-Thermosensitive in Situ Vaginal Gel of the Gel Flake-Solid Dispersion of Itraconazole for Enhanced Antifungal Activity in the Treatment of Vaginal Candidiasis. *ACS Applied Materials and Interfaces*, 13(15), 18128–18141. https://doi.org/10.1021/ACSAMI.1C03422/SUPPL_FILE/AM1C03422_SI_001.PDF
- Pettinelli, N., Rodríguez-Llamazares, S., Bouza, R., Barral, L., Feijoo-Bandín, S., & Lago, F. (2020). Carrageenan-based physically crosslinked injectable hydrogel for wound healing and tissue repairing applications. *International Journal of Pharmaceutics*, 589, 119828. <https://doi.org/10.1016/j.ijpharm.2020.119828>

- Pinnaratip, R., Bhuiyan, M. S. A., Meyers, K., Rajachar, R. M., & Lee, B. P. (2019). Multifunctional Biomedical Adhesives. *Advanced Healthcare Materials*, 8(11), 1801568. <https://doi.org/10.1002/adhm.201801568>
- Ponrasu, T., Veerasubramanian, P. K., Kannan, R., Gopika, S., Suguna, L., & Muthuvijayan, V. (2018). Morin incorporated polysaccharide-protein (psyllium-keratin) hydrogel scaffolds accelerate diabetic wound healing in Wistar rats. *RSC Advances*, 8(5), 2305–2314. <https://doi.org/10.1039/c7ra10334d>
- Prescient & Strategic Intelligence. (2022, October). *Wound Dressing Market Size, Share | Industry Report 2023*. Wound Dressing Market Overview. <https://www.psmarketresearch.com/market-analysis/wound-dressings-market>
- Qin, H., Wang, J., Wang, T., Gao, X., Wan, Q., & Pei, X. (2018). Preparation and Characterization of Chitosan/ β -Glycerophosphate Thermal-Sensitive Hydrogel Reinforced by Graphene Oxide. *Frontiers in Chemistry*, 6(NOV), 565. <https://doi.org/10.3389/fchem.2018.00565>
- Qu, J., Zhao, X., Liang, Y., Zhang, T., Ma, P. X., & Guo, B. (2018). Antibacterial adhesive injectable hydrogels with rapid self-healing, extensibility and compressibility as wound dressing for joints skin wound healing. *Biomaterials*, 183(August), 185–199. <https://doi.org/10.1016/j.biomaterials.2018.08.044>
- Rahman, L., Lembang, R. S., Lallo, S., Handayani, S. R., Usmanengsi, & Permana, A. D. (2021). Bioadhesive dermal patch as promising approach for improved antibacterial activity of bioactive compound of Zingiber cassumunar Roxb in ex vivo Staphylococcus aureus skin infection model. *Journal of Drug Delivery Science and Technology*, 63, 102522. <https://doi.org/10.1016/J.JDDST.2021.102522>
- Rakhshaei, R., & Namazi, H. (2017). A potential bioactive wound dressing based on carboxymethyl cellulose/ZnO impregnated MCM-41 nanocomposite hydrogel.

Materials Science and Engineering C, 73, 456–464.
<https://doi.org/10.1016/j.msec.2016.12.097>

Rashtbar, M., Hadjati, J., Ai, J., Shirian, S., Jahanzad, I., Azami, M., Asadpour, S., & Sadroddiny, E. (2018). Critical-sized full-thickness skin defect regeneration using ovine small intestinal submucosa with or without mesenchymal stem cells in rat model. *Journal of Biomedical Materials Research. Part B, Applied Biomaterials*, 106(6), 2177–2190. <https://doi.org/10.1002/JBM.B.34019>

Ren, Z., Ke, T., Ling, Q., Zhao, L., & Gu, H. (2021). Rapid self-healing and self-adhesive chitosan-based hydrogels by host-guest interaction and dynamic covalent bond as flexible sensor. *Carbohydrate Polymers*, 273, 118533. <https://doi.org/10.1016/J.CARBPOL.2021.118533>

Rice-Evans, C. A., Miller, N. J., & Paganga, G. (1997). Antioxidant properties of phenolic compounds. *Trends in Plant Science*, 2(4), 152–159. [https://doi.org/10.1016/S1360-1385\(97\)01018-2](https://doi.org/10.1016/S1360-1385(97)01018-2)

Rouyère, C., Serrano, T., Frémont, S., & Echard, A. (2022). Oxidation and reduction of actin: Origin, impact in vitro and functional consequences in vivo. *European Journal of Cell Biology*, 101(3), 151249. <https://doi.org/10.1016/J.EJCB.2022.151249>

Sağdıç, O., Özkan, G., Özcan, M., & Özçelik, S. (2005). A Study on inhibitory effects of Sığla tree (*Liquidambar orientalis* Mill. var. *orientalis*) storax against several bacteria. *Phytotherapy Research*, 19(6), 549–551. <https://doi.org/10.1002/ptr.1654>

Sağdıç, O., Özkan, G., Özcan, M., Özçelik, S., Sağdıç, O., Özkan, G., Özcan, M., & Özçelik, S. (2005). A study on inhibitory effects of sığla tree (*Liquidambar orientalis* Mill. var. *orientalis*) storax against several bacteria. *Phytotherapy Research*, 19(6), 549–551. <https://doi.org/10.1002/ptr.1654>

Sahiner, N., Sagbas, S., Sahiner, M., Silan, C., Aktas, N., & Turk, M. (2016). Biocompatible and biodegradable poly(Tannic Acid) hydrogel with

antimicrobial and antioxidant properties. *International Journal of Biological Macromolecules*, 82, 150–159.
<https://doi.org/10.1016/J.IJBIOMAC.2015.10.057>

Saiz-Poseu, J., Mancebo-Aracil, J., Nador, F., Busqué, F., & Ruiz-Molina, D. (2019). The Chemistry behind Catechol-Based Adhesion. In *Angewandte Chemie - International Edition* (Vol. 58, Issue 3, pp. 696–714). Wiley-VCH Verlag.
<https://doi.org/10.1002/anie.201801063>

Shafique, M., Sohail, M., Minhas, M. U., Khaliq, T., Kousar, M., Khan, S., Hussain, Z., Mahmood, A., Abbasi, M., Aziz, H. C., & Shah, S. A. (2021). Bio-functional hydrogel membranes loaded with chitosan nanoparticles for accelerated wound healing. *International Journal of Biological Macromolecules*, 170, 207–221.
<https://doi.org/10.1016/j.ijbiomac.2020.12.157>

Shao, K., Han, B., Gao, J., Song, F., Yang, Y., & Liu, W. (2015a). Synthesis and characterization of a hydroxyethyl derivative of chitosan and evaluation of its biosafety. *Journal of Ocean University of China*, 14(4), 703–709.
<https://doi.org/10.1007/s11802-015-2544-x>

Shao, K., Han, B., Gao, J., Song, F., Yang, Y., & Liu, W. (2015b). Synthesis and characterization of a hydroxyethyl derivative of chitosan and evaluation of its biosafety. *Journal of Ocean University of China*, 14(4), 703–709.
<https://doi.org/10.1007/s11802-015-2544-x>

Shchipunov, Y. A. (2020). Structure of Polyelectrolyte Complexes by the Example of Chitosan Hydrogels with lambda-carrageenan. *Polymer Science - Series A*, 62(1), 54–61. <https://doi.org/10.1134/S0965545X20010101>

Sheikhi, A., de Rutte, J., Haghniaz, R., Akouissi, O., Sohrabi, A., Di Carlo, D., & Khademhosseini, A. (2019). Modular microporous hydrogels formed from microgel beads with orthogonal thermo-chemical responsivity: Microfluidic fabrication and characterization. *MethodsX*, 6, 1747–1752.
<https://doi.org/10.1016/J.MEX.2019.07.018>

- Shirzaei Sani, E., Portillo Lara, R., Aldawood, Z., Bassir, S. H., Nguyen, D., Kantarci, A., Intini, G., & Annabi, N. (2019). An Antimicrobial Dental Light Curable Bioadhesive Hydrogel for Treatment of Peri-Implant Diseases. *Matter*, *1*(4), 926–944. <https://doi.org/10.1016/j.matt.2019.07.019>
- Shou, Y., Zhang, J., Yan, S., Xia, P., Xu, P., Li, G., Zhang, K., & Yin, J. (2020). Thermoresponsive Chitosan/DOPA-Based Hydrogel as an Injectable Therapy Approach for Tissue-Adhesion and Hemostasis. *ACS Biomaterials Science and Engineering*, *6*(6), 3619–3629. <https://doi.org/10.1021/acsbiomaterials.0c00545>
- Shu, X., Wei, Y., Luo, X., Liu, J., Mao, L., Yuan, F., & Gao, Y. (2023). κ -Carrageenan/konjac glucomannan composite hydrogel filled with rhamnolipid-stabilized nanostructured lipid carrier: Improvement of structure and properties. *Food Hydrocolloids*, *134*, 108088. <https://doi.org/10.1016/J.FOODHYD.2022.108088>
- Singh, B., Sharma, S., & Dhiman, A. (2013). Design of antibiotic containing hydrogel wound dressings: Biomedical properties and histological study of wound healing. *International Journal of Pharmaceutics*, *457*(1), 82–91. <https://doi.org/10.1016/j.ijpharm.2013.09.028>
- Singh, B., Singh, J., & Rajneesh. (2021a). Application of tragacanth gum and alginate in hydrogel wound dressing's formation using gamma radiation. *Carbohydrate Polymer Technologies and Applications*, *2*, 100058. <https://doi.org/10.1016/J.CARPTA.2021.100058>
- Singh, B., Singh, J., & Rajneesh. (2021b). Application of tragacanth gum and alginate in hydrogel wound dressing's formation using gamma radiation. *Carbohydrate Polymer Technologies and Applications*, *2*, 100058. <https://doi.org/10.1016/j.carpta.2021.100058>
- Singh, P., Verma, C., Mukhopadhyay, S., Gupta, A., & Gupta, B. (2022). Preparation of thyme oil loaded κ -carrageenan-polyethylene glycol hydrogel membranes as

wound care system. *International Journal of Pharmaceutics*, 618, 121661.
<https://doi.org/10.1016/j.ijpharm.2022.121661>

Sohn, D. G., Hong, M. W., Kim, Y. Y., & Cho, Y. S. (2015). Fabrication of Dual-pore Scaffolds Using a Combination of Wire-Networked Molding (WNM) and Non-solvent Induced Phase Separation (NIPS) Techniques. *Journal of Bionic Engineering* 2015 12:4, 12(4), 565–574. [https://doi.org/10.1016/S1672-6529\(14\)60146-3](https://doi.org/10.1016/S1672-6529(14)60146-3)

Spanò, R., Muraglia, A., Todeschi, M. R., Nardini, M., Strada, P., Cancedda, R., & Mastrogiacomo, M. (2018). Platelet-rich plasma-based bioactive membrane as a new advanced wound care tool. *Journal of Tissue Engineering and Regenerative Medicine*, 12(1), e82–e96. <https://doi.org/10.1002/term.2357>

Sumitha, N. S., Prakash, P., Nair, B. N., & Sailaja, G. S. (2021). Degradation-Dependent Controlled Delivery of Doxorubicin by Glyoxal Cross-Linked Magnetic and Porous Chitosan Microspheres. *ACS Omega*, 6(33), 21472–21484.
https://doi.org/10.1021/ACSOMEGA.1C02303/SUPPL_FILE/AO1C02303_S1_001.PDF

Sun, T., Tao, H., Xie, J., Zhang, S., & Xu, X. (2010). Degradation and antioxidant activity of κ -carrageenans. *Journal of Applied Polymer Science*, 117(1), 194–199. <https://doi.org/10.1002/APP.31955>

Swain, S. K., Bhattacharyya, S., & Sarkar, D. (2015). Fabrication of porous hydroxyapatite scaffold via polyethylene glycol-polyvinyl alcohol hydrogel state. *Materials Research Bulletin*, 64, 257–261.
<https://doi.org/10.1016/j.materresbull.2014.12.072>

Tan, H., Jin, D., Sun, J., Song, J., Lu, Y., Yin, M., Chen, X., Qu, X., & Liu, C. (2021). Enlisting a Traditional Chinese Medicine to tune the gelation kinetics of a bioactive tissue adhesive for fast hemostasis or minimally invasive therapy.

Bioactive Materials, 6(3), 905–917.
<https://doi.org/10.1016/J.BIOACTMAT.2020.10.011>

Tan, S., Wood, M., & Maher, P. (1998). Oxidative Stress Induces a Form of Programmed Cell Death with Characteristics of Both Apoptosis and Necrosis in Neuronal Cells. *Journal of Neurochemistry*, 71(1), 95–105.
<https://doi.org/10.1046/J.1471-4159.1998.71010095.X>

Tavakoli, S., Mokhtari, H., Kharaziha, M., Kermanpur, A., Talebi, A., & Moshtaghian, J. (2020a). A multifunctional nanocomposite spray dressing of Kappa-carrageenan-polydopamine modified ZnO/L-glutamic acid for diabetic wounds. *Materials Science and Engineering: C*, 111(February), 110837.
<https://doi.org/10.1016/j.msec.2020.110837>

Tavakoli, S., Mokhtari, H., Kharaziha, M., Kermanpur, A., Talebi, A., & Moshtaghian, J. (2020b). A multifunctional nanocomposite spray dressing of Kappa-carrageenan-polydopamine modified ZnO/L-glutamic acid for diabetic wounds. *Materials Science and Engineering C*, 111(February), 110837.
<https://doi.org/10.1016/j.msec.2020.110837>

Tavakoli, S., Mokhtari, H., Kharaziha, M., Kermanpur, A., Talebi, A., & Moshtaghian, J. (2020c). A multifunctional nanocomposite spray dressing of Kappa-carrageenan-polydopamine modified ZnO/L-glutamic acid for diabetic wounds. *Materials Science and Engineering C*, 111(February), 110837.
<https://doi.org/10.1016/j.msec.2020.110837>

Tayebi, T., Baradaran-Rafii, A., Hajifathali, A., Rahimpour, A., Zali, H., Shaabani, A., & Niknejad, H. (2021). Biofabrication of chitosan/chitosan nanoparticles/polycaprolactone transparent membrane for corneal endothelial tissue engineering. *Scientific Reports*, 11(1), 7060.
<https://doi.org/10.1038/s41598-021-86340-w>

- Taylor, M., Urquhart, A. J., Zelzer, M., Davies, M. C., & Alexander, M. R. (2007). Picoliter water contact angle measurement on polymers. *Langmuir*, 23(13), 6875–6878. <https://doi.org/10.1021/la070100j>
- Timur, S. S., Yüksel, S., Akca, G., & Şenel, S. (2019). Localized drug delivery with mono and bilayered mucoadhesive films and wafers for oral mucosal infections. *International Journal of Pharmaceutics*, 559(May 2018), 102–112. <https://doi.org/10.1016/j.ijpharm.2019.01.029>
- Toumi, S., Yahoum, M. M., Lefnaoui, S., & Hadjsadok, A. (2021). Synthesis, characterization and potential application of hydrophobically modified carrageenan derivatives as pharmaceutical excipients. *Carbohydrate Polymers*, 251, 116997. <https://doi.org/10.1016/j.carbpol.2020.116997>
- Türkkan, S., Pazarçeviren, A. E., Keskin, D., Machin, N. E., Duygulu, Ö., & Tezcaner, A. (2017). Nanosized CaP-silk fibroin-PCL-PEG-PCL/PCL based bilayer membranes for guided bone regeneration. *Materials Science and Engineering: C*, 80, 484–493. <http://www.ncbi.nlm.nih.gov/pubmed/28866191>
- Urie, R., McBride, M., Ghosh, D., Fattahi, A., Nitiyanandan, R., Popovich, J., Heys, J. J., Kilbourne, J., Haydel, S. E., & Rege, K. (2021). Antimicrobial laser-activated sealants for combating surgical site infections. *Biomaterials Science*, 9(10), 3791–3803. <https://doi.org/10.1039/D0BM01438A>
- Varshosaz, J., Tavakoli, N., Moghaddam, F., & Ghassami, E. (2015). Polyelectrolyte complexes of chitosan for production of sustained release tablets of bupropion HCl. *Farmacia*, 63(1), 65–73.
- Vowden, K., & Vowden, P. (2017). Wound dressings: principles and practice. *Surgery (Oxford)*, 35(9), 489–494. <https://doi.org/10.1016/J.MPSUR.2017.06.005>
- Vreeman, H. J., Snoeren, T. H. M., & Payens, T. A. J. (1980). Physicochemical investigation of k-carrageenan in the random state. *Biopolymers*, 19(7), 1357–1374. <https://doi.org/10.1002/BIP.1980.360190711>

- Wang, J., Wang, L., Wu, C., Pei, X., Cong, Y., Zhang, R., & Fu, J. (2020). Antibacterial Zwitterionic Polyelectrolyte Hydrogel Adhesives with Adhesion Strength Mediated by Electrostatic Mismatch. *ACS Applied Materials & Interfaces*. <https://doi.org/10.1021/ACSAMI.0C14959>
- Wang, L., Wang, W., Liao, J., Wang, F., Jiang, J., Cao, C., & Li, S. (2018). Novel bilayer wound dressing composed of SIS membrane with SIS cryogel enhanced wound healing process. *Materials Science and Engineering: C*, 85, 162–169. <https://doi.org/10.1016/J.MSEC.2017.11.024>
- Watson, E., Tatara, A. M., Kontoyiannis, D. P., & Mikos, A. G. (2016). Inherently Antimicrobial Biodegradable Polymers in Tissue Engineering. *ACS Biomaterials Science and Engineering*, 3(7), 1207–1220. <https://doi.org/10.1021/ACSBIOMATERIALS.6B00501>
- Wei, Q., Chen, K., Zhang, X., Ma, G., Zhang, W., & Hu, Z. (2022). Facile preparation of polysaccharides-based adhesive hydrogel with antibacterial and antioxidant properties for promoting wound healing. *Colloids and Surfaces B: Biointerfaces*, 209, 112208. <https://doi.org/10.1016/J.COLSURFB.2021.112208>
- Wei, R., Chen, T., Wang, Y., Xu, Q., Feng, B., Weng, J., Peng, W., & Wang, J. (2021). By Endowing Polyglutamic Acid/Polylysine Composite Hydrogel with Super Intrinsic Characteristics to Enhance its Wound Repair Potential. *Macromolecular Bioscience*, 21(5), 2000367. <https://doi.org/10.1002/MABI.202000367>
- Winkler, L. W. (1888). Die Bestimmung des im Wasser gelösten Sauerstoffes. *Berichte Der Deutschen Chemischen Gesellschaft*, 21(2), 2843–2854. <https://doi.org/10.1002/cber.188802102122>
- Wittaya-areekul, S., & Prahsarn, C. (2006). Development and in vitro evaluation of chitosan–polysaccharides composite wound dressings. *International Journal of*

Pharmaceutics, 313(1–2), 123–128.
<https://doi.org/10.1016/J.IJPHARM.2006.01.027>

Xiang, S., Li, T., Wang, Y., Ma, P., Chen, M., & Dong, W. (2016). Long-chain branching hydrogel with ultrahigh tensibility and high strength by grafting: Via photo-induced polymerization. *New Journal of Chemistry*, 40(10), 8650–8657. <https://doi.org/10.1039/c6nj01843b>

Xing, W., Yin, M., Lv, Q., Hu, Y., Liu, C., & Zhang, J. (2014). Oxygen Solubility, Diffusion Coefficient, and Solution Viscosity. In *Rotating Electrode Methods and Oxygen Reduction Electrocatalysts* (pp. 1–31). Elsevier B.V. <https://doi.org/10.1016/B978-0-444-63278-4.00001-X>

Xu, Y., Kim, C. S., Saylor, D. M., & Koo, D. (2017). Polymer degradation and drug delivery in PLGA-based drug–polymer applications: A review of experiments and theories. *Journal of Biomedical Materials Research Part B: Applied Biomaterials*, 105(6), 1692–1716. <https://doi.org/10.1002/JBM.B.33648>

Yamanlar, S., Sant, S., Boudou, T., Picart, C., & Khademhosseini, A. (2011). Surface functionalization of hyaluronic acid hydrogels by polyelectrolyte multilayer films. *Biomaterials*, 32(24), 5590–5599. <https://doi.org/10.1016/j.biomaterials.2011.04.030>

Yang, J., Bai, R., Chen, B., & Suo, Z. (2020). Hydrogel Adhesion: A Supramolecular Synergy of Chemistry, Topology, and Mechanics. *Advanced Functional Materials*, 30(2), 1901693. <https://doi.org/10.1002/ADFM.201901693>

Yang, J., Chen, Y., Zhao, L., Feng, Z., Peng, K., Wei, A., Wang, Y., Tong, Z., & Cheng, B. (2020). Preparation of a chitosan/carboxymethyl chitosan/AgNPs polyelectrolyte composite physical hydrogel with self-healing ability, antibacterial properties, and good biosafety simultaneously, and its application as a wound dressing. *Composites Part B: Engineering*, 197, 108139. <https://doi.org/10.1016/j.compositesb.2020.108139>

- Yang, Q., Tang, L., Guo, C., Deng, F., Wu, H., Chen, L., Huang, L., Lu, P., Ding, C., Ni, Y., & Zhang, M. (2021). A bioinspired gallol-functionalized collagen as wet-tissue adhesive for biomedical applications. *Chemical Engineering Journal*, *417*, 127962. <https://doi.org/10.1016/J.CEJ.2020.127962>
- Yang, Y., Liang, Y., Chen, J., Duan, X., & Guo, B. (2022). Mussel-inspired adhesive antioxidant antibacterial hemostatic composite hydrogel wound dressing via photo-polymerization for infected skin wound healing. *Bioactive Materials*, *8*, 341–354. <https://doi.org/10.1016/J.BIOACTMAT.2021.06.014>
- Yen, C., He, H., Lee, L. J., & Ho, W. S. W. (2009). Synthesis and characterization of nanoporous polycaprolactone membranes via thermally- and nonsolvent-induced phase separations for biomedical device application. *Journal of Membrane Science*, *343*(1–2), 180–188. <https://doi.org/10.1016/j.memsci.2009.07.024>
- Ying, H., Zhou, J., Wang, M., Su, D., Ma, Q., Lv, G., & Chen, J. (2019). In situ formed collagen-hyaluronic acid hydrogel as biomimetic dressing for promoting spontaneous wound healing. *Materials Science and Engineering: C*, *101*, 487–498. <https://doi.org/10.1016/J.MSEC.2019.03.093>
- Yoon, H. Y., Son, S., Lee, S. J., You, D. G., Yhee, J. Y., Park, J. H., Swierczewska, M., Lee, S., Kwon, I. C., Kim, S. H., Kim, K., & Pomper, M. G. (2014). Glycol chitosan nanoparticles as specialized cancer therapeutic vehicles: Sequential delivery of doxorubicin and Bcl-2 siRNA. *Scientific Reports*, *4*(1), 1–12. <https://doi.org/10.1038/srep06878>
- Yu, R., Li, M., Li, Z., Pan, G., Liang, Y., Guo, B., Yu, R., Liang, Y., Guo, B., Li, M., Li, Z., & Pan, G. (2022). Supramolecular Thermo-Contracting Adhesive Hydrogel with Self-Removability Simultaneously Enhancing Noninvasive Wound Closure and MRSA-Infected Wound Healing. *Advanced Healthcare Materials*, *11*(13), 2102749. <https://doi.org/10.1002/ADHM.202102749>

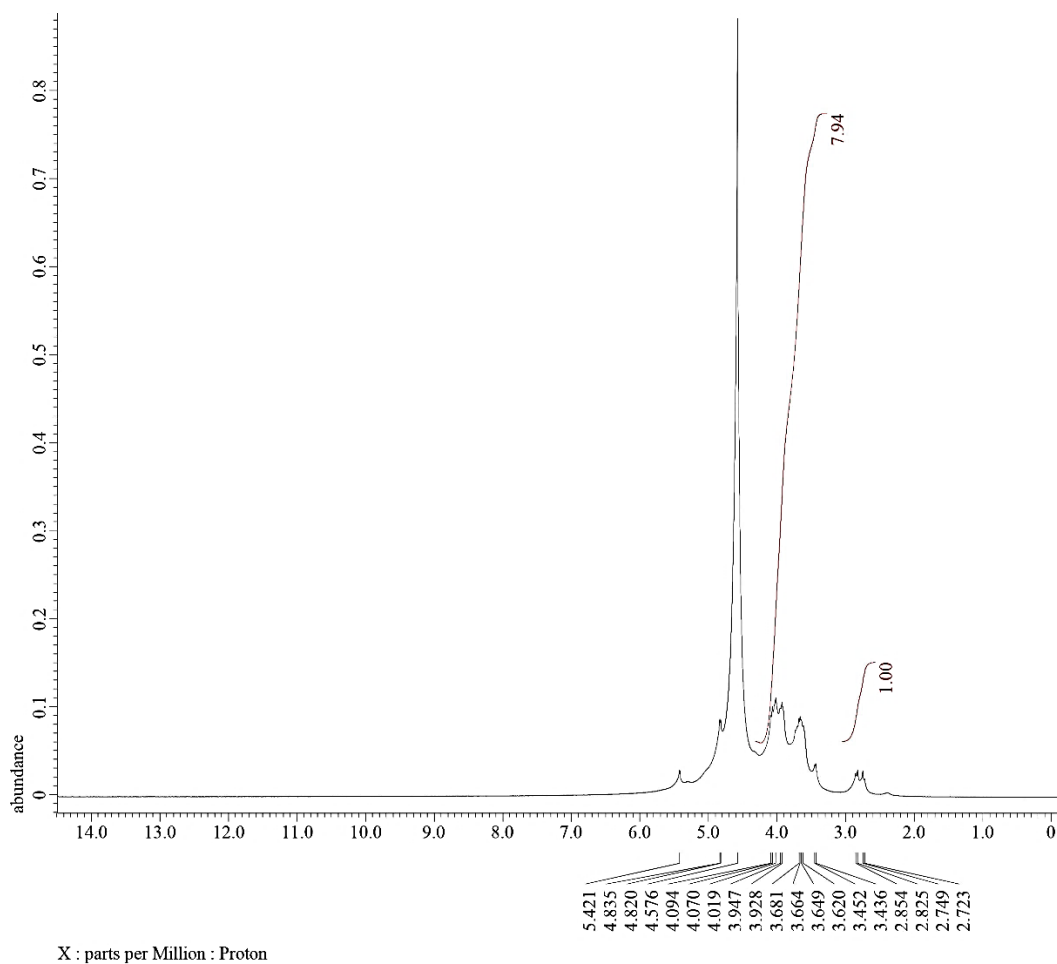
- Zahid, S., Khalid, H., Ikram, F., Iqbal, H., Samie, M., Shahzadi, L., Shah, A. T., Yar, M., Chaudhry, A. A., Awan, S. J., Khan, A. F., & Rehman, I. ur. (2019). Bi-layered α -tocopherol acetate loaded membranes for potential wound healing and skin regeneration. *Materials Science and Engineering: C*, *101*, 438–447. <https://doi.org/10.1016/j.msec.2019.03.080>
- Zeb, A. (2020). Concept, mechanism, and applications of phenolic antioxidants in foods. *Journal of Food Biochemistry*, *44*(9). <https://doi.org/10.1111/JFBC.13394>
- Zehtabchi, S., Tan, A., Yadav, K., Badawy, A., & Lucchesi, M. (2012). The impact of wound age on the infection rate of simple lacerations repaired in the emergency department. *Injury*, *43*(11), 1793–1798. <https://doi.org/10.1016/J.INJURY.2012.02.018>
- Zepon, K. M., Marques, M. S., da Silva Paula, M. M., Morisso, F. D. P., & Kanis, L. A. (2018). Facile, green and scalable method to produce carrageenan-based hydrogel containing in situ synthesized AgNPs for application as wound dressing. *International Journal of Biological Macromolecules*, *113*, 51–58. <https://doi.org/10.1016/j.ijbiomac.2018.02.096>
- Zepon, K. M., Martins, M. M., Marques, M. S., Heckler, J. M., Dal Pont Morisso, F., Moreira, M. G., Ziulkoski, A. L., & Kanis, L. A. (2019a). Smart wound dressing based on κ -carrageenan/locust bean gum/cranberry extract for monitoring bacterial infections. *Carbohydrate Polymers*, *206*, 362–370. <https://doi.org/10.1016/j.carbpol.2018.11.014>
- Zepon, K. M., Martins, M. M., Marques, M. S., Heckler, J. M., Dal Pont Morisso, F., Moreira, M. G., Ziulkoski, A. L., & Kanis, L. A. (2019b). Smart wound dressing based on κ -carrageenan/locust bean gum/cranberry extract for monitoring bacterial infections. *Carbohydrate Polymers*, *206*, 362–370. <https://doi.org/10.1016/j.carbpol.2018.11.014>

- Zein, A. B., & Kabanov, V. A. (1982). A New Class of Complex Water-soluble Polyelectrolytes. *Russian Chemical Reviews*, 51(9), 833–855. <https://doi.org/10.1070/rc1982v051n09abeh002921>
- Zhang, X., Pan, Y., Li, S., Xing, L., Du, S., Yuan, G., Li, J., Zhou, T., Xiong, D., Tan, H., Ling, Z., Chen, Y., Hu, X., & Niu, X. (2020). Doubly crosslinked biodegradable hydrogels based on gellan gum and chitosan for drug delivery and wound dressing. *International Journal of Biological Macromolecules*, 164, 2204–2214. <https://doi.org/10.1016/j.ijbiomac.2020.08.093>
- Zhao, X., Liang, Y., Huang, Y., He, J., Han, Y., & Guo, B. (2020). Physical Double-Network Hydrogel Adhesives with Rapid Shape Adaptability, Fast Self-Healing, Antioxidant and NIR/pH Stimulus-Responsiveness for Multidrug-Resistant Bacterial Infection and Removable Wound Dressing. *Advanced Functional Materials*, 30(17), 1910748. <https://doi.org/10.1002/adfm.201910748>
- Zheng, W., & Wang, S. Y. (2001). Antioxidant Activity and Phenolic Compounds in Selected Herbs. *Journal of Agricultural and Food Chemistry*, 49(11), 5165–5170. <https://doi.org/10.1021/jf010697n>
- Zheng, Z., Bian, S., Li, Z., Zhang, Z., Liu, Y., Zhai, X., Pan, H., & Zhao, X. (2020). Catechol modified quaternized chitosan enhanced wet adhesive and antibacterial properties of injectable thermo-sensitive hydrogel for wound healing. *Carbohydrate Polymers*, 249, 116826. <https://doi.org/10.1016/J.CARBPOL.2020.116826>
- Zhou, J., Yao, D., Qian, Z., Hou, S., Li, L., Jenkins, A. T. A., & Fan, Y. (2018). Bacteria-responsive intelligent wound dressing: Simultaneous In situ detection and inhibition of bacterial infection for accelerated wound healing. *Biomaterials*, 161, 11–23. <https://doi.org/10.1016/j.biomaterials.2018.01.024>

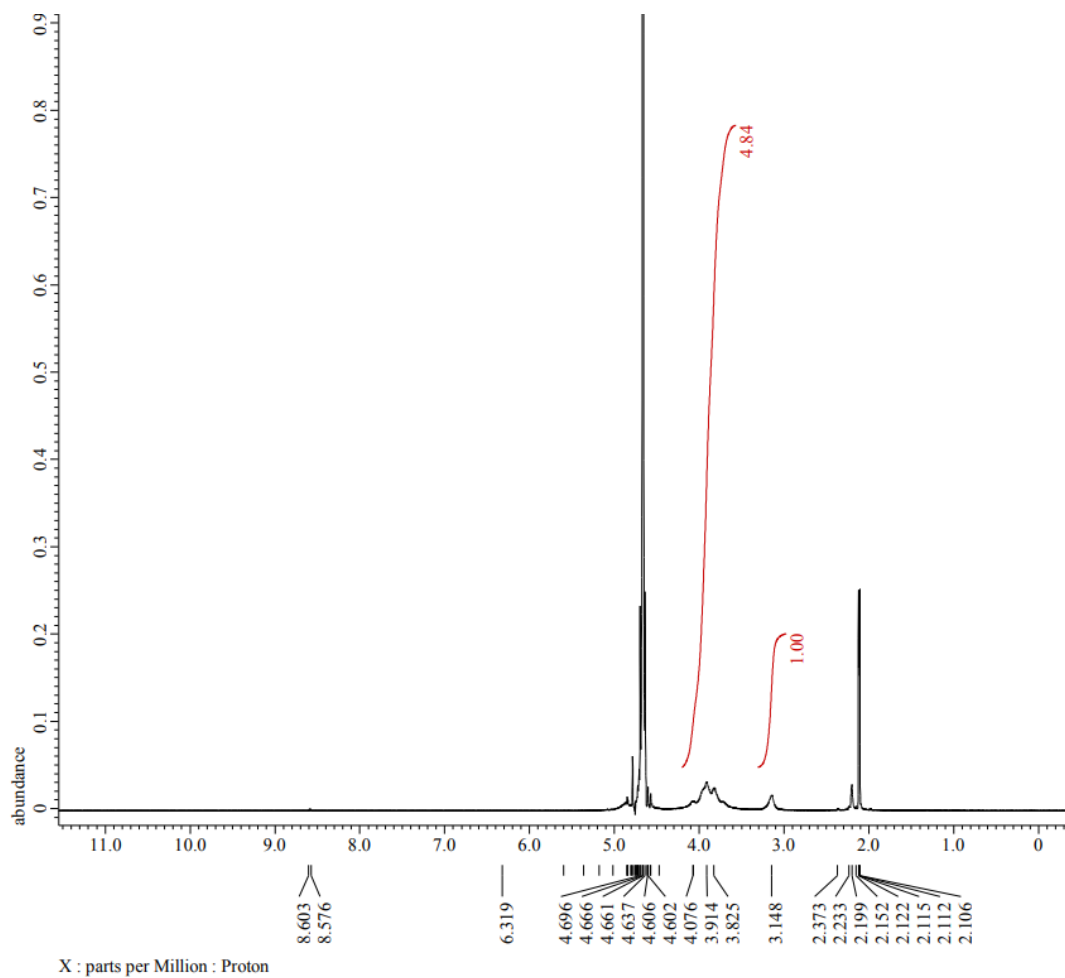
- Zhu, H., Tian, J., Mao, H., & Gu, Z. (2021). Bioadhesives: Current hotspots and emerging challenges. *Current Opinion in Biomedical Engineering*, 18, 100271. <https://doi.org/10.1016/J.COBME.2021.100271>
- Zuidema, J. M., Rivet, C. J., Gilbert, R. J., & Morrison, F. A. (2014). A protocol for rheological characterization of hydrogels for tissue engineering strategies. *Journal of Biomedical Materials Research Part B: Applied Biomaterials*, 102(5), 1063–1073. <https://doi.org/10.1002/jbm.b.33088>
- Zuppolini, S., Cruz-Maya, I., Guarino, V., & Borriello, A. (2020). *Functional Biomaterials Optimization of Polydopamine Coatings onto Poly-ε-Caprolactone Electrospun Fibers for the Fabrication of Bio-Electroconductive Interfaces*. <https://doi.org/10.3390/jfb11010019>

APPENDICES

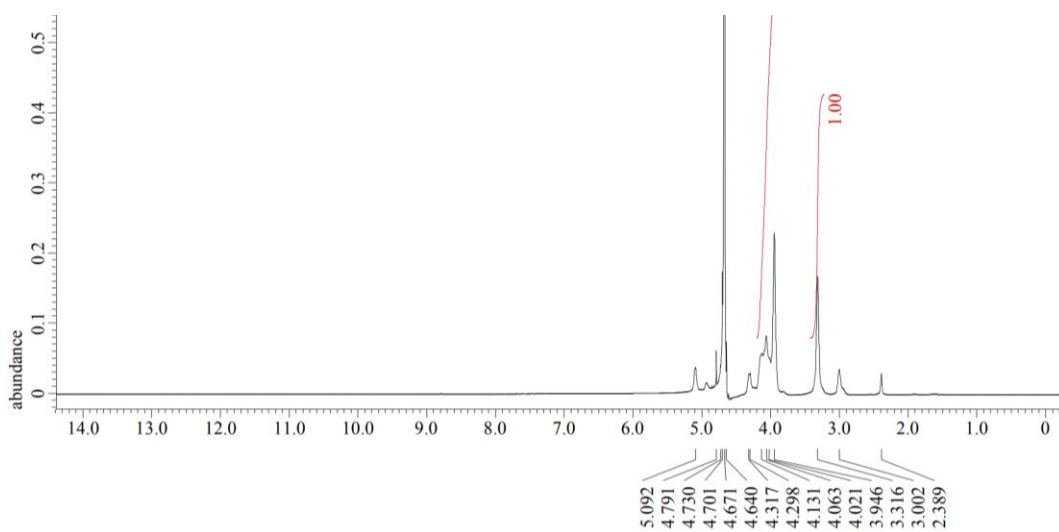
A. ^1H NMR of Polymers Used in the Preparation of HECS:kC Hydrogels



Appendix A Figure 1. ^1H NMR of kC



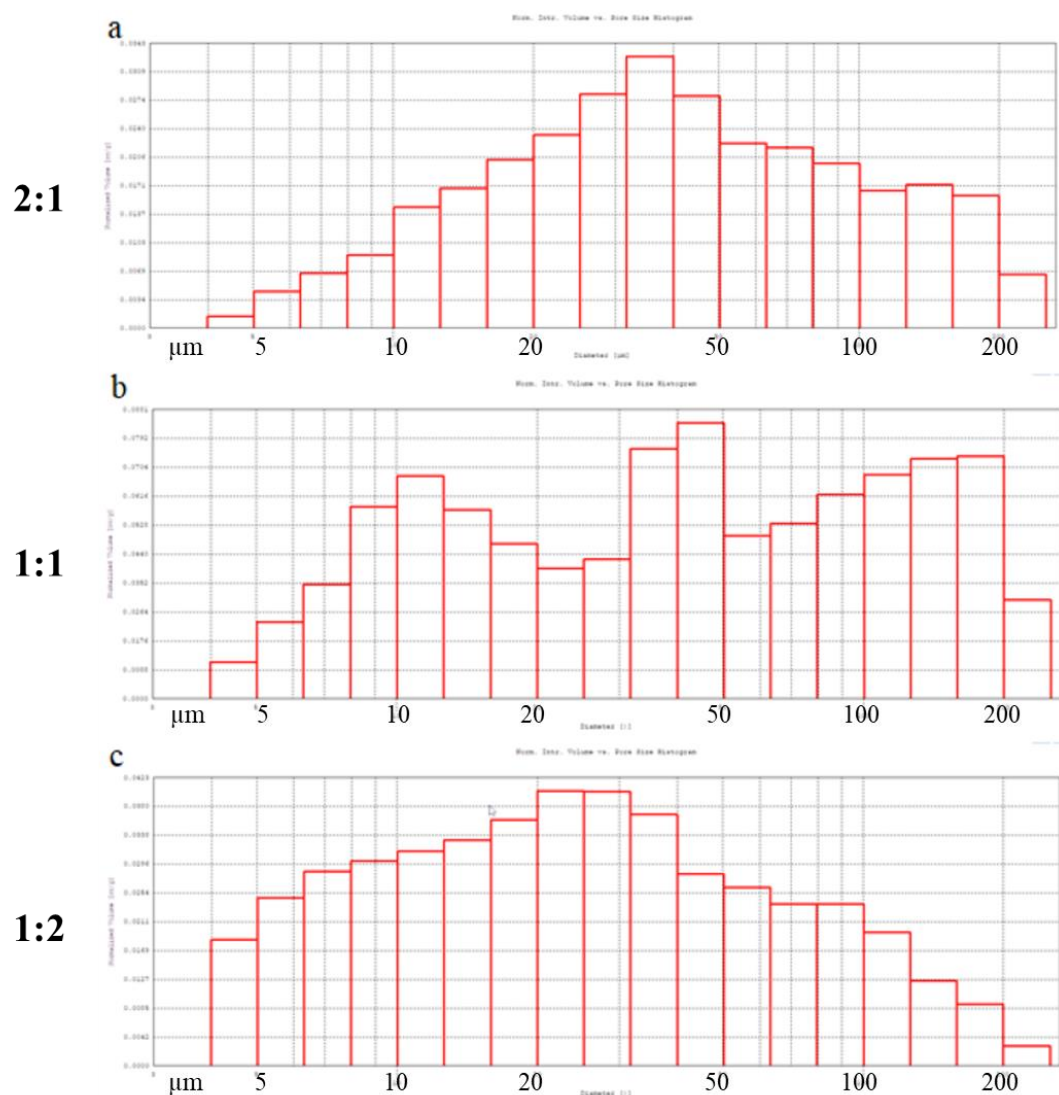
Appendix A Figure 2. ^1H NMR of CS



X : parts per Million ; Proton

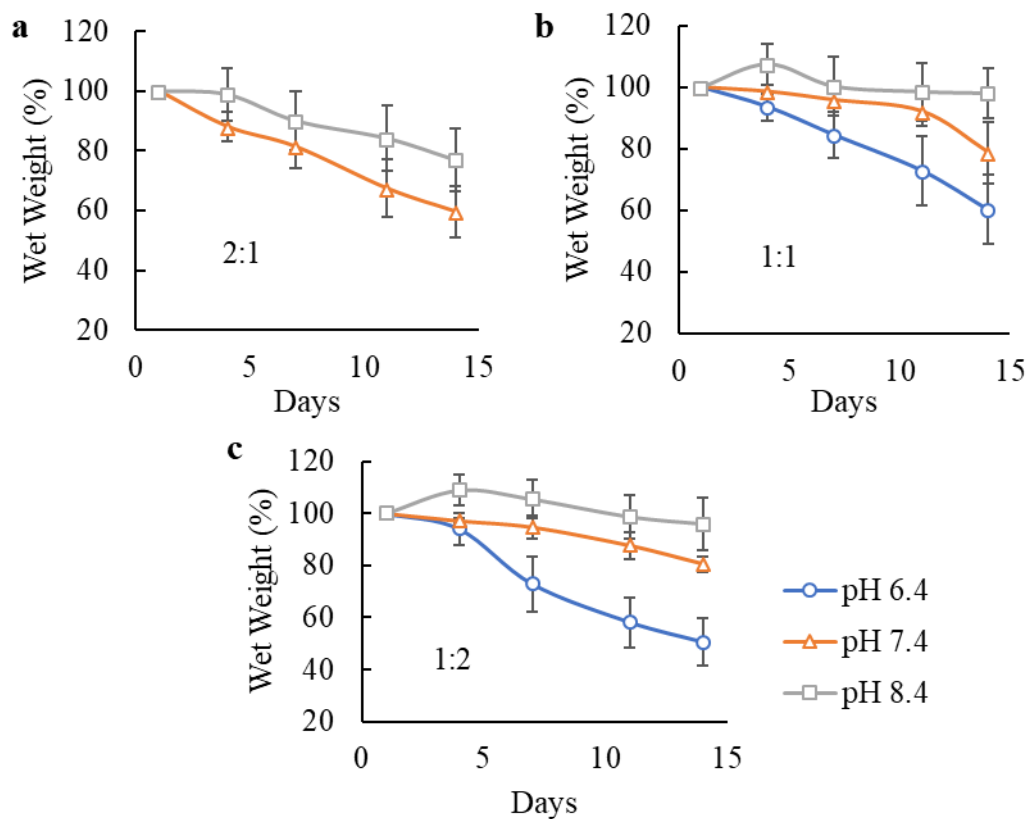
Appendix A Figure 3. ¹H NMR of HECS

B. Pore Size Distribution of HECS-kC Hydrogels

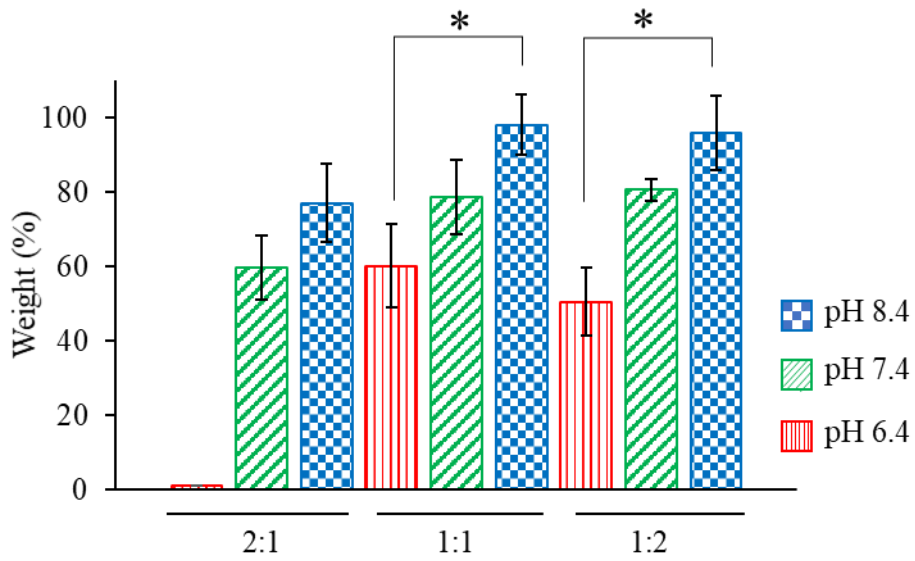


Appendix B Figure 1. Pore size distribution of hydrogels with HECS:kC ratios of 2:1, 1:1 and 1:2.

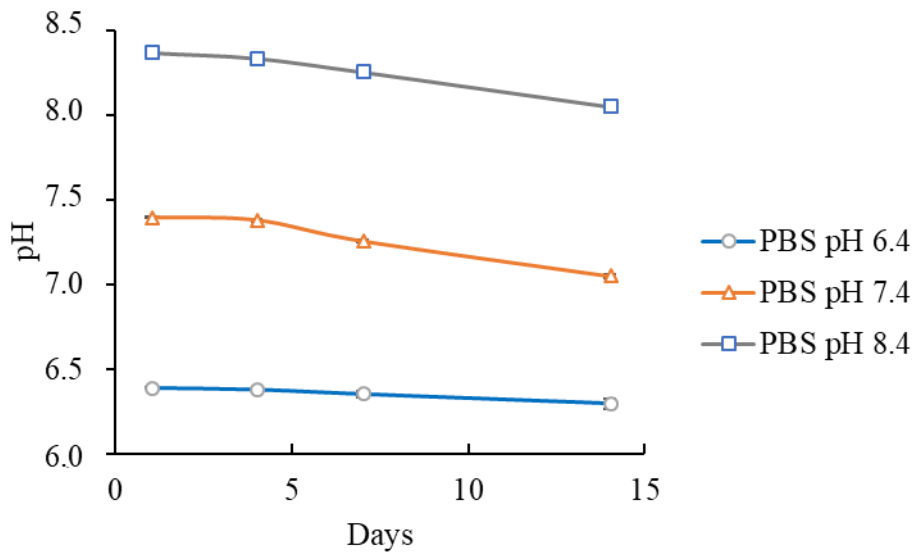
C. Wet Weight Change of HECS-kC Hydrogels and Incubation Buffer pH



Appendix C Figure 1. Wet weight change of HECS:kC hydrogels with 2:1 (a) 1:1 (b) 1:2 (c) ratio at 37°C. The hydrogel samples incubated in buffer at pH 6.4 were lost within 1 day and the results are not shown in the graph (n=3).



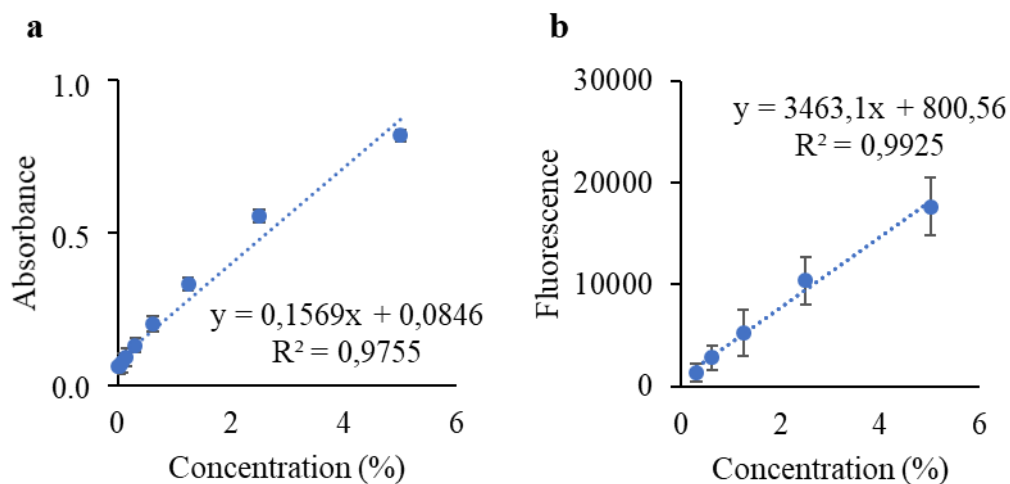
Appendix C Figure 2. *In vitro* degradation of the hydrogels in PBS after 14 days of incubation at 37°C. The hydrogel samples incubated in buffer at pH 6.4 were lost within 1 day and the results are not shown in the graph. The mean differences between groups pH 6.4-pH 8.4 are significant (n=3, p<0.05).



Appendix C Figure 3. Change in the pH of incubation buffers during the degradation study Standard deviations are very small and cannot be seen in the graph (n=3).

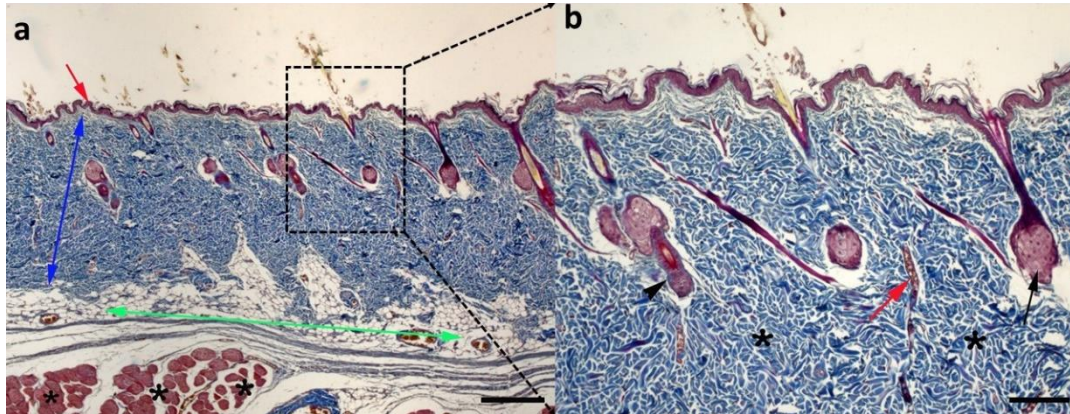
D. Storax Standard Curve

Storax standard curve was obtained via absorbance measurement at 363 nm and fluorescence at 565 nm excitation and 685 nm emission. Storax at different concentrations were dissolved in absolute ethanol.

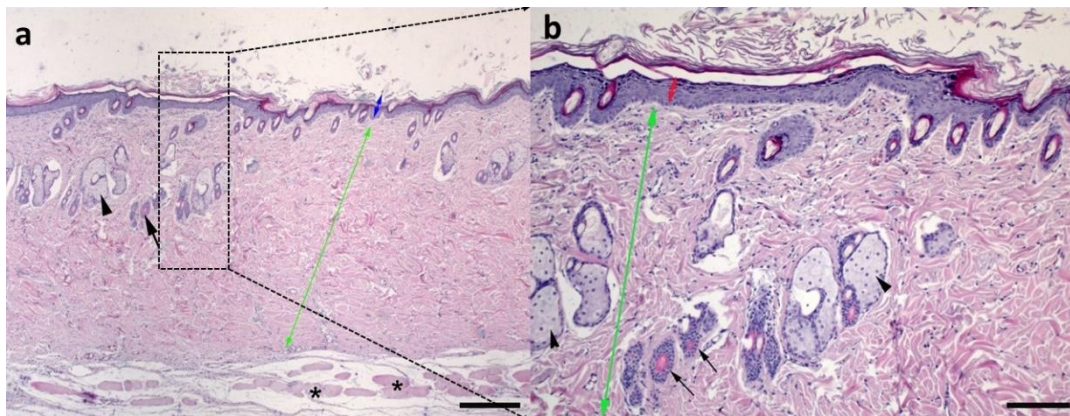


Appendix D Figure 1. Standard curve constructed with different concentrations of storax (n=3) using spectrophotometry at a wavelength of 363 nm (a) fluorimetry (excitation wavelength: 565 nm and emission wavelength: 685 nm) (n=3).

E. Masson's Trichrome and Hematoxylin-Eosin Staining of Normal Rat Skin



Appendix E Figure 1. Histological evaluation of normal rat skin. Masson's trichrome staining, scale bar (a): 250 μm ; scale bar (b): 150 μm . (a) Epidermis (red arrow), dermis (blue arrow), hypodermis (green arrow), muscle tissue (asterix). (b) sebaceous gland (black arrow), hair follicle (arrow head), collagen fibers (asterix), blood vessels (red arrow).



Appendix E Figure 2. Histological evaluation of normal rat skin. Hematoxylin-eosin staining; scale bar (a): 250 μm ; scale bar (b): 150 μm . (a) epidermis (blue arrow), dermis (green arrow), sebaceous gland (arrow head), hair follicle (black arrow). (b) epidermis (red arrow), dermis (green arrow), sebaceous gland (arrow head), hair follicle (black arrow).

CURRICULUM VITAE

Surname, Name: Nakipoğlu, Mustafa

EDUCATION

| Degree | Institution | Year of Graduation |
|-------------|------------------------------------|--------------------|
| MS | METU, Biotechnology, Ankara | 1999 |
| BS | Osmangazi Uni., Biology, Eskişehir | 2012 |
| High School | Fatih Sultan Mehmed Lisesi, Ankara | 2006 |

FOREIGN LANGUAGES

English

PUBLICATIONS

- 1- NAKIPOGLU M., YILMAZ F., IÇGEN B. (2016). vanA Gene Harboring Enterococcal and Non enterococcal Isolates Expressing High Level Vancomycin and Teicoplanin Resistance Reservoired in Surface Waters. Bulletin of Environmental Contamination and Toxicology, 1-8., Doi: 10.1007/s00128-016-1955-8
- 2- NAKIPOGLU M., YILMAZ F., IÇGEN B. (2016). vanA targeted oligonucleotide DNA probe designed to monitor vancomycin and teicoplanin resistant bacteria in surface waters. Environmental Monitoring and Assessment, 188(10), Doi: 10.1007/s10661-016-5578-7
- 3- K. MOHAMMED-AHMED H., NAKIPOGLU M., TEZCANER A., KESKIN D., EVIS Z. (2023). Functionalization of graphene oxide quantum dots for anticancer drug delivery. Journal of Drug Delivery Science and Technology, Doi: 80-104199, 10.1016/j.jddst.2023.104199

INTERESTS

World history, Ancient architecture, Swimming, Trekking, Video Games, Movies